수의학박사학위논문

Effects of surface-modified gold nanoparticles on cell viability and osteogenic differentiation

표면 변형된 금 나노 입자의 세포 생존도 및 골분화에 대한 작용

2015년 8월

서울대학교 대학원

수의학과 수의생명과학 전공

(수의약리학)

최 선 영

Doctoral Thesis

Effects of surface-modified gold nanoparticles on cell viability and osteogenic differentiation

Seon Young Choi

Academic advisor: So Yeong Lee, DVM, PhD

Graduate School

Seoul National University

August 2015

ABSTRACT

Researches regarding application of nanoparticles (NPs) had unique physical and chemical characteristics in biomedical fields such as drug delivery, targeting specific cancer cell, and tissue regeneration have been progressed. In case of AuNPs known to be less toxic than other NPs, a colloidal form of AuNPs dispersed in liquid are widely used. Thus, AuNPs are synthesized with stabilizer to prevent electrochemical instability of AuNPs. AuNPs modified with stabilizer are applied in drug delivery system and diagnostic tools due to stability and easy combination with antibody. Moreover, AuNPs are investigated as therapeutic tools to stimulate differentiation of adult stem cells in tissue regeneration. However, the toxicity of AuNPs for cells according to the size, shape, and surface charge has been reported. Moreover, it is reported that the physiological and biological effects of AuNPs on cells are cell type dependent. In this study, cytotoxicity of AuNPs stabilized with citrate- and chitosan on human lung cancer cells were measured and the change of microRNA expression by exposure of AuNPs stabilized with citrate- and chitosan was predicted. Furthermore, the promoting effect of AuNPs stabilized with chitosan on osteogenic differentiation of human adipose-derived mesenchymal stem cells (hADSCs) was investigated.

The results of this study revealed that differently charged AuNPs which were modified with citrate and chitosan showed toxicity in human lung cancer cells in dose-dependent manners through apoptosis and necrosis. Moreover, the

expression of microRNAs that were regarded as post-transcriptional regulators was altered by exposure to citrate- and chitosan-AuNPs in human lung cancer cells. The microRNAs up-regulated by citrate-AuNPs were related to migration and metastasis. The microRNAs up-regulated by chitosan-AuNPs were related to cell proliferation, apoptosis, and differentiaton. In addition, the microRNAs down-regulated by chitosan-AuNPs were related to proliferation, apoptosis, and development signaling pathway. In a study regarding cell differentiation, chitosan-AuNPs at the concentration that does not decrease cell viability stimulate the osteogenic differentiation of hADSCs through the activation of the Wnt/β-catenin signaling pathway. Therefore, results in this study suggest that AuNPs stabilized with citrate- and chitosan should be applied as therapeutic tools for regeneration of damaged tissue, and evaluating cytotoxicity of citrate- and chitosan-AuNPs should be estimated prior to biomedical application.

This study focuses on (1) the cytotoxic effect of citrate- and chitosan-AuNPs (Chapter I and II); (2) alteration in the expression of microRNAs by citrate- and chitosan-AuNPs (Chapter III) in human lung cancer cells; and (3) the promotion of osteogenic differentiation of hADSCs by chitosan-AuNPs (Chapter IV).

Keyword: citrate-gold nanoparticle, chitosan-gold nanoparticle, cytotoxicity, microRNA, human adipose derived mesenchymal stem cells, mineralization, Wnt/β-catenin

Student Number : 2009-21640

CONTENTS

LIST OF FIGURES

LITERATURE REVIEW

CHAPTER I

CHAPTER II

CHAPTER III

CHAPTER IV

GENERAL CONCLUSION

LIST OF TABLE

CHAPTER I

CHAPTER II

CHAPTER III

CHAPTER IV

ABBREVIATIONS

ALP	Alkaline phosphatase
ARS	Alizarin red s
AuNPs	Gold nanoparticles
BSP	Bone sialoprotein
CCK-8	Cell counting kit-8
CHX	Cyclohexamide
DAPI	4', 6-diamidino-2-phenylindole
DAVID	The database for annotation, visualization and integrated discovery
DMSO	Dimethyl sufoxide
DPBS	Dublecco's phospho buffered saline
FDA	Food and Drug Administration
FBS	Fetal bovine serum
GM	Growth medium
GO	Gene ontology
hADSCs	Human adipose tissue-derived mesenchymal stem cells
H_2O_2	Hydrogen peroxide
ICP-MS	Inductively coupled plasma-mass spectrometry
IC_{50}	Half maximal inhibitory concentration
KEGG	Kyoto encyclopedia of genes and genomes
LDH	Lactate dehydrogenase
MAPK	Mitogen-activated protein kinase
MSCs	Mesenchymal stem cells
MTT	3-(4,5-Dimethylthiazol-2-yl)-2,5-Diphenyltetrazolium bromide)
MWCNTs	Multiwall carbon nanotubes
NPs	Nanoparticles
OD	Optical density

OM	Osteogenic-inducing medium
OPN	Osteopontin
ORO	Oil red o
OSC	Osteocalcin
PCR	Polymerase chain reaction
PI	Propidinium iodide
ROS	Reactive oxygen species
RT-PCR	Reverse transcription polymerase chain reaction
SE	Standard error
TEM	Transmission electron microscopic
TGF-β	Transforming growth factor-beta
TiO_2	Titanium dioxide
TNF-α	Tumor necrosis factor-alpha
VEGF	Vascular endothelial growth factor

LITERATURE REVIEW

Properties of gold nanoparticles

Nanoparticles (NPs) with an average diameter of 1 to 100 nm are inorganic materials modified according to their surface, size, and composition (Alivisatos, 1996; Tervonen et al., 2009). The surface of NPs is coated with polymers or biomolecules for improved stability and selective targeting of biological molecules (Fang et al., 2009; Sperling and Parak, 2010). The final size of NPs is dependent on the surfactant additives, temperatures, and solvents present during their synthesis (Peer et al., 2007). Thus, the chemical, electrical and optical characteristics of NPs can differ from those of the bulk solid type (Burda et al., 2005).

All NPs have a large ratio in terms of surface area to volume, which makes them advantageous as carriers since their surface is coated with many molecules (El-Sayed, 2004; Gupta and Gupta, 2005; Lee et al., 1999). Also, the behavior of NPs is determined by the electrons they contain (Godovski, 1995; Xu and Tanaka, 1999). NP electrons can generate light or heat after absorbing energy (Govorov and Richardson, 2007; Richardson et al., 2009). Moreover, the chemical composition of NPs determines the electron's characteristics (McConnell et al., 2000). The larger magnetic fields of individual NPs, which are generated by the movement of electrons, can increase the contrast in magnetic resonance imaging (Blasiak et al., 2013; Issa et al., 2013; Kim et al., 2010).

Of the various NP types, gold nanoparticles (AuNPs) have emerged as the most attractive nanomaterials for biomedical applications due to their physical and chemical properties (Eustis and el-Sayed, 2006; Jain et al., 2008; Zhang, 2015). AuNPs absorb and scatter visible light upon excitation of their surface plasmon oscillation, and the light-scattering signal is consequently much brighter than fluorophores (Levy et al., 2010; Tong et al., 2009; Yguerabide and Yguerabide, 1998). Furthermore, AuNPs can be functionalized easily by anchoring thiol linkers in their monolayers (Ghosh et al., 2008a; Levy et al., 2004; Levy, 2006; Tiwari et al., 2011). In some studies, functional nano-conjugates have been obtained using peptides, antibodies, and nucleic acid (Boisselier and Astruc, 2009; Huang et al., 2013; Pantic and Markovic, 2011). These properties allow AuNPs to act as multifunctional platforms for therapeutic and diagnostic purposes (Khan et al., 2014; Mieszawska et al., 2013; Paciotti et al., 2006).

Applications of gold nanoparticles in the biomedical fields

Nanomaterials have already been approved by the Food and Drug Administration (FDA) for use in humans (Kim et al., 2010). Iron oxide of the type contained in the commercial products, Feridex® and Resovist®, is applied in magnetic resonance imaging diagnoses targeting the liver, while paclitaxel albumin-stabilized NPs are applied to treat lung cancer (Bose et al., 2014; Wang et al., 2013b). Therefore, many NPs are studied *in vitro* and *in vivo* for use as drug carriers or as contrast agents for diagnosis purposes (Huang et al., 2015a;

Lu et al., 2009; Palombo et al., 2014). First, NPs can easily penetrate the blood-brain barrier and cytoplasm, and can accumulate in tumors owing to their enhanced permeability and retention effect, as well as their tailored composition (Ferrari, 2005; Murphy et al., 2005; Oberdorster et al., 2004). The high ratio of surface area to volume in the case of NPs permits a high loading of therapeutic agents and drug molecules within a single carrier particle (Mahapatro and Singh, 2011; Tosi et al., 2013). Moreover, the fine-tuned composition of NPs can increase their half-life in the blood circulation (Kamaly et al., 2012; Zhang and Saltzman, 2013). Also, the use of NPs can minimize the adverse effects of drugs by preventing nonspecific uptake in tissue (De Jong and Borm, 2008; Kim et al., 2010; Zapol and Curtiss, 2007). Second, in cancer imaging, NPs are used to amplify detection in diagnostic tests (Castro-Sesquen et al., 2014; Nie et al., 2007). Super paramagnetic iron oxide nanoparticles are used in cancer imaging owing to a difference in the frequency of the protons, and a contrast is observed between tissues using super paramagnetic iron oxide nanoparticles (Alwi et al., 2012; Harisinghani et al., 2003).

For application in biomedical fields, a colloidal form of AuNPs dispersed in a liquid medium is prepared through the reduction of gold salts in the presence of stabilizing agents like sodium citrate and chitosan to prevent agglomeration and to control growth (Daniel and Astruc, 2004; Turkevich et al., 1951). Sodium citrate (Figure 1A) is both reducing agent and stabilizer to provide long-term stability and to control the size of AuNPs (Kumar et al., 2007). In addition, chitosan (Figure 1B) as reducing and stabilizing agent has biocompatible and biodegradable characteristics. Moreover, AuNPs stabilized

with chitosan will not introduce toxicity and biological hazard to environment (Huang and Yang, 2004). The colloid AuNPs, together with the stabilizing agent, allow AuNPs to be functionalized easily by means of polymer linkers on their surfaces (Delong et al., 2010; Sharma et al., 2009; Uehara, 2010). The uses of functionalized AuNPs include single-molecule targeting, sensing, drug delivery, and diagnostics (Boisselier and Astruc, 2009; Ghosh et al., 2008a; Ghosh et al., 2008b; Levy et al., 2010). In addition, functionalized AuNPs can be engineered to accumulate in tumor cells using targeting ligands, thus providing a tool for cancer diagnosis and gene therapy (Ghosh et al., 2008a; Kodiha et al., 2015; Levy et al., 2010). Also, the optical properties of AuNPs, such as strong elastic light scattering, can be applied in photothermal therapy for cancer (Alkilany and Murphy, 2010; Dembereldorj et al., 2014).

Furthermore, AuNPs are used in genomic detections without polymerase chain reaction (PCR) amplification, a method that has been approved by the FDA for genetic screening (Bakthavathsalam et al., 2012; Nam et al., 2003; Su et al., 2015). The citrate-AuNPs directly detect deletion mutation in exon 19 and L858R point mutation in exon 21 of epidermal growth factor receptor in non-amplified genomic deoxyribonucleic acids (Lee et al., 2010). This colorimetric method using AuNPs has advantages due to its high speed and low cost. AuNPs-DNA biosensors also detect non-PCR amplified genomic *Salmonella enterica serovar Enteritidis* (*S. enterica ser. Enteritidis*) DNA (Vetrone et al., 2012).

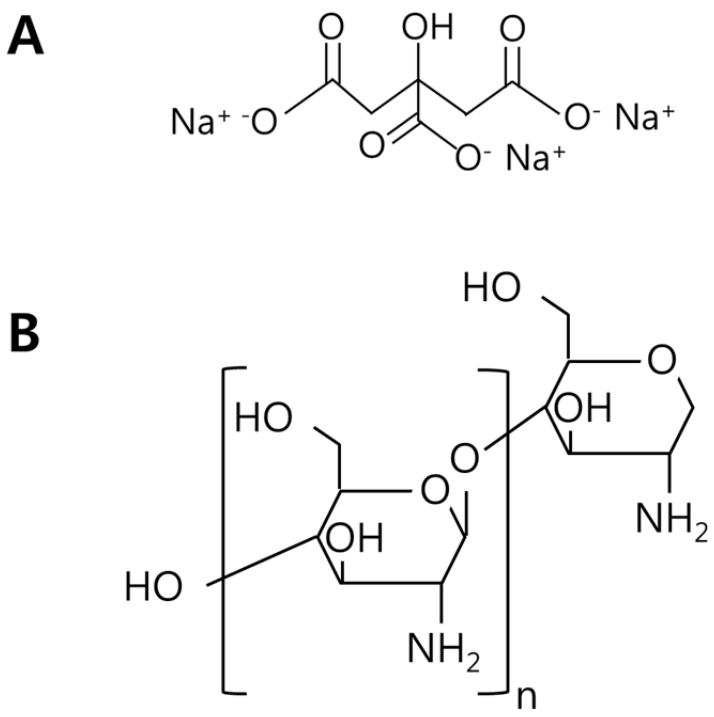

FIGURE 1. Molecular formulas of sodium citrate and chitosan. (A) sodium citrate (B) chitosan. The formulas were quoted from Sigma-aldrich (St. Louis, USA).

Toxicity of gold nanoparticles in cells

Although the investigation of NPs has become more extensive in the biomedical field, the impact of NPs on human health remains unclear (Bouwmeester et al., 2009; Lan and Yang, 2012; Maynard et al., 2006; Nel et al., 2006). An increasing number of scientific reports suggest that nanomaterial has a toxic effect on cell viability (Hussain et al., 2005; Karlsson et al., 2009; Sohaebuddin et al., 2010). The metal oxide particles show toxicity in human lung cancer cells (Karlsson et al., 2009; Sahu et al., 2013; Yildirimer et al., 2011), and NPs such as titanium dioxide (TiO_2) and silver reduce rat liver cell viability (Hussain et al., 2005; Kawata et al., 2009; Shi et al., 2013).

According to several recent studies, AuNPs known to be non-toxic have a cytotoxic effect on cell viability depending on the size, shape, and type of cell (Khlebtsov and Dykman, 2011; Uboldi et al., 2009; Yah, 2013). For example, a cetyl trimethylammonium bromide-AuNPs have a toxic effect depending on the shape and size of the AuNPs in mammalian cells (Chithrani et al., 2006). AuNPs with a diameter of 15 nm are not toxic, but AuNPs of 1.2 nm in diameter induce apoptosis in human prostate cancer cells (Pan et al., 2007). Also, AuNPs with a diameter of 1.9 nm have less toxicity in normal cells but significant cytotoxicity in radiated cells (Coulter et al., 2012). In addition, AuNPs have little toxicity depending on type of stabilizer such as starch and Gum Arabic, and have a non-toxic for sodium citrate and chitosan (Jena et al., 2012; Pokharkar et al., 2009; Vijayakumar and Ganesan, 2012). Moreover, AuNPs decrease cell viability depending on the surface charge (Arnida et al.,

2010; Schaeublin et al., 2011). Negatively or positively charged AuNPs trigger mitochondrial in human keratinocyte cells, but neutral AuNPs do not (Schaeublin et al., 2011). Also, the surface charge of AuNPs influences toxicity and the distribution of AuNPs in organ (Hirn et al., 2011; Khlebtsov and Dykman, 2011).

Recently, several studies have suggested that the exposure of NPs alters the microRNAs expression profiles relating to disease in cells (Bollati et al., 2010; Bourdon et al., 2012; Burklew et al., 2012; Frazier et al., 2014). Metal-rich particles, for example, modify the expression of miR-222, 21, and 146, which relate to inflammations in peripheral blood leukocytes (Bollati et al., 2010), while the inhalation of diesel particles disrupts the expression of microRNAs that is linked to tumorigenesis-associated pathways in human airway cells (Jardim et al., 2009). Further examples are carbon black NPs, which change the expression of the microRNAs (miR-135b) relating to disease in mouse lung (Bourdon et al., 2012), and TiO_2 NPs, which affect the cell growth and microRNA expression of tobacco (Burklew et al., 2012).

Tissue regeneration using gold nanoparticles

Mesenchymal stem cells (MSCs) are considered a useful strategy in regenerative medicine because of their many properties including self-renewal and multipotency (Pittenger et al., 1999; Ren et al., 2012; Vemuri et al., 2011). MSCs are obtained from bone marrow, adipose tissue, and umbilical cord blood, and they are capable of differentiation into specific cell fates, such as

osteoblasts, adipocytes, and chondrocytes, depending on their induction (Halleux et al., 2001; Kern et al., 2006; Pittenger et al., 1999). In particular, stem cells isolated from the adipose tissue, called adipose-derived stem cells, have great potential due to less expensive acquisition and greater available quantities than bone marrow (Toupadakis et al., 2010; Wagner et al., 2005).

In tissue engineering, various types of nanomaterial have recently been estimated as tools to control the specific differentiation of MSCs (Heymer et al., 2008; Kim et al., 2013; Ricles et al., 2011; Spadaccio et al., 2009). Biodegradable and biocompatible NPs with the ability to target stem cells and release their pay-load into the cytoplasm activate signaling cascades (Ilie et al., 2012). Human MSCs show chondrocyte-like phenotypes when placed in a culture together with poly-L-lactic acid loaded with hydroxyapatite scaffold (Spadaccio et al., 2009). The multiwall carbon nanotubes (MWCNT) induce the adipogenic differentiation of mouse myoblastic cells (C2C12 cells) through lipid accumulation in the cytoplasm (Tsukahara and Haniu, 2011), and graphene oxides accelerate the differentiation of MSCs toward adipogenic differentiation (Lee et al., 2011). The poly-L-ornithine-CNTs and poly(methacrylic acid)-grafted CNTs promote the differentiation of human embryonic stem cells into neurons (Chao et al., 2009; Chao et al., 2010). Moreover, TiO_2 and polyethylene glycol-MWCNT support the osteogenic differentiation of MSCs (Nayak et al., 2010; Park et al., 2009).

Recently, AuNPs have been reported to be an osteogenic inducing agent for bone tissue regeneration and also a suitable material for tissue engineering because of their non-toxic characteristics (Shevach et al., 2014; Zhang et al.,

2008a). The AuNP-decellularized matrix hybrids promote the contraction forces of cardiac cells during culture (Shevach et al., 2014). In particular, the citrate-AuNPs stimulate the osteogenic differentiation of bone marrow-derived mesenchymal stem cells through the mitogen-activated protein kinase signaling pathway (Yi et al., 2010). Also, AuNPs with a diameter of both 20 and 40 nm lead to an increase in the osteogenic differentiation rate of the primary mouse osteoblast (Zhang et al., 2014).

Hypothesis and purpose

Several reports suggest that AuNPs can be applied as therapeutic tools in the biomedical fields, such as delivery of drugs and genes into tumor cells. Moreover, many reports in regenerative medicine show that NPs stimulate the differentiation of hMSCs toward a specific lineage including osteoblasts, adipocytes, chondrocytes, and neurons.

Although NPs stimulate the regeneration of damaged tissue, NPs, including AuNPs, also have negative effects on cells such as cell growth inhibition and cell death through apoptosis or necrosis. Thus, it is important that the toxicity of NPs is evaluated prior to applying NPs to tissue regeneration. In view of the positive and negative effects of NPs, I hypothesized that negatively or positively charged AuNPs through stabilizing with citrate and chitosan have toxic effects on cell viability and positively charged AuNPs stabilized with chitosan can promote osteogenic differentiation of hMSCs at the concentration that does not decrease cell viability. Accordingly, the research regarding the

cytotoxic effect of AuNP stabilized with citrate and chitosan in concentration-dependent manner was measured (Chapter I and II), as was the change in the expression profile of microRNAs by comparing the expression of microRNAs in non-treated cells and in AuNP stabilized with citrate- and chitosan-treated cells (Chapter III). The promoting effect of chitosan-AuNPs on the osteogenic differentiaton of MSCs (Chapter IV) was also investigated.

CHAPTER I

In vitro toxicity of citrate-gold nanoparticles in human lung adenocarcinoma cells

ABSTRACT

Gold nanoparticles (AuNPs) have a potential cytotoxic effect on cells. In the present study, the cytotoxicity effect of citrate-AuNPs in the human lung carcinoma (A549) cells was examined. Negatively charged citrate-AuNPs were prepared by chemical reduction using citrate. To investigate the uptake of citrate-AuNPs in cells, transmission electron microscopy was perfomed. Also, both methylthiazol tetrazolium and lactate dehydrogenase assays revealed that the citrate-AuNPs were toxic, as determined by their half-maximal inhibitory concentration. A flow cytometric and real-time RT-PCR analysis of apoptotic genes suggested that citrate-AuNPs induce cell damages through extrinsic and intrinsic apoptotic pathways.

These results demonstrate that citrate-AuNPs decrease cell viability and increase the expression of the marker genes related to apoptosis. Therefore, the cytotoxic effect of citrate-AuNPs should be considered in nano-biotechnology applications.

INTRODUCTION

Numerous studies show that nanoparticles (NPs) are efficient to drug, protein and gene delivery for cancer therapies (Duchesne et al., 2008; Sperling et al., 2008). In addition, gold nanoparticles (AuNPs) have been studied because of size- and shape-dependent physiochemical properties which are applied to biomedicine (Daniel and Astruc, 2004; Sardar et al., 2009). The synthesis of AuNPs base on the single phase aqueous reduction of tetracholoauric acid by sodium citrate still remains the most commonly aqueous method possible to control the size of AuNPs by simple reaction conditions (Bastus et al., 2011). Some report shows the biocompatibility, uptake, and subcellular distribution of citrate-AuNPs in biological applications (Patra et al., 2007).

Despite the increasing interest of NPs in biomedical applications, there has been a growing concern of the potential risks and adverse effects of NPs on living systems (Haynes, 2010). Among various types of NPs, silver nanoparticles using in antimicrobial process induce toxic effects to plant through reactive oxygen species (ROS) production (Panda et al., 2011). In addition, exposure of silver nanoparticles causes impairment of mitochondrial function of rat liver cells (Teodoro et al., 2011). Thus, to develop successful biomedical applications for nano-biotechnology, an understanding of the cytotoxic effects of NPs (Vamanu et al., 2008) should be essential.

Recently, the cytotoxicity of AuNPs toward alveolar type II cell lines was reported (Uboldi et al., 2009). Moreover, the surface charge of AuNPs was

found to modulate the membrane potential of different cell types and subsequent downstream intracellular events (Arvizo et al., 2010).

However, the report regarding the mechanism of toxicity induced by negatively charged AuNPs stabilized with citrate in human lung adenocarcinoma cells has not been reported in details. Therefore, in order to investigate the effect of negatively charged citrate-AuNPs on cell viability, *in vitro* cytotoxicity and apoptosis induced by citrate-AuNPs were studied using cell viability assay, flow cytometric and mRNA expression analysis.

MATERIALS AND METHODS

Preparation of AuNPs

Citrate-AuNPs were provided by Dr. Sang-woo Joo (Soongsil University). Colloidal dispersions of negatively charged AuNPs were prepared using the citrate reduction method (Lee and Meisel, 1982). Transmission electron microscropy (TEM) was used to observe the morphology of the AuNP aggregates. Quantum electronics and laser science and zeta potential measurements monitored the hydrodynamic radius and surface potential of the particles, respectively, with a Malvern Nano-ZS instrument and an Ostuka ELS Z2 analyser. The percentage of Au in the NP solutions was measured using the Perkin-Elmer OPTIMA 4300DV ICP-AES. The shape of citrate-AuNPs was nearly spherical, and the average diameters of citrate-AuNPs were 17.0 ± 1.7 nm. The zeta potentials of citrate-AuNPs were measured to be -37.5 ± 6.3 mV. The hydrodynamic diameters of citrate-AuNPs were 36.0 ± 1.7 nm from dynamic light scattering measurements.

Cell culture

Human lung carcinoma cells (A549; ATCC CCL-185, NCI-H1975; ATCC CRL-5908) and human epidermoid carcinoma cells (A431; ATCC CRL-2592) were cultured in RPMI 1640 medium, supplemented with 10% fetal bovine serum (FBS) and antibiotics at 37°C in a 5% CO_2 incubator. For the methylthiazol tetrazolium (MTT) and lactate dehydrogenase (LDH) assays, the cells were

seeded in 96-well plates at a concentration of 1×10^4 cells/well. They were cultured for one day (90% confluence) before the assays. RPMI 1640 and FBS were obtained from WelGene (Daegu, Korea). Antibiotics (antibiotic-antimycotic stabilized solution), MTT, and dimethyl sulfoxide (DMSO) were purchased from Sigma-Aldrich (St. Louis, USA). Lactate, 2-*p*-iodophenyl-3-*p*-nitrophenyl tetrazolium chloride, phenazine methosulfate, and 1.3 mM nicotineamide adenine dinucleotide used to examine LDH leakage was purchased from Sigma-Aldrich (St. Louis, USA). Karnovsky's fixative, 0.05 M sodium carcodylated buffer, 1% osmium tetroxide, 0.5% uranyl acetate, propylene oxide, and Spurr's resin were obtained from the National Instrumentation Center for Environmental Management (NICEM) at Seoul National University, Korea. For the cell cycle analysis, propidium iodide (PI) and RNase A were purchased from Sigma-Aldrich (St. Louis, USA) and Amresco (OH, USA), respectively. For the annexin V/PI double staining, a fluorescein isothiocynate annexin V apoptosis detection kit was purchased from BD science (CA, USA). Finally, M-MLV for reverse transcription and GoTaq were purchased from Invitrogen (NY, USA) and Promega (WI, USA), respectively.

TEM

The uptake of citrate-AuNPs was also examined using transmission electron microscopy (TEM). Before exposure to the citrate-AuNPs, the A549 cells were plated at a concentration of 1×10^6 cells per dish on a 100-mm culture dish

(SPL, Korea) containing growth medium. The citrate-AuNPs were then added, and the cells were incubated at 37°C with 5% CO_2. After 24 h, the cells were washed twice with dulbecco's phosphate buffered saline (DPBS), fixed with Karnovsky's fixative for 24 h, and post-fixed with 0.5 M osmium tetroxide. After fixation, the specimens were rinsed and dehydrated in a graded series of 30%, 50%, 70%, 80%, and 90% ethanol and treated three times with 100% ethanol for 15 min each. The samples were then embedded in a mixture of resin in propylene oxide polymerized at 80°C. Ultrathin sections for TEM were prepared using a diamond knife and the samples were analyzed using a transmission electron microscope. Raman spectra were obtained using a Raman confocal system model 1000 spectrometer (Renishaw, United Kingdom) equipped with an integral microscope (Leica DM LM, Germany).

ICP-MS measurements

The relative uptake amounts for citrate-AuNPs were determined by inductively coupled plasma-mass spectrometry (ICP-MS). A549 cells were plated at a concentration of 1×10^6 cells per dish on a 100 mm cell culture dish (SPL, Korea) containing growth medium. Citrate-AuNPs were added and the cells were incubated at 37°C with 5% CO_2. After 24 h, the cells were harvested and washed with DPBS. After DPBS was removed, the cell pellet was stored at -20°C. The samples were analyzed using a Varian inductively coupled plasma-mass spectrometer.

MTT and LDH release assay

Cell viability was assessed using the MTT assay. Briefly, the culture medium was removed, and 0.5 mg/mL of MTT solution was added. The 96-well plates were then incubated at 37°C for 4 h to allow for the formation of MTT formazan. The MTT solution was replaced with 200 μL of DMSO to dissolve the formazan crystals, and the optical density (OD) at 570 nm was determined using a microplate analyzer (Bio-Rad, CA, USA). The results were presented as a percentage of the control values.

LDH release from damaged cells was measured using a colorimetric assay that quantitatively measures LDH, a stable cytosolic enzyme that is released upon cell lysis (Mitchell et al., 1980).The released LDH in culture supernatants is measured with a 30-min coupled enzymatic assay resulting in the conversion of a tetrazolium salt into a red formazan product. The intensity of the color produced is proportional to the number of lysed cells. Twenty-four hours after seeding, the cells were treated with the citrate-AuNPs at different concentrations and incubated for another 24 h. Then, 50 μL of cell culture medium was collected from each well and plated on a new microtiter plate. Next, 50 μL of substrate mixture (54 mM L(+) lactate, 0.66 mM 2-*p*-iodophenyl-3-*p*-nitrophenyl tetrazolium chloride, 0.28 mM phenazine methosulfate, and 1.3 mM nicotinamide adenine dinucleotide in 0.2 M Tris buffer, pH 8.2) was added to the wells, and the plates were incubated for 30 min at room temperature. The OD at 490 nm was measured with a standard microplate reader. Each experiment was performed in triplicate. The LDH

release (%) relative to the control wells containing cells ~~culture medium~~ without NPs, was calculated as ((sample OD – control OD)/(maximum OD-control OD)) × 100, where sample OD was the absorbance of the citrate-AuNPs treated cells and control OD was the absorbance of the untreated control cells. Maximum OD was the absorbance of the lysed cells with triton-x.

Analysis of cell cycle by flow cytometry

For cell cycle analysis, cellular DNA was stained with PI, then fluorescence was measured using flow cytometry. Approximately 10^5 A549 cells were placed in six-well culture plates (SPL, Korea). The cells treated with citrate-AuNPs for 24 h were washed in 1 × trypsinized DPBS. The pellet was washed in DPBS, fixed in ice-cold ethanol (70%), and stored at –20°C. Before flow cytometric analysis, the cells were stained with PI in RNase A (40 μg/mL PI and 50 μg/mL RNase A) at 37°C for 40 min. Flow cytometric analysis was performed with FACS Calibur (Becton Dickinson, Canada). Data collected for 10^4 cells were analyzed using WinMDI 2.8 (Scripps Research Institute, USA). Data from raw histograms were extracted using WinMDI 2.8 software and the percentage of cells in each phase of the cell cycle was compared with the number of cells in a control group.

Real-time RT-PCR analysis

cDNA was synthesized using 1 μg of total RNA from cells both treated and not treated with citrate-AuNPs for 24 h by using M-MLV (Invitrogen, NY, USA)

reverse transcriptase and random primers (Promega, WI, USA). Real-time RT-PCR was performed with cDNAs and gene-specific primers mixed with SYBR Green premix (Takara, Japan) by using ABI STEPONE PLUS (Applied Biosystems, USA). The PCR conditions were an initial step at 95°C for 10 sec and 40 denaturation cycles of 95°C for 15 sec and annealing at 60°C for 30 sec. A step at 95°C for 15 sec, 60°C for 1 min, and 95°C for 15 sec was added to minimize nonspecific products. The results were analyzed by comparing the $2^{-[delta][delta]Ct}$ values of the mRNA of cells treated with NPs to those of the control test. Table 1 represents the list of primers used for real-time RT-PCR.

Table 1. Primers for real-time RT-PCR analysis

Gene (Acc. No.)	Sequences	Product size (bp)
bak (NM_001188)	F 5'-ATCCCGTCCTCCACTGAGAC-3' R 5'-AACCTCCTCTGTGTCCTGGG-3'	135
bax (NM_138764)	F 5'-GAGGTCTTTTTCCGAGTGGC-3' R 5'-AGGAAGTCCAATGTCCAGCC-3'	164
caspase-3 (NM_004346)	F 5'-AGGATGGCTCCTGGTTCATC-3' R 5'-CTGTTGCCACCTTTCGGTTA-3'	111
caspase-8 (NM_001228)	F 5'-TTCAGCAAAGGGGAGGAGTT-3' R 5'-TATCCCCGAGGTTTGCTTTT-3'	126
GAPDH (NM_002046.4)	F 5'- CTCTGCTCCTCCTGTTCGAC -3' R 5'- ACGACCAAATCCGTTGACTC-3'	112

Statistical analysis

Each experiment was repeated three times with at least six replicates per experiment. The results were expressed as a percentage of the non-treated cells. This study used a student's *t*-test to analyze the statistical significance of the data. Differences were considered significant when $p < 0.05$. The concentrations in the NP-response (cell viability) curves were analyzed using the Boltzmann function ($Y = 1/1 + \exp(IC_{50} - X/\text{slope factor})$ (Origin 5.0, OriginLab Corporation, USA) where IC_{50} represents a half-maximal inhibitory concentration.

RESULTS

Internalization of negatively charged citrate-AuNPs in A549 cells

The uptake of citrate-AuNPs was examined by TEM experiment added 2.43 μg/mL of citrate-AuNPs. The TEM images of the cells showed that citrate-AuNPs were internalized into the cytosol within 24 h (Figure 1A). According to the TEM images, we observed the citrate-AuNPs into cytosol loaded into several endosomal vesicles as shown in Figure 1B. Also, we measured the amount of citrate-AuNPs taken into the cells using an ICP-MS method. The result showed that the uptake rate of citrate-AuNPs is 2.27% as summarized in Table 2.

Cytotoxicity of negatively charged citrate-AuNPs

The cytotoxicity of citrate-AuNPs was examined by determining their IC_{50} values in a MTT assay, which represented the mitochondrial function in live cells. The relative cytotoxicity (%) was expressed as a percentage of the non-treated cells (100% cell viability). The results of the MTT viability assay showed that citrate-AuNPs were significantly cytotoxic toward the A549, NCI-H1975, and A431 cells that were exposed for 24 h. When the cells were exposed to the citrate-AuNPs for 24 h, their viability was reduced by 47% (A549), 47.7% (NCI-H1975), and 34.8% (A431) at 48.1 μg/mL. In dose-response curve fitting,

Table 2. ICP-MS data for cellular uptake of citrate-AuNPs

Concentration of NPs	ICP-MS	Uptake Rate
36.7 μg	0.834 μg	2.27%

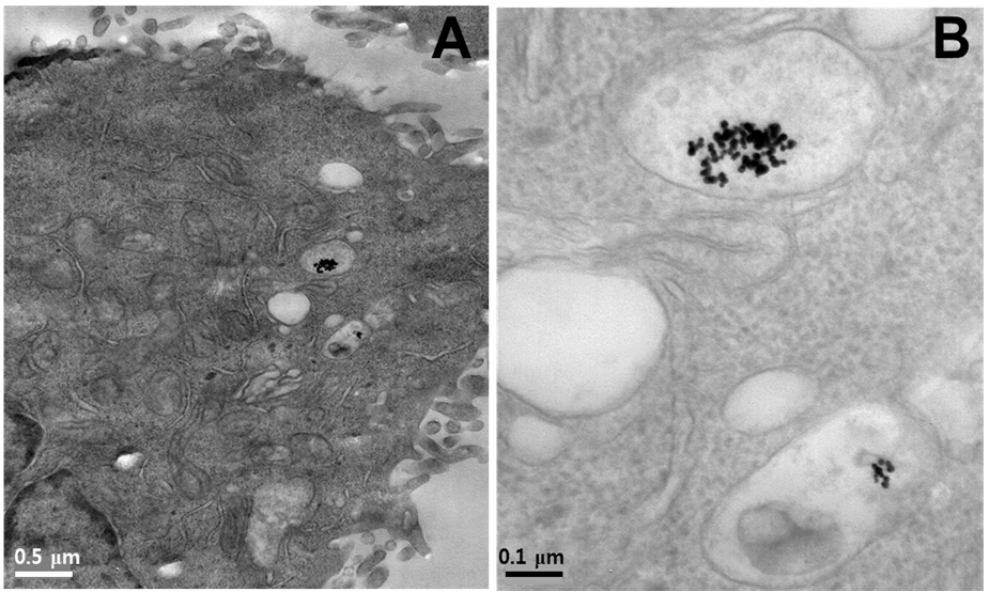

Figure 1. TEM images of cells exposed to citrate-AuNPs. A549 cells were exposed to citrate-AuNPs for 24 h and then fixed for TEM. (A) citrate-AuNPs were internalized in cytosol. (B) citrate-AuNPs were located in endosomal vesicles. Figure B was magnified from figure A. The scale bars represent 0.5 μm (A) and 0.1 μm (B).

IC_{50} values were calculated at 48.94 μg/mL (A549), 52.3 μg/mL (NCI-H1975), and at 65.2 μg/mL (A431), respectively, as shown in Figure 2A. The IC_{50} values were also calculated based on the surface area (mm^2) because when cytotoxicity is determined, the number of citrate-AuNPs in contact with the cell surface could be more important than the fluid (culture media) volume in the petri dish as summarized in Table 3. Although not shown here, the cell viability exposed for 72 h appeared to be not significantly different from that of the cell viability that was exposed for 24 h.

In addition to mitochondrial function, LDH release was measured as another indicator of citrate-AuNP-induced cytotoxicity. LDH release, due to membrane damage, was noted after cells were exposed to citrate-AuNPs for 24 h as shown in Figure 2B. As shown in Figure 2B, LDH release was increased in the A549 (n = 3), NCI-H1975 (n = 9), and A431 cells (n = 4) treated with citrate-AuNPs. As described in the Method section, the relative LDH release (%) was expressed as a percentage of the non-treated cells (0% LDH release).

Cell death mechanisms by negatively charged citrate-AuNPs in A549 cells

To examine citrate-AuNPs-induced cell viability loss, cell cycle analysis was performed after treatment with citrate-AuNPs. As shown in Figure 3, most cell populations of non-treated cells were found to be in the G_1 phase (55.7% ± 1.89) (n = 3). In addition, when treated with 0.3 × IC_{50} of citrate-AuNPs, most cell populations were found to be in the G_1 phase (39.7% ± 6.82) (n = 3).

Table 3. IC_{50} values calculated based on fluid volume and surface area

A549		NCI-H1975		A431	
μg/mL	μg/mm^2	μg/mL	μg/mm^2	μg/mL	μg/mm^2
48.9	0.3	52.3	0.32	65.2	0.4

Figure 2. Cytotoxicity induced by citrate-AuNPs. (A) MTT cell viability assay. A549 (n = 3), NCI-H1975 (n = 8) and A431 cells (n = 6) were exposed to different concentrations of citrate-AuNPs for 24 h. The value of the control (unexposed) cells was taken as 100% and the percentage decrease in the optical density of the citrate-AuNPs-exposed cells was calculated. (B) LDH assay as an index of cytotoxicity. LDH release was measured after 24 h of exposure to citrate-AuNPs. The value of the control (not exposed) cells was taken as 0% and the value of positive control (triton-x exposed) cells was taken as 100%. The percentage increase of the optical density of citrate-AuNPs-exposed cells was then calculated accordingly. The data are expressed as mean ± standard error of three and four independent experiments. *Significant difference ($p < 0.05$) compared to control. Origin version 5.0 software for Windows was used for the statistical analysis.

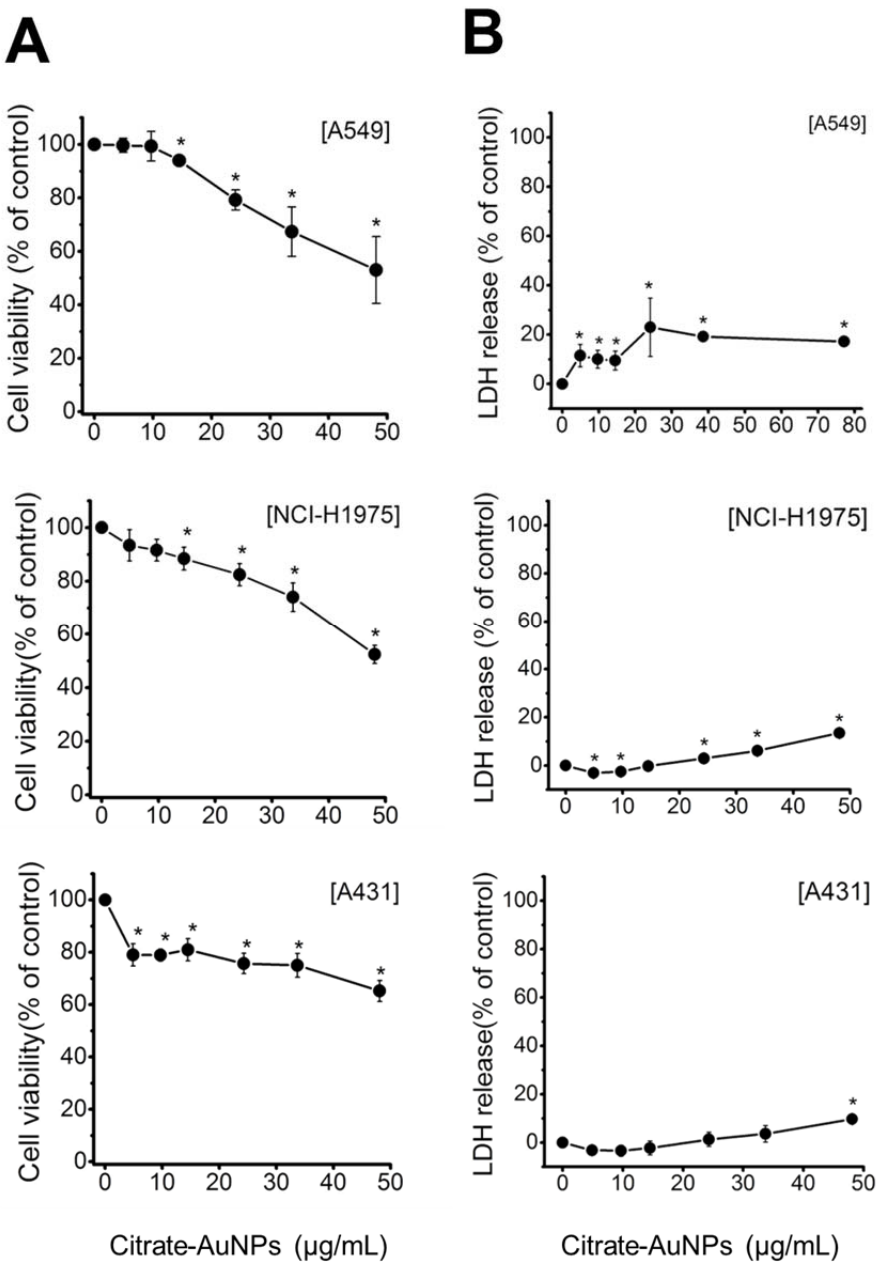
A
B
[A549]
[NCI-H1975]
[A431]
Cell viability (% of control)
Cell viability(% of control)
LDH release (% of control)
LDH release(% of control)
Citrate-AuNPs (μg/mL)
Citrate-AuNPs (μg/mL)

Also, Figure 3 shows that in the citrate-AuNP-treated cells, the sub-G_1 population was significantly larger ($p < 0.05$). The sub-G_1 population in the non-treated cells was 0.66% ± 0.14 (n = 3), while 37.53% ± 6.93 (n = 3) in citrate-AuNP-treated cells. Our flow cytometry results suggest that citrate-AuNPs induced apoptosis since the population of the sub-G1 phase increased, indicating damage to cell proliferation.

We compared the expression levels of the apoptotic genes of bax, bak, caspase-3, and caspase-8 after citrate-AuNPs treatment. As shown in Figure 4, according to the real-time RT-PCR analysis of apoptosis-related genes, citrate-AuNPs induced an increase in the mRNA expression of bax and bak, which are pro-apoptotic members of the Bcl-2 family. Citrate-AuNPs also induced the caspase-8 expression, which is associated with an extrinsic apoptotic pathway. Citrate-AuNPs provoked the expression of caspase-3, which is a common downstream effector of both extrinsic and intrinsic apoptosis pathways. Based on result, citrate-AuNPs also evoked an extrinsic apoptotic pathway in addition to an intrinsic pathway. Therefore, the apoptosis induced by citrate-AuNPs is mediated by both intrinsic and extrinsic pathways as illustrated in Figure 5.

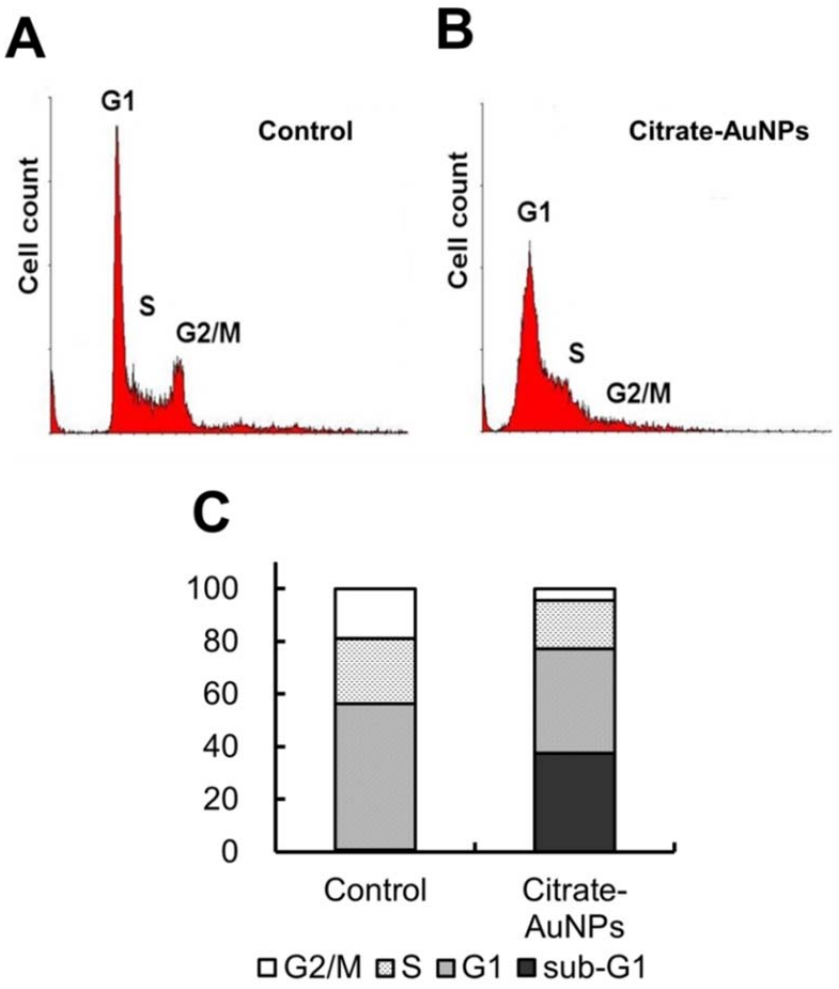

Figure 3. Cell cycle analysis. Cellular DNA was stained with PI, and the fluorescence was then flow cytometrically analyzed. (A) control without treatment ($0.3 \times IC_{50}$) with (B) citrate-AuNPs. Among the citrate-AuNPs treated cells, the number of cells in the sub-G1 phase was increased. The plot (C) was generated by WinMDI 2.8 software.

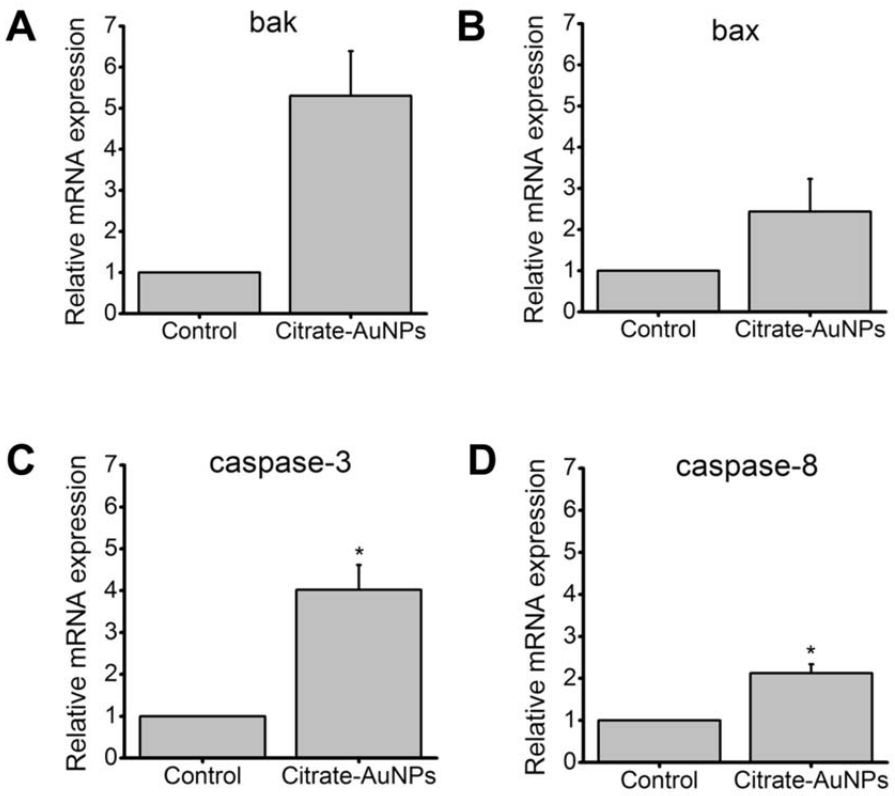

Figure 4. mRNA expression analysis of apoptosis-related genes after cells were treated with a 1 × IC_{50} of citrate-AuNPs. (A) bak (n = 3) (B) bax (n = 5) (C) caspase-3 (n = 3), and (D) caspase-8 (n = 3). *Significant difference ($p < 0.05$) compared to control. Origin version 5.0 software for Windows was used for the statistical analysis.

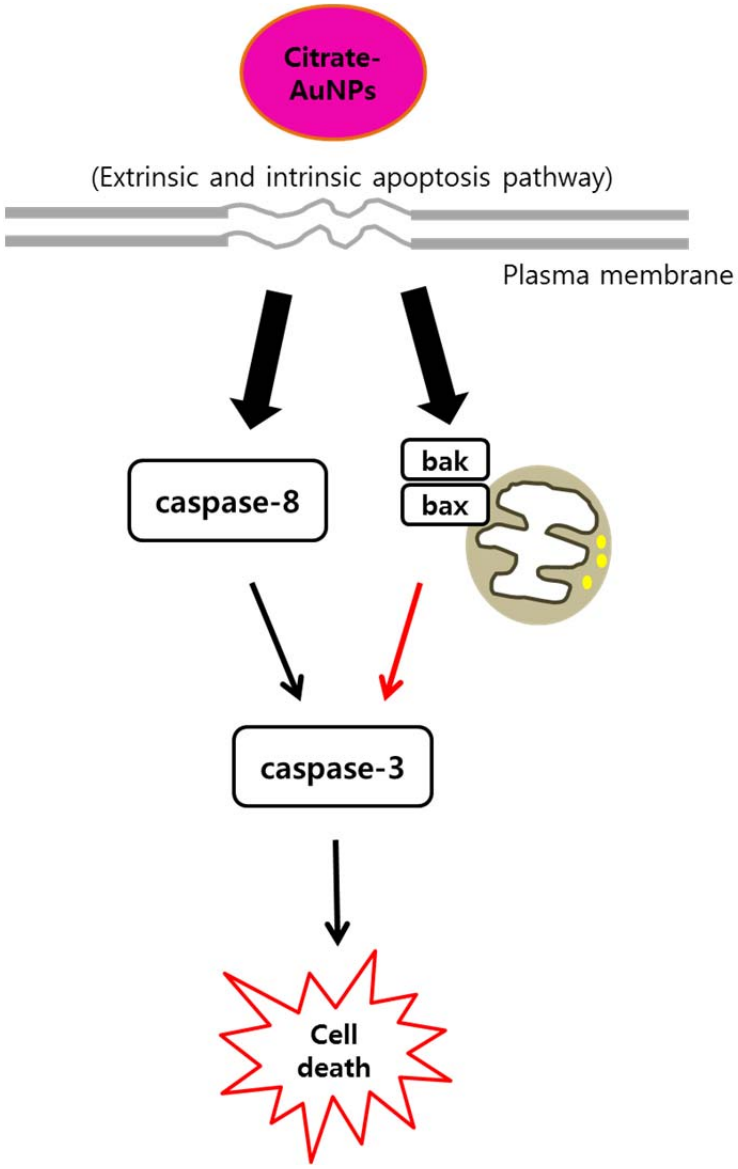

Figure 5. Schemes of cell death induced by negatively charged citrate-AuNPs. Citrate-AuNPs provoke apoptotic pathway. The exposure of citrate-AuNPs on cells induces cell membrane damage. The viability of cells with citrate-AuNPs is decreased through activation of extrinsic and intrinsic apoptosis.

DISCUSSION

In the present study, citrate-AuNPs were internalized into A549 cell. And, viability of A549, NCI-H1975, and A431 cells was reduced by citrate-AuNPs through apoptotic pathway.

Many putative mechanisms may explain the uptake of NP into cells, including phagocytosis, clathrin-mediated endocytosis, caveolae-mediated endocytosis, non-clathrin, and non-caveolae-mediated endocytosis (Unfried et al., 2007). Negatively charged quantum dots enter cells via an endocytosis mediated by a low-density lipoprotein receoptor and G-protein-coupled receptor-associated proteins. Their uptake is not primarily mediated by either clathrin or cavelolae (Zhang and Monteiro-Riviere, 2009). In our result, most of the internalized citrate-AuNPs were observed in membrane-bound vesicles. Uptake of other NPs such as silver induces releasing metal ion in cells, resulting in cytotoxicity (Beer et al., 2012; Kim et al., 2009). However, in case of AuNPs, blockade of vesicular trafficking by AuNPs, not releasing ion, induces cell death (Albanese and Chan, 2011; Brandenberger et al., 2010).

Sodium citrate using in synthesis of AuNPs as a stabilizer has known to be a non-toxic agent (Agawane et al., 2012). In colloidal AuNPs, citrate as a common stabilizer induces negative charge to surface of AuNPs (Darlington et al., 2009). AuNPs with negative charges are appeared to be toxic in macrophages depending on endocytotic pathways (Frohlich, 2012; Yen et al.,

2009). The differences in the sizes and charges of the AuNPs induce different toxic effect on cells (Yen et al., 2009). Moreover, there is different toxicity of the NPs depending on plasma membrane surface charges between J774 A1 macrophages and adenocarcinoma or epithelial carcinoma cells (Clift et al., 2008; Geiser et al., 2005). In this study, negatively charged citrate-AuNPs decrease cell viability of human lung adenocarcinoma cells and epidermoid carcinoma cell.

Numerous reports have proposed a mechanism of NP-induced cytotoxicity (Arora et al., 2008; Cregan et al., 1999; Kang et al., 2010; Khan et al., 2007). Irreversible cell damage may undergo apoptosis and may lead to an increase in the cell population in the sub-G1 phase (Banker et al., 1997; Shen et al., 2008; Wang et al., 2009; Ye et al., 2001). Corresponding with previous studies, most cell populations of citrate-AuNPs-treated cells were found in sub-G1 phase.

Bax and bak, which are pro-apoptotic members of the Bcl-2 family, are responsible for the induction of intrinsic mitochondria apoptosis (Orrenius et al., 2003). Caspase-8 expression is increased in activation of extrinsic apoptotic pathway (Boatright and Salvesen, 2003). The results indicate that extrinsic and intrinsic apoptosis-related genes are increased by citrate-AuNPs.

CHAPTER II

Cellular uptake and cytotoxicity of chitosan-gold nanoparticles in human lung adenocarcinoma cells

ABSTRACT

Gold nanoparticles (AuNPs) stabilized with chitosan were applied as delivery carriers for drug and gene in biomedical fields. However, there are increasing concerns regarding toxicity of AuNPs depending on surface modifications of AuNPs.

Positively charged chitosan-AuNPs were prepared by chemical reduction using chitosan. The cellular uptake, cytotoxicity and mechanisms of cytotoxicity of the positively charged chitosan-gold nanoparticles (AuNPs) were examined in the A549 cells, which comprise one of the most characterized pulmonary cellular systems. The uptake of chitosan-AuNPs into A549 cells was also monitored using transmission electron microscopy. The cytotoxic assay, using both methylthiazol tetrazolium and lactate dehydrogenase assays revealed that positively charged chitosan-AuNPs decreased cell viability. Flow cytometry, DNA fragmentation, real-time RT-PCR, and Western blot analysis suggest that chitosan-AuNPs provoke cell damage through both the apoptotic and necrotic pathways.

INTRODUCTION

Nanoparticles (NPs) conjugated with chitosan have recently gained increased attention for the development of safe and effective drug or gene delivery systems because of their positively charged physicochemical and biocompatible characteristics due to low toxicity (Duceppe and Tabrizian, 2010; Jeong et al., 2011). In particular, chitosan as a stabilizer have a great potential for carrying a functional biopolymer into surface of NPs (Marie et al., 2002). Moreover, the size and shape of gold nanoparticles (AuNPs) are controlled by reduction with chitosan (Huang and Yang, 2004).

Some report suggests that the uptake of positively charged NPs should be higher than that of negatively charged NPs (Gratton et al., 2008). Cationic dendrimers appear to be taken into cells by adsorptive endocytosis through interaction with specific, negatively-charged proteoglycans in the cell membrane (Perumal et al., 2008). The surface charges of the cells and NPs, and the resulting interaction, may play a significant role in the uptake of NPs (Zhang et al., 2008b). In addition, cell membrane potential is also known to be important when determining intracellular uptake of positively charged AuNPs (Arvizo et al., 2010).

To develop safe applications for bio-nanotechnology, a better understanding of the cytotoxic effects of NPs is required (Ahamed et al., 2011; Akhtar et al., 2010; Liu et al., 2010). Furthermore, there has been an increased recognition of the harmful effects of NPs on living systems (Haynes, 2010).

NPs in contact with a biological environment are in a dynamic exchange with biomolecules, such as proteins and lipids (Lynch et al., 2009).

Although positively charged AuNPs were noted as delivery tools for anti-cancer drug and genes, their toxicity and molecular mechanisms of cell death by positively charged AuNPs still remain controversial (Auffan et al., 2009; Nel et al., 2006). In addition, toxicity of AuNPs is depending on their size, concentration, and surface modification (Simpson et al., 2010; Uboldi et al., 2009; Yen et al., 2009).

Lung epithelial cells are one of the most exposed tissues to NPs, and used in earlier cytotoxicological studies of carbon black and silica (Limbach et al., 2007; Rothen-Rutishauser et al., 2006). Thus, in the present study, human lung carcinoma A549 cells were chosen to characterize the potential cytotoxicity of chitosan-AuNPs, The uptake of the chitosan-AuNPs in A549 cells were examined by transmission electron microscopy (TEM). Furthermore, the molecular cell death mechanisms mediating the cytotoxicity induced by the positively charged chitosan-AuNPs were investigated.

MATERIALS AND METHODS

Preparation of AuNPs

Chitosan-AuNPs were provided by Sang-woo Joo (Soongsil University). Colloidal dispersions of positively charged chitosan-AuNPs were prepared using the chitosan reduction method (Wei and Qian, 2008). TEM was used to observe the morphology of the chitosan-AuNP aggregates. Quantum electronics and laser science and zeta potential measurements monitored the hydrodynamic radius and surface potential of the particles, respectively, with a Malvern Nano-ZS instrument and an Ostuka ELS Z2 analyser. The percentage of Au in the NP solutions was measured using the Perkin-Elmer OPTIMA 4300DV ICP-AES. The average diameters of chitosan-AuNPs were 16.9 ± 2.6 nm. The zeta potentials of chitosan-AuNPs were measured to be +41.5 ± 5.7 mV. The hydrodynamic diameters of chitosan-AuNPs appeared to be 39.8 ± 5.7 nm from dynamic light scattering measurements.

Cell culture

A549 human lung carcinoma cells (ATCC CCL-185), NCI-H460 (ATCC HTB-177) and A431 (ATCC CRL-2592) were cultured in RPMI 1640 medium (WelGene, Daegu, Korea) containing 10% inactivated fetal bovine serum (FBS) (WelGene, Daegu, Korea) and 1% antibiotics (Antibiotic-antimycotic solution, Sigma-Aldirch, St. Louis, USA) at 37°C in a 5% CO_2 incubator.

TEM

The uptake of chitosan-AuNPs was examined by using transmission electron microscopy (TEM). The A549 cells were plated into a 100 mm culture dish (SPL, Korea) at 1×10^6 cells per dish containing growth medium and incubated at 37°C. The chitosan-AuNPs were then added, and the cells were incubated at 37°C with 5% CO_2. After 24 h, the cells were washed with dulbecco's phosphate buffered saline (DPBS) and fixed with Karnovsky's fixative (Choi et al., 2012). After fixation, the specimens were dehydrated in a graded series of ethanols. The samples were then embedded in a mixture of resin at 80°C. Ultrathin sections were prepared for TEM by using a diamond knife, and the samples were analyzed using a transmission electron microscope. Karnovsky's fixative, 0.05 M sodium carcodylated buffer, 1% osmium tetroxide, 0.5% uranyl acetate, propylene oxide, and Spurr's resin were obtained from the National Instrumentation Center for Environmental Management (NICEM) at Seoul National University, Korea.

ICP-MS measurements

The relative uptake amounts for chitosan-AuNPs were determined by inductively coupled plasma-mass spectrometry (ICP-MS) (Choi et al., 2012). A549 cells were seeded at a concentration of 1×10^6 cells per dish on a 100 mm cell culture dish (SPL, Korea) containing growth medium. Chitosan-AuNPs were added and the cells were incubated at 37°C with 5% CO_2. After 24 h, the cells were harvested and washed with DPBS. The samples were analyzed using

a Varian ICP-MS.

MTT and LDH release assay

For the methylthiazol tetrazolium (MTT) and lactate dehydrogenase (LDH) assays, the cells were seeded in 96-well plates at a concentration of 1×10^4 cells per well. Cell viability was measured using MTT assay. Briefly, 0.5 mg/mL of thiazolyl blue tetrazolium (MTT, Sigma-Aldrich, St. Louis, USA) solution was added to the cells. The MTT formazan was dissolved with dimethyl sulfoxide (DMSO) (Sigma-Aldrich, St. Louis, USA) and the optical density (OD) at 570 nm was determined using a microplate analyzer (Bio-Rad, CA, USA). The results were presented as a percentage of the control values.

LDH release was measured by means of a colorimetric assay that quantitatively measures LDH, a stable cytosolic enzyme that is released upon cell lysis (Mitchell et al., 1980). The released LDH in culture supernatants is measured with a 30 min enzymatic assay. The cells were treated with the chitosan-AuNPs at different concentrations and incubated for another 24 h. Then, 50 μL of cell culture medium was collected from each well and plated on a new microtiter plate. Next, 50 μL of substrate mixture was added to the wells, and the plates were incubated for 30 min at room temperature. The OD at 490 nm was measured with a standard microplate reader. Each experiment was performed in triplicate. The LDH release (%) relative to the control wells containing cells without NPs, was calculated as ((sample OD – control OD)/(maximum OD-control OD)) × 100, where sample OD was the absorbance

of the citrate-AuNPs treated cells and control OD was the absorbance of the untreated control cells. Maximum OD was the absorbance of the lysed cells with triton-x.

Flow cytometry

Cellular DNA was stained with propidium iodide (PI) for cell cycle analysis (Choi et al., 2012). Approximately 1×10^6 A549 cells were plated in 100 mm cell culture dish (SPL, Korea). The medium was harvested following a 24 h treatment with chitosan-AuNPs. The cells were washed in 1× trypsinized DPBS, collected in the stored medium, and centrifuged. The pellet was washed in DPBS, fixed in ice-cold ethanol (70%), and stored at –20°C. Prior to flow cytometric analysis, the cells stained with PI in RNase A (40 μg/mL PI and 50 μg/mL RNase A) and incubated at 37°C for 40 min, followed by incubation at 4°C until analysis. Flow cytometric analysis was performed with FACS Calibur (Becton Dickinson, Canada). Data were analyzed using WinMDI 2.8 (Scripps Research Institute, USA).

Apoptosis analysis by double-staining annexin V-PI method

A549 cells were plated in 100 mm cell culture dish at a density of 1×10^6 cells per dish in RPMI1640 medium with 10% FBS and 1% antibiotics. Chitosan-AuNPs were added and the cells were incubated at 37°C with 5% CO_2. After 24 h, the cells were harvested and washed twice with cold DPBS and then resuspended in 400 μL of 1 × binding buffer (Choi et al., 2012). Next, 100 μL

of the solution was transferred to a 5 mL culture tube. After adding 1 μL of fluorescein isothiocyanate (FITC) annexin V and 1 μL PI to the solution, the cells were incubated for 15 min at room temperature in the dark. Next, 400 μL of 1 × binding buffer was added to each tube and analyzed by flow cytometry within 1 h. Apoptotic cells and necrotic cells were calculated by Cell Quest software (BD Biosciences, CA, USA). For the annexin V/PI double staining, a FITC annexin V apoptosis detection kit was purchased from BD.

DNA fragmentation assay

A549 cells treated with chitosan-AuNPs were scrapped with genomic extraction buffer (0.1 M NaCl, 0.01 M EDTA, 0.3 M Tris-HCl, 0.2 M sucrose) and the cells were spun down. The supernatant was incubated with 5 M potassium acetate on ice. Tris-EDTA buffer and RNase A (10 mg/ml) were added, and then DNA was extracted with phenol-chloroform. After electrophoresis on a 1.5% agarose gel, DNA fragmentation was visualized with ethidium bromide staining.

Real-time RT-PCR analysis

cDNA was synthesized using total RNA (1 μg) from cells both treated and not treated with NPs for 24 h. Real-time RT-PCR was performed using cDNAs and gene-specific primers mixed with SYBR Green premix (Takara, Japan) by using ABI STEPONE PLUS (Applied Biosystems, USA) (Choi et al, 2012). The PCR conditions were an initial step at 95°C for 10 sec and 40 denaturation cycles of 95°C for 15 sec and annealing at 60°C for 30 sec. Steps at 95°C for 15 sec,

60°C for 1 min, and 95°C for 15 sec was added to minimize nonspecific products. The results were analyzed by comparing the $2^{-[delta][delta]Ct}$ values of the mRNA of cells treated with NPs to those of the control test. Table 1 represents the list of primers used for real-time RT-PCR.

Table 1. Primers for real-time RT-PCR analysis

Gene (Acc. No.)	Sequences	Product size (bp)
bak (NM_001188)	F 5'-ATCCCGTCCTCCACTGAGAC-3' R 5'-AACCTCCTCTGTGTCCTGGG-3'	135
bax (NM_138764)	F 5'-GAGGTCTTTTTCCGAGTGGC-3' R 5'-AGGAAGTCCAATGTCCAGCC-3'	164
caspase-3 (NM_004346)	F 5'-AGGATGGCTCCTGGTTCATC-3' R 5'-CTGTTGCCACCTTTCGGTTA-3'	111
caspase-8 (NM_001228)	F 5'-TTCAGCAAAGGGGAGGAGTT-3' R 5'-TATCCCCGAGGTTTGCTTTT-3'	126
GAPDH (NM_002046.4)	F 5'- CTCTGCTCCTCCTGTTCGAC -3' R 5'- ACGACCAAATCCGTTGACTC-3'	112

Western blotting assay

A549 cells were treated with different concentrations of chitosan-AuNPs and incubated for 24 h. Both adherent and floating cells were collected, and then the cell pellets were suspended in lysis buffer (Promega, WI, USA) and incubated for 40 min on ice. The protein content of the supernatant was determined using bicinchoninic acid protein assay kit (Thermo Scientific, MA, USA). The protein lysates were separated by electrophoresis in 10% sodium dodecyl sulfate polyacrylamide gel and blotted on a polyvinylidene difluoride membrane. Proteins were detected using anti-caspase-8 monoclonal antibody (Abcam, MA, U.S.A.). The proteins were visualized using anti-rabbit IgG conjugated with peroxidase (GeneDepot, TX, USA).

Statistical analysis

Mann-Whitney tests or Wilcoxon Rank sum tests were used to consider the statistical significance of the data. Origin version 5.0 software for Windows was used for the statistical analysis. Differences were considered significant when $p < 0.05$. A half-maximal inhibitory concentration, IC_{50} values were calculated using the Boltzmann function ($Y = 1/1 + \exp(IC_{50} – X/\text{slope factor})$ (Origin 5.0, OriginLab Corporation, USA).

RESULTS

Uptake of positively charged chitosan-AuNPs in A549 cells

The uptake of chitosan-AuNPs was examined by using TEM. The amount of chitosan-AuNPs added for TEM was 8.04 μg/mL. Most of the internalized chitosan-AuNPs were detected in membrane-bound vesicles as shown in Figure 1A. According to the TEM images, we detected the particles loading into a number of endosomal vesicles, as shown in Figure 1A and Figure 1B. It is also noteworthy that chitosan-AuNPs were found as an aggregated form at the cellular membrane as shown in Figure 1C and Figure 1D. We measured the amount of chitosan-AuNPs taken into the cells using an ICP-MS. The result showed that the uptake rate of positively charged chitosan-AuNPs is 5.40% as demonstrated in Table 2.

Cytotoxicity of positively charged chitosan-AuNPs

MTT and LDH assay were used to study the cytotoxicity of chitosan-AuNPs. The MTT viability assay demonstrated that chitosan-AuNPs were significantly cytotoxic for 24 h. The IC_{50} value of chitosan-AuNPs treatment was 23.0 μg/mL as shown in Figure 2. The IC_{50} values were also derived from the surface area (mm^2) of the petri dish because a number of NPs in contact with the cell surface could be more significant than the fluid (culture media) volume in the petri dish in calculating the IC_{50} value, 0.14 $\mu g/mm^2$. LDH release was also measured as

Table 2. ICP-MS data for cellular uptake of chitosan-AuNPs

Concentration of NPs	ICP-MS	Uptake Rate
11.6 μg	0.623 μg	5.40%

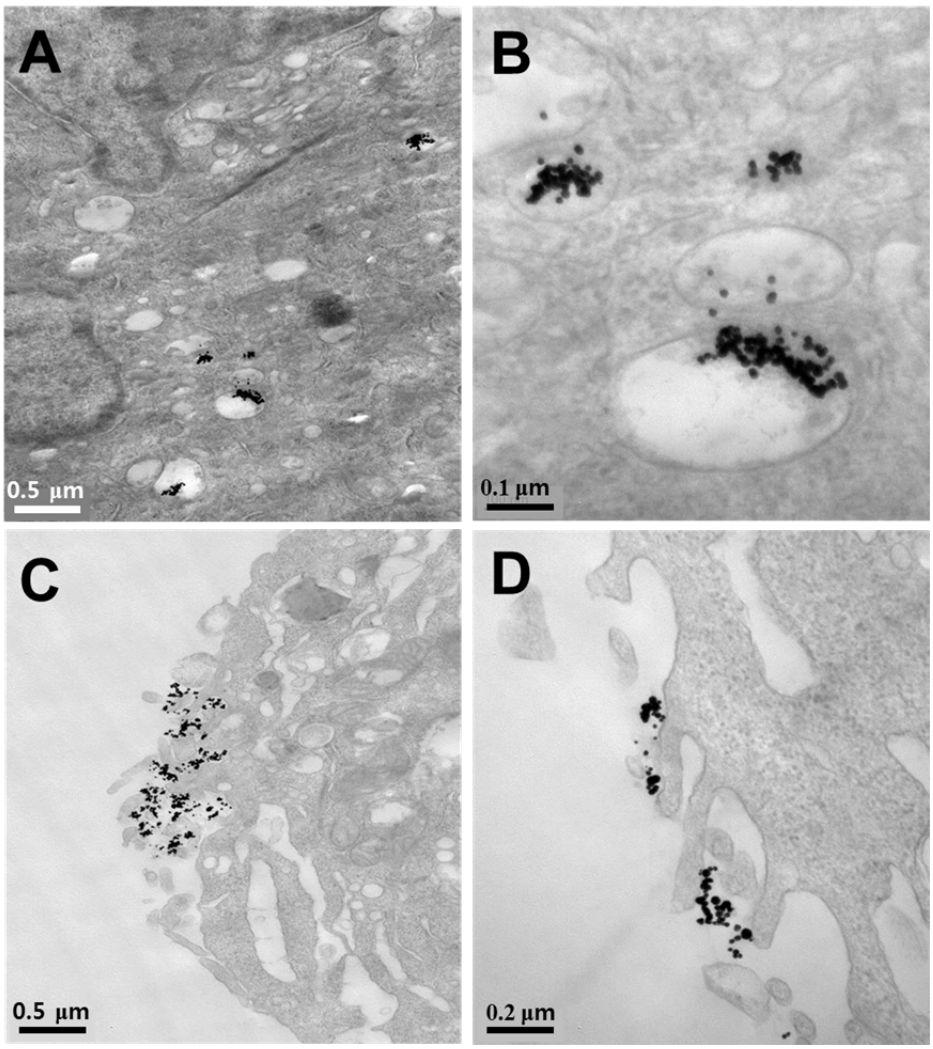

Figure 1. TEM images of cells exposed to chitosan-AuNPs. A549 cells were exposed to chitosan-AuNPs for 24 h and then fixed for TEM. (A), (B) chitosan-AuNPs were internalized in endosomal compartment as magnified in the right image. (C), (D) chitosan-AuNPs found at the membrane indicating the surface change interactions.

another indicator of chitosan-AuNPs-induced cytotoxicity. As shown in Figure 2, LDH release was increased in cells treated with chitosan-AuNPs. We also performed the cytotoxicity assay of chitosan-AuNPs under the conditions of both 10% and 1% FBS media in order to better estimate the role of the serum-coated chitosan-AuNPs using lung cancer cells, A549, NCI-H460, and epidermoid A431 cells (n = 5). As shown in the Figure 3, the toxicity behaviors did not appear much different in the two serum protein conditions ($p > 0.05$).

Cell death mechanisms by positively charged chitosan-AuNPs in A549 cells

In order to identify the specific mechanisms of the cytotoxicity of chitosan-AuNP, cell cycle analysis was carried out after treatment with chitosan-AuNPs and without chitosan-AuNPs treatment. Cells treated with concentrations of 0.1 × IC_{50} (2.54% ± 0.04), 0.2 × IC_{50} (13.13% ± 1.40), 0.3 × IC_{50} (38.27% ± 7.24), and 1 × IC_{50} (21.29% ± 3.58) of the chitosan-AuNPs demonstrated that the sub-G_1 population was increased compared to the control, which suggests that chitosan-AuNPs induce cell death (n = 5) (Figure 4A, B). The result of the DNA fragmentation assay also demonstrated that DNA was fragmented at chitosan-AuNPs concentrations of 0.2 × IC_{50} and 0.3 × IC_{50}, and a spot of low molecular weight DNA, sign of complete DNA degradation, was detected at chitosan-AuNPs concentrations of 0.5 × IC_{50} and 1 × $IC_{50.}$ Hydrogen peroxide (H_2O_2) and sodium selenite were used as positive controls (Figure 4C). Additionally, annexin V/PI double staining results indicate that increasing the concentration

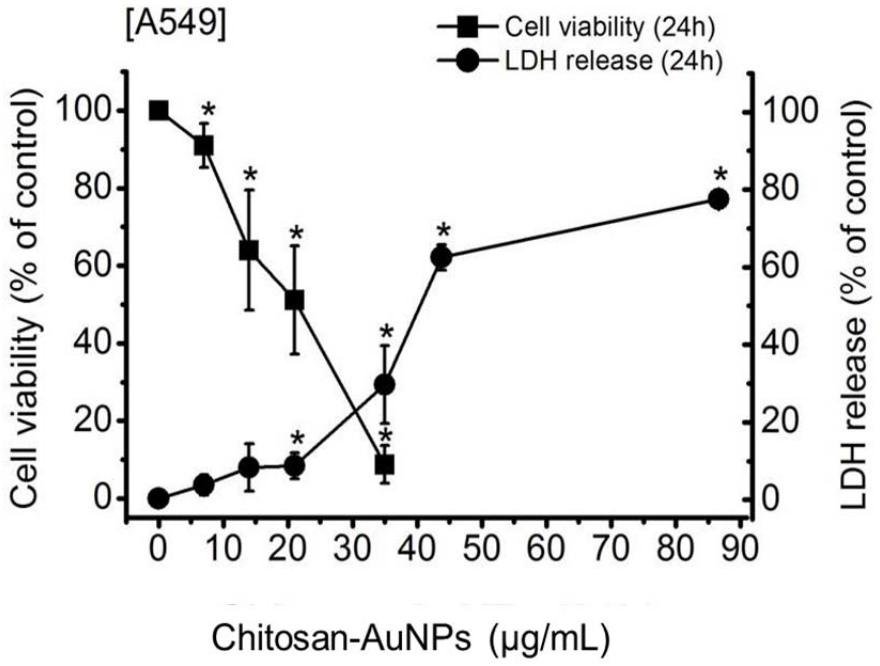

Figure 2. **Cytotoxicity induced by chitosan-AuNPs.** MTT cell viability assay was performed using A549 cells exposed to various concentrations of chitosan-AuNPs for 24 h (n = 5). LDH release was measured after 24 h of exposure to chitosan-AuNPs (n = 3). The Data are expressed as mean ± standard error (SE) of three or four independent experiments. *Significant difference ($p < 0.05$) compared to control (0 μg/ mL).

Figure 3. Cytotoxicity induced by chitosan-AuNPs in A549 (A), NCI-H460 (B), and A431 (C) cells with 1% and 10% FBS. Cytotoxicity was measured using an MTT cell viability assay using cells exposed to a range of concentrations of chitosan-AuNPs for 24 h. The Data are expressed as mean ± SE of three or four independent experiments. *Significant difference ($p < 0.05$) compared to control (0 μg/ mL).

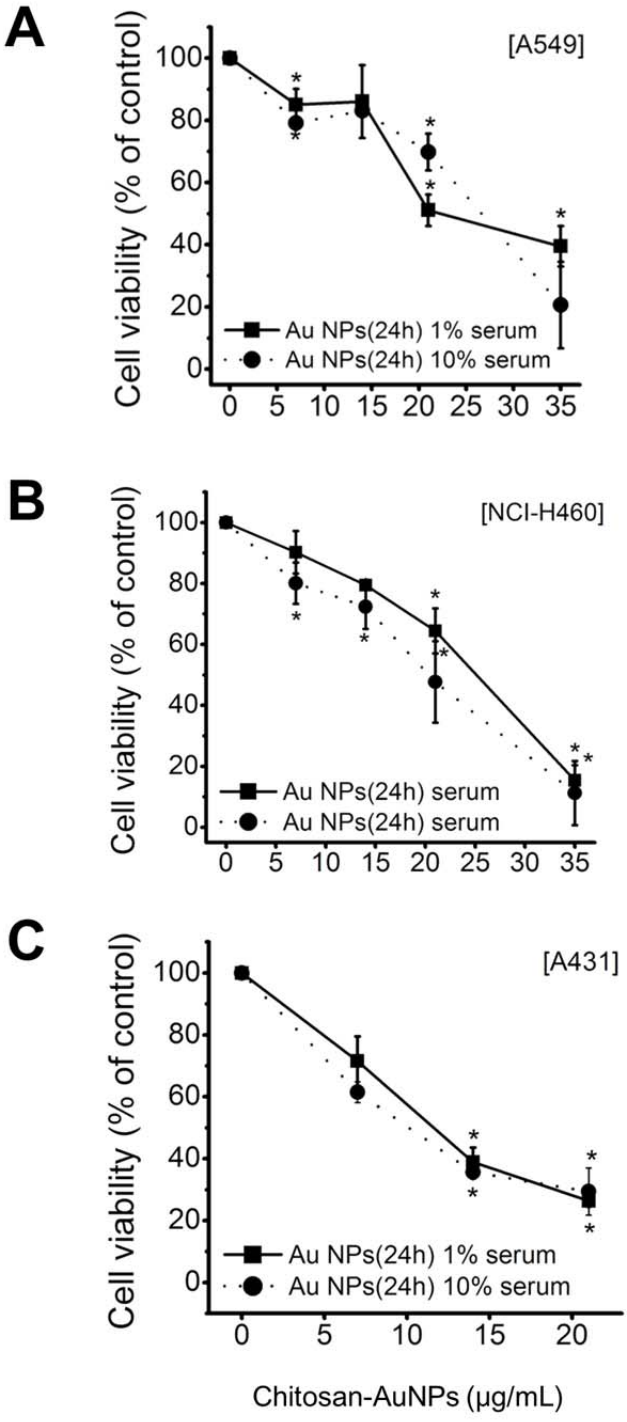
A
[A549]
Cell viability (% of control)
Au NPs(24h) 1% serum
Au NPs(24h) 10% serum
B
[NCI-H460]
Cell viability (% of control)
Au NPs(24h) serum
Au NPs(24h) serum
C
[A431]
Cell viability (% of control)
Au NPs(24h) 1% serum
Au NPs(24h) 10% serum
Chitosan-AuNPs (μg/mL)

of chitosan-AuNPs up to 0.2 × IC_{50}, 0.3 × IC_{50}, 0.5 × IC_{50}, and 1 × IC_{50} activated apoptotic (PI negative and annexin V positive), necrotic (PI positive and annexin V positive) and fully lysed necrotic (PI positive and annexin V negative) cell death (Figure 5). In the positive control, the cells were treated with 1 mM hydrogen peroxide (H_2O_2) which is known to increase apoptotic portion (Hu et al., 2011).

In order to investigate whether the chitosan-AuNPs regulate apoptosis-related genes, we compared the expression levels of apoptotic genes of bak, bax, and caspase-3 before and after chitosan-AuNPs treatment. As shown in Figure 6A, chitosan-AuNPs activated an increase in mRNA expression of bak (2.10 ± 0.88 fold) and bax (1.49 ± 0.26) fold, which are pro-apoptotic members of the Bcl-2 family, and caspase-3 (3.29 ± 0.89), which is a downstream effector of apoptotic pathways (n = 6). In statistical analysis, the p-value of bak (p = 0.058), bax (p = 0.092), and caspse-3 (p = 0.051) was not significant. Furthermore, in order to measure the protein level of caspase-8 as an initiator of an extrinsic apoptotic pathway, western blotting assay was performed. As shown in Figure 6B, the alteration of protein level of caspase-8 was detected. The cleavage of procaspase-8 was increased at chitosan-AuNPs concentrations of 0.2 × IC_{50}, 0.3 × IC_{50} and 0.5 × IC_{50} when the expression level was normalized to β-actin. At chitosan-AuNPs concentration of 1 × IC_{50}, the protein of caspase-8 was not detected because cells were completely lysed by necrotic cell death.

Figure 4. Flow cytometric analysis demonstrating cell cycle distribution. (A) flow cytometric analysis of cell cycle distribution after treatment of chitosan-AuNPs. The number of cells in the sub-G1 phase was increased among the chitosan-AuNPs treated cells. (B) the plot of cell cycle distribution with and without treatment using chitosan-AuNPs. (C) DNA fragmentation induced by chitosan-AuNPs. Cells were treated with different concentrations of chitosan-AuNPs for 24 h. H_2O_2 and sodium selenite were used as positive controls.

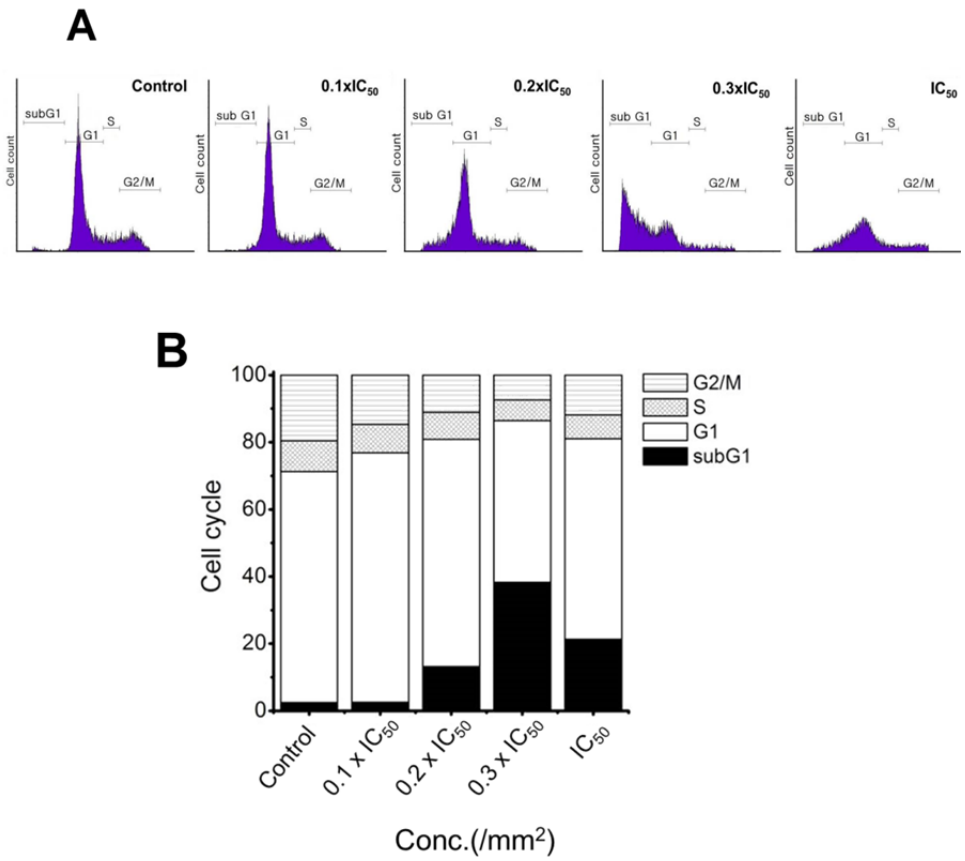
A
Control
0.1xIC50
0.2xIC50
0.3xIC50
IC50
subG1
G1
S
G2/M
Cell count
B
Cell cycle
100
80
60
40
20
0
G2/M
S
G1
subG1
Control
0.1 x IC50
0.2 x IC50
0.3 x IC50
IC50
Conc.(/mm2)
C
Marker
Control
0.1 x IC50
0.2 x IC50
0.3 x IC50
0.5 x IC50
1 x IC50
H2O2
Sodium-selenite
1kb
500bp

Figure 5. Annexin V/PI double staining. Cells were treated with different concentration of chitosan-AuNPs as noted for 24 h, and were then stained with annexin V and PI, and assayed by flow cytometery. H_2O_2 (1 mM) was used as positive control.

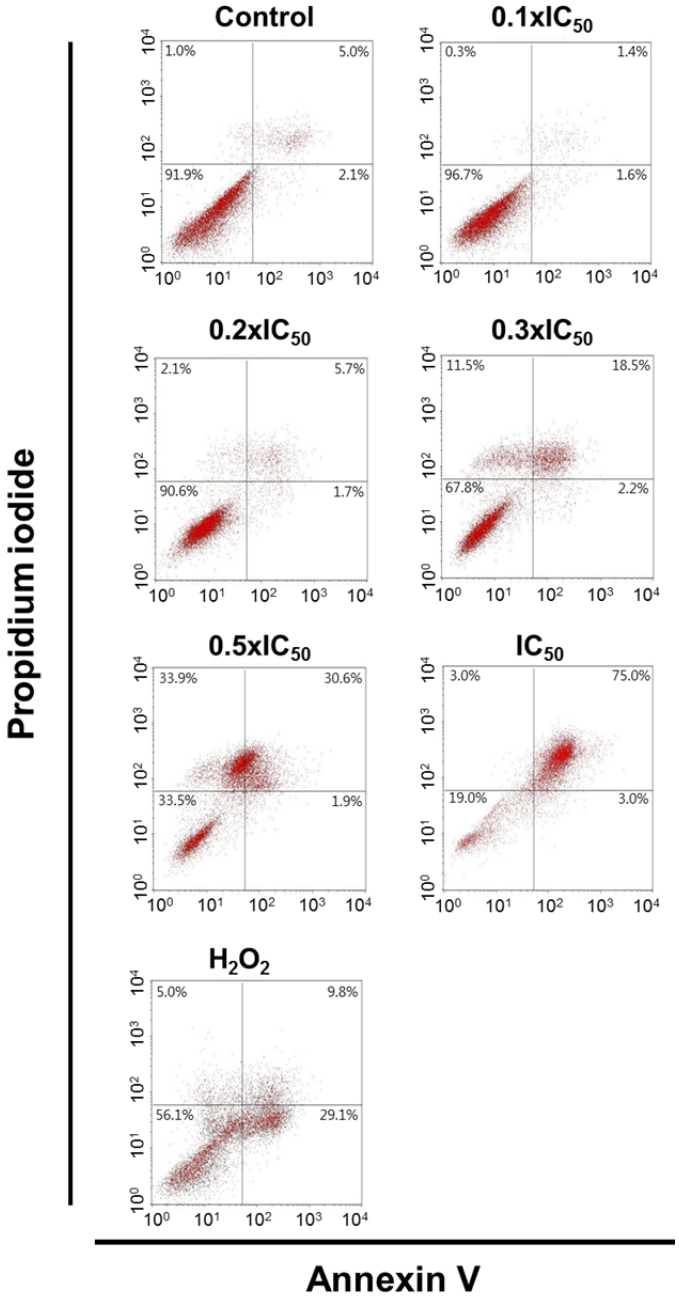
Control
1.0%
5.0%
91.9%
2.1%
0.1xIC50
0.3%
1.4%
96.7%
1.6%
0.2xIC50
2.1%
5.7%
90.6%
1.7%
0.3xIC50
11.5%
18.5%
67.8%
2.2%
0.5xIC50
33.9%
30.6%
33.5%
1.9%
IC50
3.0%
75.0%
19.0%
3.0%
H2O2
5.0%
9.8%
56.1%
29.1%
Propidium iodide
Annexin V

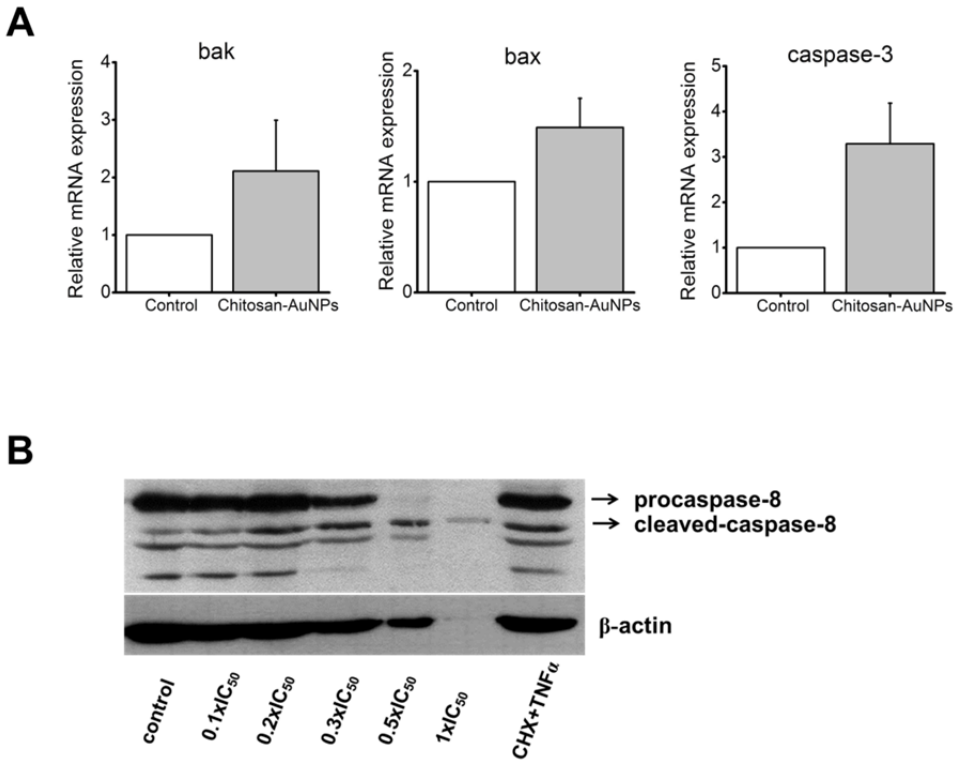

Figure 6. Expression of apoptosis-related mRNAs and protein. (A) mRNA expression analysis of apoptosis-related gene, bak, bax, and caspase-3. After cells were treated with a 1 × IC_{50} of chitosan-AuNPs, real-time RT-PCR analysis was performed using gene specific primers. (B) western blot analysis of caspase-8. The alteration of protein level of caspase-8 was detected in cells treated with chitosan-AuNPs for 24 h. Positive controls displaying 24 h exposures to cycloheximide (CHX) and tumor necrosis inducing factor alpha (TNF-α).

DISCUSSION

Recently, AuNPs have been suggested for several potential uses, including diagnostics, biosensing and drug/gene delivery into the cells. With increasing prospective applications of AuNPs, the uptake and cytotoxicity mechanisms of NPs are of particular importance.

The related mechanisms of uptake of NPs into cells have been proposed (Unfried et al., 2007). TEM results suggest that positively charged chitosan-AuNPs can be internalized into endosomes. In this study, uptake may affect the cytotoxicity induced by positively charged AuNPs. It was expected that the positively charged chitosan-AuNPs could easily attach on the negatively charged cellular membrane. These characteristics of chitosan-AuNPs could be preferable factors since positively charged chitosan-AuNPs are more efficient in interacting with cells compared to the neutral or negatively charged chitosan-AuNPs. However, It is also closely related to the cytotoxicity of positively charged AuNPs (Lin et al., 2010a).

Much attention has been paid to understanding the interactions between NPs and biological systems including protein coronae in nano-therapeutics (Faunce et al., 2008). The interactions between proteins and NPs should be understood, especially when seeking to achieve controlled delivery into the cell. To examine the effect of the serum proteins on cytotoxicity, we performed a cell viability assay under the serum protein conditions of both 1% and 10%. Based on our cytotoxicity test at 1% and 10%, the serum protein coating did not affect

the cell viability presumably due to the highly positive charge of chitosan-AuNPs. The serum-protein did not greatly affect the cell viability test in contrast to the recent report on the FBS-coated graphene oxide (Hu et al., 2011).

At the present time, the cytotoxicity and cytotoxic mechanisms induced by chitosan-AuNPs are controversial (Arvizo et al., 2010; Connor et al., 2005; Goodman et al., 2004; Pan et al., 2007; Pernodet et al., 2006; Uboldi et al., 2009; Yen et al., 2009). AuNPs do not cause acute cytotoxicity toward the K562 leukemia cell line (Connor et al., 2005). Chitosan, biological hydrophilic polymer, is widely regarded as being a non-toxic (Kean and Thanou, 2010). On the other hand, chitosan has little toxicity depending on molecular weight and degree of deacetylation (Richardson et al., 1999). In addition, several reports have indicated the cytotoxicity of AuNPs toward alveolar type II cell lines (Uboldi et al., 2009) and human dermal fibroblasts (Pernodet et al., 2006). Also, toxicity of AuNPs was size-dependent (Pan et al., 2007). Recently, the surface charge of AuNPs was found to modulate membrane potential of different cell types and subsequent downstream intracellular events (Arvizo et al., 2010).

Several reports have suggested cytotoxic mechanisms of NPs (Arora et al., 2008; Kang et al., 2010; Khan et al., 2007). However, more precise cytotoxic mechanisms induced by positively charged AuNPs are still unknown. Recently, it has been demonstrated that positively charged using trimethylammonium ethanethiol increased the apoptosis through the expression of p53 and caspase 3 in HaCaT keratinocyte cells (Schaeublin et al., 2011). Moreover, AuNPs cytotoxicity is known to be associated with necrosis in HeLa cells (Pan et al., 2009).

Results in this study show that positively charged chitosan-AuNPs decreased mitochondrial function and induce severe membrane leakage as concentration dependent manner. In addition, flow cytometry analysis revealed that chitosan-AuNPs treatment increased the sub-G1 phase which represents DNA fragmentation-induced cell death. Also, apoptotic genes related to the intrinsic apoptotic pathways such as Bak, Bax and caspase 3 were significantly increased. Additionally, the cleaved protein of procaspase-8 increased at AuNPs concentrations of 0.2 × IC_{50}, 0.3 × IC_{50} and 0.5 × IC_{50}. Furthermore, annexin V/PI double staining results demonstrated the mechanism of cell death by positively charged chitosan-AuNPs lacks integrity of the plasma membrane. Specifically, excessive cell damage (presumably necrosis) was activated at the concentrations of 0.2 × IC_{50}, 0.3 × $IC_{50,}$ 0.5 × IC_{50} and 1 × IC_{50}. This suggests that positively charged chitosan-AuNPs induce excessive cell death of most likely necrosis at a certain range of chitosan-AuNPs concentration. In other words, sudden external stimuli could be a cause of cell death for the positively charged chitosan-AuNPs.

Therefore, the elucidation of cytotoxic mechanisms is essential prior to the biological applications of positively charged chitosan-AuNPs.

CHAPTER III

The alteration of microRNA expression by surface-modified gold nanoparticles in human lung adenocarcinoma cells

ABSTRACT

MicroRNAs are important non-coding regulators that bind to target mRNA. Several studied indicate that nanoparticles (NPs) induce alterations in microRNAs expression relating to cell development and progressive diseases. However, the alteration of microRNA expression by surface-modified gold nanoparticles (AuNPs) in A549 cells has not been reported.

In order to investigate the patterns of microRNA expression, we analyzed data from a microRNA's microarray. Results show that the expression of microRNA (hsa-miR-198) in cells treated with citrate-AuNPs significantly differed from non-treated cells, the expression of 12 microRNAs in cells treated with chitosan-AuNPs significantly differed from non-treated cells. Furthermore, the predicted target genes of microRNAs were related to proliferation, apoptosis, and cell differentiation including the mitogen-activated protein kinase, ErbB, Wnt signaling pathway. Thus, the alteration of microRNA expression profiles by citrate- and chitosan-AuNPs would mediate the regulation of the cell processes.

INTRODUCTION

Non-coding RNAs that are 22 nucleotides long, such as microRNA, are critical molecules of the post-transcriptional regulator (Bartel, 2004). The microRNAs usually suppress their target expression by using the RNA-induced silencing complex in target mRNAs to bind in a partial complementary sequence. The primary microRNA is initially transcribed by RNA polymerase II and processed to a stem-loop-containing precursor microRNA (pre-microRNA) by the microprocessor complex in the nucleus. Finally, the pre-microRNA is exported to the cytoplasm where it is cleaved by Dicer to form the mature microRNA (Kim, 2005; Lagos-Quintana et al., 2001).

It is known that a single microRNA can target hundreds mRNAs, so subtle changes in microRNA expression can elicit important cellular effects (Baek et al., 2008; Selbach et al., 2008). Many reports suggest that microRNAs, as post-transcriptional regulators, are involved in many biological processes, including the cell development and diseases (Alvarez-Garcia and Miska, 2005; Calin et al., 2004; Minones-Moyano et al., 2011). MicroRNA expression was different in chronic lymphocytic leukemia compared to normal B cells (Calin et al., 2004). In addition, down-regulation of miR-34b/c expression triggers alteration in mitochondrial dysfunction in Parkinson's disease (Minones-Moyano et al., 2011). Thus, microRNAs may be useful as biomarkers for disease diagnosis (Volinia et al., 2006). Moreover, the expression of microRNAs is specific to the tissue and the developmental stage (Xu et al., 2007). The

expression of 13 microRNAs related to developmental processes was altered during the chondrogenic differentiation of mouse retina (Yang et al., 2011).

Recently, the exposure of nanoparticles (NPs) has induced a change in microRNA (Bourdon et al., 2012; Burklew et al., 2012; Halappanavar et al., 2011) in cells. The aluminum oxide NPs altered the expression of microRNAs related to stress responses in tobacco (Burklew et al., 2012). In addition, the exposure of carbon black NPs changed the expression of mmu-miR-135b, mmu-miR-146b, and mmu-miR-21 relating to inflammation in mouse lung (Bourdon et al., 2012). Moreover, diesel exhaust particles alter the expression of microRNAs relating to regulation of cell process in tumorigenesis (Jardim et al., 2009).

However, research regarding the effect of surface-modified gold nanoparticles (AuNPs) in changing microRNA expression patterns has not been reported. Therefore, the expression of microRNAs altered in cells treated with citrated- and chitosan-AuNPs using microRNA microarray analysis technology was investigated.

MATERIALS AND METHODS

Preparation of AuNPs

Citrate- and chitosan-AuNPs were provided by Sang-woo Joo (Soongsil University). The average diameters of citrate-AuNPs were 17.0 ± 1.7 nm. The zeta potentials of citrate-AuNPs were measured to be -37.5 ± 6.3 mV. The average diameters of chitosan-AuNPs were 16.9 ± 2.6 nm. The zeta potentials of chitosan-AuNPs were measured to be +41.5 ± 5.7 mV.

Cell culture

The human lung cancer cell line A549 was obtained from the Korea Cell Bank. They were cultured in RPMI 1640 media (Welgene, Daegu, Korea) and supplemented with 10% fetal bovine serum (FBS), and 1% antibiotic solution (Sigma-Aldrich, St. Louis, USA). The cells were maintained at 37°C in a humidified incubator with 5% CO_2.

Nanoparticles treatment and cell viability assay

The viability of cells treated with nanoparticles was assessed with methylthiazol tetrazolium (MTT) assay. Briefly, 0.1 mg/well of MTT solution was added in cells, and then cells were incubated at 37°C for 4 h to allow for the formation of MTT formazan. The MTT formazan was dissolved in 200 μL of dimethyl sulfoxide and the optical density was measured at 570 nm using a microplate

analyzer (Tecan, Austria). Results are presented as a percentage of the control values. All experiments were carried in triplicates.

Total RNA isolation

Total RNA was extracted from both groups with a QIAZOL reagent (Qiagen, USA) according to the manufacturer's protocols. Briefly, cells were lysed by QIAZOL. Chloroform was then added, mixed by inverting and cells were incubated at room temperature for 10 min. The RNA was extracted by adding isopropyl alcohol and centrifuged for 10 min at 12,000 rpm to precipitate the RNA. Finally, the total RNA was eluted with nuclease-free water. RNA quantity and quality were analyzed using NanoDrop spectrophotometer. The experiment was performed three times.

MicroRNA microarray analysis

The microRNA microarray analysis was performed by DNAlink (Korea) using an Affymeterix genechip miRNA 2.0 array. The assay was performed on small RNA in the total RNA sample. The small RNA was then extended at the 3'-end with a poly(A) tail using poly(A) polymerase, followed by ligation of an oligonucleotide tag to the poly(A) tail for later fluorescent staining. Two different tags (Cy3 and Cy5) were used for the two different RNA samples. The two RNA samples were then hybridized overnight on a microchip using a microcirculation pump. These probes consisted of chemically modified nucleotide coding sequences that complemented the target microRNAs and a

spacer segment of polyethylene glycol to extend the coding sequence away from the substrate. Each microRNA was analyzed 4 times and the controls were repeated 4 times.

Statistical analysis of microRNA data

The analysis of the microarray data was performed by DNAlink (Korea). The microarray data was analyzed by subtracting the background and then the signals were normalized using a filter. To identify microRNAs whose expression differed between control and AuNPs treated A549 cells, a statistics analysis was performed. The ratio of the two sets of detected signal (control and AuNPs treated) was calculated and expressed in $\log_2$ for each microRNA. MicroRNAs with p-values < 0.01 and $\log_2$ ratio > 0.5 were considered to be significantly differentially expressed.

Target prediction of microRNAs

The microRNAs that showed altered expression after citrate- and chitosan-AuNPs exposure were selected for target prediction. In the present study, the microRNA target prediction was done using four different programs. The programs used include mirWalk v2.0 (Dweep et al., 2011), TargetScan (Creighton et al., 2008), PicTar (Krek et al., 2005) and miRanda (Betel et al., 2008). The use of different computational algorithms helped reduce the potential false positives and increase the accuracy of prediction (Zhang and Pan, 2009). The predicted target genes were sorted according to the individual scores

from each program.

Functional analysis of predicted targets

The potential target genes for selected microRNAs were classified according to biological function determined using the gene ontology (GO) system. To determine a possible overlap of biological functions among the microRNAs, significantly overrepresented GO terms among selected microRNAs were searched for by using the Database for Annotation, Visualization and Intergrated Discovery (DAVID) version 6.2 (http://david.abcc.ncifcrf.gov). The DAVID program determined all the annotated GO terms associated with predicted target genes and then counted the number of apperances of each GO term for these genes. In addition, pathway analysis of the predicted target genes was performed using the DAVID database (Huang da et al., 2009).

RESULTS

Effect of citrate- and chitosan-AuNPs on A549 cell viability

To determine the viability of A549 cells treated with citrate- and chitosan-gold nanoparticles, cell viability assays were performed (Figure 1). The viability of cells treated with citrate-AuNPs decreased by 21% at a 10 μg/mL concentration. The viability of cells treated with chitosan-AuNPs decreased by 22% at a 10 μg/mL concentration.

Alteration of microRNA expression profiles in A549 cells after citrate- and chitosan-AuNPs exposure

To examine the responses of microRNAs to AuNPs, a microRNA microarray was performed by using total RNAs extracted from A549 cells treated with citrate- and chitosan-AuNPs at 10 μg/mL concentration.

After 24h incubation, the expression level of one microRNA was significantly altered by citrate-AuNPs exposure, and the expression level of 16 microRNAs was significantly altered by chitosan-AuNPs exposure compared with non-treated cells (Figure 2 and Table 1). Statistical analysis of differentially expressed microRNAs showed that 17 microRNAs were significantly dysregulated with $p < 0.05$ and 1.5-fold changes. In citrate-AuNPs treated cells, hsa-mir-198 was up-regulated with 1.51-fold. In chitosan-AuNPs treated cells, four microRNAs (hp_hsa-mir-548i-4 (1.92-fold), hsa-mir-570

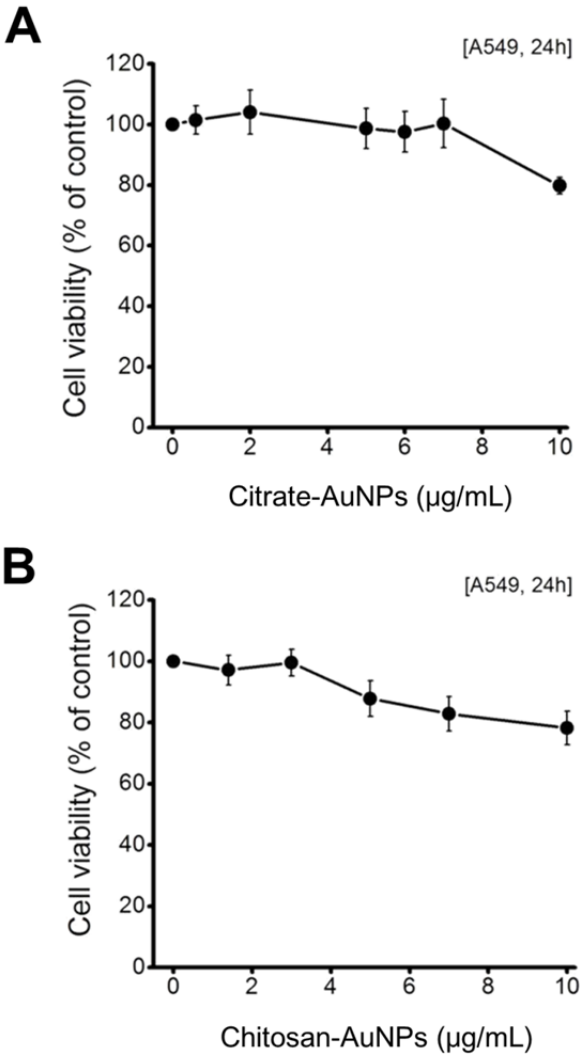

Figure 1. Effect of citrate- and chitosan-AuNPs on A549 cell viability. MTT cell viability assay was performed using A549 cells exposed to (A) citrate- (B) chitosan-AuNPs for 24 h (n = 5). The value of untreated cells was taken as 100%, and the percentage decrease in the optical density of the NP-exposed cells was calculated.

(1.76-fold), has-mir-606 (1.73-fold), has-mir-548a-3p (1.55-fold)) were up-regulated, whereas 12 microRNAs (hp_hsa-miR-2116 (1.56-fold), hp_hsa-miR-502-x (1.63-fold), hsa-miR-342-3p (1.66-fold), hp_hsa-miR-149 (1.73-fold), hsa-miR-149 (1.78-fold), hsa-miR-93 (1.77-fold), hsa-miR-744 (1.85-fold), hsa-miR-34c-3p (1.85-fold), hsa-miR-423-3p (1.86-fold), hsa-miR-501 (2.05-fold), hsa-miR-1180 (2.57-fold), hsa-miR-1303 (3.18-fold)) were down-regulated.

Prediction of target genes of differentially expressed microRNAs

To investigate the probable biological function of the differentially expressed microRNAs, we predicted the putative targets of 17 microRNAs. The four different computational programs including mirWalk, TargetScan, PicTar and miRanda were used following the manufacturer's instructions. The total putative target genes of the each microRNA were selected for functional analysis. A total of 3,121 genes were selected as significantly putative targets of hsa-mir-198 microRNAs in citrated-AuNPs treated cells. A total of 11,747 genes from four up-regulated microRNAs and a total of 15,362 genes from 12 down-regulated microRNAs were selected as significant putative targets in chitosan-AuNPs treated cells (Table 2).

Functional annotation analysis for AuNPs induced-differently expressed microRNAs

Table 1. Fold change in the expression of significantly changed microRNAs by citrate- and chitosan-AuNPs

Probe_ID	Citrate-AuNPs			Chitosan-AuNPs		
	Log_2 ratio	Fold change	P-value	Log_2 ratio	Fold change	P-value
Up-regulated						
hsa-miR-198	0.599	1.515	0.012			
hp_hsa-mir-548i-4				0.944	1.924	0.021
hsa-miR-570				0.815	1.760	0.010
hsa-miR-606				0.789	1.729	0.026
hsa-miR-548a-3p				0.640	1.558	0.039
Down-regulated						
hp_hsa-mir-2116				-0.645	-1.56439	0.04894
hp_hsa-mir-502_x				-0.708	-1.63392	0.04769
hsa-miR-342-3p				-0.734	-1.664	0.04966
hp_hsa-mir-149				-0.798	-1.73838	0.01398
hsa-miR-93				-0.828	-1.77461	0.01055
hsa-miR-149				-0.832	-1.78027	0.00135
hsa-miR-744				-0.892	-1.85511	0.0288
hsa-miR-34c-3p				-0.893	-1.85658	0.04274
hsa-miR-423-3p				-0.895	-1.86016	0.04059
hp_hsa-mir-501				-1.04	-2.05695	0.04948
hsa-miR-1180				-1.365	-2.57498	0.04361
hsa-miR-1303				-1.669	-3.18071	0.03032

*Log_2 ratio=treatment/control

Figure 2. Altered microRNAs by citrate- and chitosan-AuNPs. Profile of microRNA expression in A549 cells treated with (A) citrate-and (B) chitosan-AuNPs for 24 h (n = 4). The relative increase or decrease of the microRNAs that showed a significant change in levels of expression after AuNPs treatment compared with untreated cells.

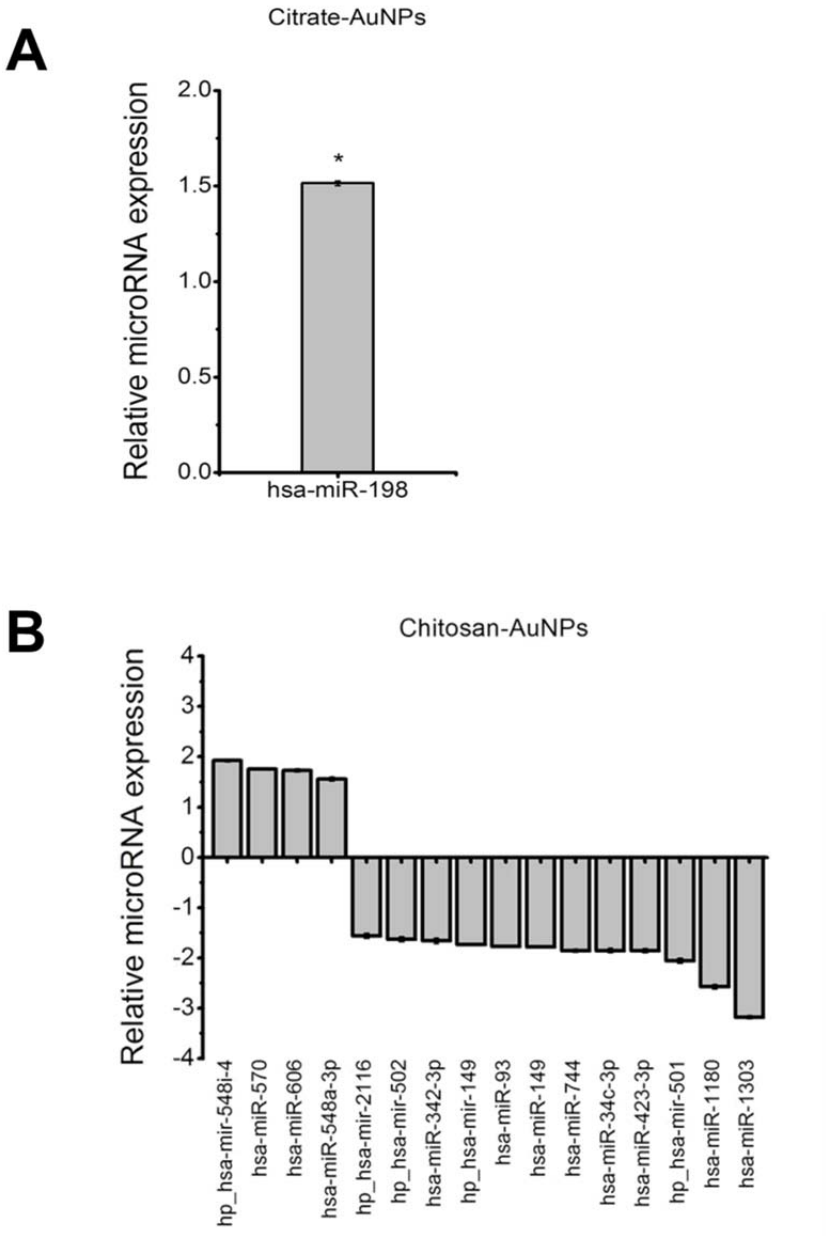
A
Citrate-AuNPs
Relative microRNA expression
2.0
1.5
1.0
0.5
0.0
*
hsa-miR-198
B
Chitosan-AuNPs
Relative microRNA expression
4
3
2
1
0
-1
-2
-3
-4
hp_hsa-mir-548i-4
hsa-miR-570
hsa-miR-606
hsa-miR-548a-3p
hp_hsa-mir-2116
hp_hsa-mir-502
hsa-miR-342-3p
hp_hsa-mir-149
hsa-miR-93
hsa-miR-149
hsa-miR-744
hsa-miR-34c-3p
hsa-miR-423-3p
hp_hsa-mir-501
hsa-miR-1180
hsa-miR-1303

The biological function of predicted target gene was classified using the gene ontology system in DAVID. The overrepresented GO terms for selected microRNAs were identified since a single gene was related to many GO terms.

Table 3 represents the biological processes associated with selected microRNAs as predicted by DAVID. The top 10 of enriched GO biological process categories with the smallest p-values for the predicted target genes of the up-regulated microRNAs treated with citrate-AuNPs were endocytosis, membrane invagination, vesicle mediated transport, leukocyte adhesion, DNA modification, membrane organization, MAPKKK cascade, DNA methylation, and regulation of small GTPase mediated signal transduction.

Tables 4 and 5 show the enriched GO biological process categories with predicted target genes of up-and down-regulated microRNAs by treatment with chitosan-AuNPs. In the target genes of up-regulated by treatment with chitosan-AuNPs, the top 10 of enriched GO categories with the smallest p-values were regulation of transcription, transcription, regulation of RNA metabolic process, mRNA metabolic process, regulation of transcription, DNA-dependent, positive regulation of RNA metabolic process, mRNA processing, positive regulation of transcription, DNA-dependent, positive regulation of macromolecule metabolic process, and regulation of transcription from RNA polymerase II promoter (Table 4). In the target genes of microRNAs by treatment with chitosan-AuNPs, the top 10 enriched GO categories with the smallest p-values were transcription, regulation of transcription, regulation of small GTPase mediated signal transduction, positive regulation of macromolecule metabolic process, positive regulation of nucleobase, nucleoside, nucleotide and nucleic acid metabolic

Table 2. Number of predicted target genes of the selected microRNAs

Type of AuNPs	Type of expression	Probe ID of microRNA	Total number of accession ID
Citrate-AuNPs	Up	hsa-mir-198	3,121
Chitosan-AuNPs	Up	hp_hsa-mir-548i-4 hsa-miR-570 hsa-miR-606 hsa-miR-548a-3p	11,747
Chitosan-AuNPs	Down	hp_hsa-mir-2116 hp_hsa-mir-502_x hsa-miR-342-3p hp_hsa-mir-149 hsa-miR-93 hsa-miR-149 hsa-miR-744 hsa-miR-34c-3p hsa-miR-423-3p hp_hsa-mir-501 hsa-miR-1180 hsa-miR-1303	15,362

Table 3. Analysis of biological processes of predicted target genes of up-regulated microRNAs by citrate-AuNPs

Term	Count	%	P value	Fold enrichment	Gene
GO:0006897~endocytosis	54	1.731	6.272E-4	1.572	HIP1R, AP1S1, EEN_B2_L3, RUFY1, CAP, GAPVD1, MYO7A, EPS15L1, AHSG, TFRC
GO:0010324~membrane invagination	54	1.731	6.267E-4	1.572	HIP1R, AP1S1, EEN_B2_L3, RUFY1, CAP, GAPVD1, MYO7A, EPS15L1, AHSG, TFRC
GO:0016192~vesicle-mediated transport	118	3.782	0.001	1.312	SYT13, MON2, AP1S1, AP4B1, SYTL1 , SAR1B, RUFY1, MYO7A, GAPVD1, AHSG
GO:0007159~leukocyte adhesion	12	0.384	0.002	2.745	VCAM1, ICAM1, ITGB1, SELPLG, APOA4, SELP, PTPRC, ITGA5, CERCAM, CD209
GO:0006304~DNA modification	13	0.416	0.003	2.523	SMUG1, OGG1, MLL, DNMT1, TDRD1, ATRX, CCNO, PICK1, TRDMT1, MLL5
GO:0016044~membrane organization	79	2.532	0.006	1.328	HIP1R, FTL, RTP2, GNAPT, AP1S1, SH3D19, SAR1B, EEN_B2_L3,ATP8B3, STX3
GO:0000165~MAPKKK cascade	43	1.378	0.006	1.497	DOK5, CRKL, C1QTNF2, ITGA1, CCM2, MAP3K2, EGF, MAP3K9, FGD4, MINK1
GO:0006305~DNA alkylation	10	0.321	0.008	2.669	MLL, DNMT1, TDRD1, ATRX, PICK1, TRDMT1, MLL5, BAZ2A, ATF71P, DNMT3A
GO:0006306~DNA methylation	10	0.321	0.008	2.669	MLL, DNMT1, TDRD1, ATRX, PICK1, TRDMT1, MLL5, BAZ2A, ATF7lP, DNMT3A
GO:0051056~regulation of small GTPase mediated signal transduction	55	1.763	0.008	1.398	CTGLF6, IQGAP2, TBC1D20, GBL, PSD, ASAP1,RGL3, GRTP1, GAPVD1, PLEKHG1

process, positive regulation of nitrogen compound metabolic process, regulation of RNA metabolic process, vesicle-mediated transport, protein amino acid phosphorylation, and positive regulation of gene expression (Table 5).

Biological pathway analysis

The predicted target genes of selected microRNAs underwent biological pathway analysis using the KEGG pathway of DAVID. The 10 high-enrichment pathways with the smallest p-values were selected. The pathways of the target genes of up-regulated microRNAs by treatment with citrate-AuNPs cells were arrhythmogenic right ventricular dardiomyopathy, adherens junction, focal adhesion, endocytosis, hypertrophic cardiomyopathy, axon guidance, leukocyte transendothelial migration, VEGF signaling, pathways in cancer, and alpha-linolenic acid metabolism (Table 6). The pathways of target genes of up-regulated microRNAs by treatment with chitosan-AuNPs cells were pathways in cancer, ubiquitin mediated proteolysis, cell cycle, Wnt signaling pathway, TGF-beta signaling pathway, colorectal cancer, adherens juction, spliceosome, Jak-STAT signaling pathway, and T cell receptor signaling pathway (Table 7). In down-regulated microRNAs by treatment with chitosan-AuNPs, the top 10 pathways were pathways in cancer, apoptosis, focal adhesion, renal carcinoma, ErbB signaling pathway, pancreatic cancer, MAPK signaling, axon guidance, neurotrophin signaling pathway, and glioma (Table 8).

Table 4. Analysis of biological processes of predicted target genes of up-regulated microRNAs by chitosan-AuNPs

Term	Count	%	P value	Fold enrichment	Gene
GO:0045449~regulation of transcription	1747	14.866	1.508E-22	1.141	CRY1, STAT1, SREBF1, IRF8, ATF3, SUPT3H, ZNF648, ATF7IP, YAP1, TGIF2
GO:0006350~transcription	1411	12.006	6.802E-18	1.141	CRY1, STAT1, GTF2H3, GLI2, SREBF1, IRF8, ZNF34, SUPT3H, ATF3, ZNF648
GO:0051252~regulation of RNA metabolic process	1208	10.279	2.797E-13	1.132	HCLS2, STAT1, GTF2H3, GLI2, SREBF1, IRF8, ZNF34, XRCC6, SUPT3H, ATF3
GO:0016071~mRNA metabolic process	284	2.417	3.967E-13	1.304	U2AF2, FUS, CSTF3, A2BP1, LSM5, SERBP1, GEMIN6, THOC4, TSEN15, HNRNPA0
GO:0006355~regulation of transcription, DNA-dependent	1174	9.989	8.599E-12	1.125	HCLS2, STAT1, GTF2H3, GLI2, SREBF1, IRF8, ZNF34, XRCC6, SUPT3H, ATF3
GO:0051254~positive regulation of RNA metabolic process	353	3.004	1.967E-11	1.246	PRDM16, GLI2, SREBF1, BCL10, RUNX1T1, XRCC6, ATF7IP, CDX2, MYOCD, ERCC6
GO:0006397~mRNA processing	246	2.093	2.263E-11	1.302	U2AF2, FUS, CSTF3, LSM5, A2BP1, GEMIN6, THOC4, TSEN15, HNRNPA0, BRUNOL5
GO:0045893~positive regulation of transcription, DNA-dependent	349	2.970	4.903E-11	1.242	PRDM16, GLI2, SREBF1, BCL10, RUNX1T1, XRCC6, ATF7IP, CDX2, MYOCD, MAP3K1
GO:0010604~positive regulation of macromolecule metabolic process	592	5.037	1.929E-10	1.173	ANAPC1, HCLS1, SREBF1, GLI2, TRAF6, XRCC6, CD28, ATF7IP, ERCC6, MAP3K1
GO:0006357~regulation of transcription from RNA polymerase II promoter	508	4.323	3.115E-10	1.187	PAX5, SOX30, GLI2, SREBF1, HDAC3, JMY, IRF8, XRCC6, SUPT3H, CHD2

Table 5. Analysis of biological processes of predicted target genes of down-regulated microRNAs by chitosan-AuNPs

Term	Count	%	P value	Fold enrichment	Gene
GO:0006350~transcription	1756	11.435	1.673E-20	1.100	CRY1, ZNF688, STAT1, SREBF1, IRF8, ATF3, SUPT3H, ZNF648, ZNF787, GATAD2A
GO:0045449~regulation of transcription	2144	13.961	4.331E-19	1.085	CRY1, ZNF688, STAT1, SREBF1, IRF8, SUPT3H, ATF3, ZNF648, ZNF787, GATAD2A
GO:0051056~regulation of small GTPase mediated signal transduction	235	1.530	1.045E-12	1.228	KALRN, IQGAP2, DEPDC2, MFN2, EV15, TBC1D2, ARHGEF19, FBXO8, RGL3, ARFGAP1
GO:0010604~positive regulation of macromolecule metabolic process	733	4.773	1.362E-12	1.126	ANAPC1, HCLS1, SREBF1, GLI2, TRAF6, XRCC6, CD28, ATF7IP, NR2E3, ERCC6
GO:0045935~positive regulation of nucleobase, nucleoside, nucleotide and nucleic acid metabolic process	543	3.536	2.973E-12	1.145	SREBF1, GLI2, XRCC6, ATF7IP, NR2E3, ERCC6, MAP3K1, YAP1, CREBBP, ALX1
GO:0051173~positive regulation of nitrogen compound metabolic process	559	3.640	3.731E-12	1.143	HRH1, SREBF1, GLI2, XRCC6, ATF7IP, NR2E3, ERCC6, MAP3K1, YAP1, CREBBP
GO:0051252~regulation of RNA metabolic process	1490	9.702	6.968E-12	1.082	HCLS1, STAT1, GTF2H3, GLI2, ZNF688, SREBF1, IRF8, XRCC6, ATF3, SUPT3H
GO:0016192~vesicle-mediated transport	502	3.269	1.241E-11	1.147	KALRN, CPNE3, LIN7C, SEC31B, ANKRD27, NKD2, ARF3, RUFY1, ARFGAP1, COLEC12
GO:0006468~protein amino acid phosphorylation	576	3.751	1.303E-11	1.137	KALRN, STAT1, MST1R, FGFR1, EPHA5, ERCC6, CAMK2G, MAP3K1, STK25, PRKDC
GO:0010628~positive regulation of gene expression	506	3.295	1.322E-11	1.146	GLI2, SREBF1, XRCC6, ATF7IP, NR2E3, MAP3K1, YAP1, CREBBP, ALX1, SMAD9

Table 6. KEGG pathway analysis of predicted target genes of up-regulated microRNA by citrate-AuNPs

KEGG pathway	Count	%	P value	Fold enrichment	Gene	Putative function
hsa05412:Arrhythmogenic right ventricular cardiomyopathy (ARVC)	23	0.737	0.001	1.993	PKP2, CTNNA2, TIGA2, ITGA3, DMD, ITGA5, SGCA, LEF1,	cell death
Chsa04520:Adherens junction	21	0.673	0.009	1.796	MET, CTNNA2, CTNND1, LEF1, PTPRB	migration
hsa04510:Focal adhesion	44	1.410	0.010	1.442	MET, PARVG, ITGA2, ITGA3, ITGA5, THBS1, SPP1, PTEN, ITGA10, COL6A2	cell survival, proliferation
hsa04144:Endocytosis	40	1.282	0.016	1.432	MET, DNAJC6, USP8, PSD, RUFY1, PSD3, PRKCZ, RAB11A, AP2A2, ARRB2,	endocytosis
hsa05410:Hypertrophic cardiomyopathy (HCM)	21	0.670	0.026	1.627	ITGB1, SLC8A1, ITGA2, ITGA3, DMD	cardiac dysorder
hsa04360:Axon guidance	29	0.929	0.028	1.480	UNC5B, SEMA4G, RGS3, NTN4, MET, PLXNA3, PPP3CA,	cell growth
hsa04670:Leukocyte transendothelial migration	27	0.865	0.028	1.507	CYBB, CTNNA2, JAM2, PTK2B, CXCL12, CLDN5, RAPGEF4, ICAM1,	migration
hsa04370:VEGF signaling pathway	19	0.608	0.028	1.669	PPP3CA, PLA2G1B, PLA2G3, PTGS2, PLA2G12B, CASP9,	growth, migration, metastasis
hsa05200:Pathways in cancer	63	2.019	0.033	1.265	MET, ITGA2, ITGA3, FGF11, RAD51, CDK4, RUNX1T1, PIAS4, LEF1, PTEN	metastasis, proliferation, apoptosis
hsa00592:alpha-Linolenic acid metabolism	7	0.224	0.043	2.562	PLA2G12A, ACOX3, JMJD7, ACOX1, PLA2G1B, PLA2G12B,	linolenic acid metabolism

Table 7. KEGG pathway analysis of predicted target genes of up-regulated microRNA by chitosan-AuNPs

KEGG pathway	Count	%	P value	Fold enrichment	Gene	Putative function
hsa05200:Pathways in cancer	29	1.949	9.692E-7	1.225	PTK2, LAMB1, MMP1, JAK1, LAMC1, DAPK1, TFG, PTCH1, MMP2, RALB	metastasis, proliferation, apoptosis
hsa04120:Ubiquitin mediated proteolysis	104	0.885	5.492E-6	1.332	UBE3A, UBE2L3, DDB1, KLHL13, UBE2K, SMURF2, MDM2, PIAS3, FBXW8, CUL3	ubiquitination
hsa04110:Cell cycle	95	0.808	1.394E-5	1.335	GADD45A, SMAD2, CDC14B, TFDP1, GSK3B, MDM2, DBF4, MCM3, PRKDC, PCNA,	cell cycle arrest, DNA repair
hsa04310:Wnt signaling pathway	112	0.953	1.447E-5	1.301	FRAT1, MAP3K7, WNT16, SMAD2, GSK3B, PRICKLE1, PPP2R5E, CACYBP, LEF1,	cell cycle, Wnt signaling
hsa04350:TGF-beta signaling pathway	69	0.587	2.503E-5	1.392	LEFTY2, INHBB, GDF6, ACVR1, SMAD2, DCN, BMP7, BMP6, THBS2, TFDP1,	cell cycle, apoptosis osteoblast-differentiation
hsa05210:Colorectal cancer	65	0.553	1.727E-4	1.358	SMAD2, RAF1, GSK3B, MAP2K1, LEF1, TCF7L1, FOS, SOS1, TGFBR1,	cell cycle, apoptosis
hsa04520:Adherens junction	60	0.510	2.357E-4	1.367	TJP1, MAP3K7, CTNND1, SMAD2, ACTB, PARD3, SORBS1, SSX2IP, PVRL2,	cell growth, differentiation
hsa03040:Spliceosome	92	0.782	2.502E-4	1.281	NCBP1, U2AF2, DHX8, DDX42, SR140, NCBP2 HSPA1A, ACIN1, LSM5, DHX15,	mRNA processing
hsa04630:Jak-STAT signaling pathway	109	0.928	6.595E-4	1.234	JAK1, IL6, IL12RB2, IFNA7, PRLR, IL10RA, STAT1, SOCS4, IFNA2, IL23R	proliferation, anti-apoptosis, development
hsa04660:T cell receptor signaling pathway	77	0.655	0.002	1.251	MAP3K7, RAF1, GSK3B, MAP2K1, NFATC4, FOS, SOS1, PPP3CC, IFNG, NFATC3,	proliferation, differentiation, immunity

Table 8. KEGG pathway analysis of predicted target genes of down-regulated microRNA by chitosan-AuNPs

KEGG pathway	Count	%	P value	Fold enrichment	Gene	Putative function
hsa05200:Pathways in cancer	293	1.907	1.556E-11	1.197	PTK2, FAS, AKT1, JAK1, DAPK1, PTCH1, TRAF3, IKBKG	metastasis, proliferation, apoptosis
hsa04210:Apoptosis	85	0.553	3.230E-8	1.309	FAS, AKT1, TNFRSF1A, IKBKG, IL1RAP	apoptosis, p53 signaling, cell cycle
hsa04510:Focal adhesion	180	1.172	1.624E-7	1.200	PTK2, MET, AKT1, LAMC1, ACTB, VASP, VAV1, ITGA11,	cell survival, proliferation
hsa05211:Renal cell carcinoma	69	0.449	3.285E-7	1.321	MET, AKT1, EGLN2, RAF1, RAP1A, MAP2K1, HRAS	proliferation, VEGF signaling, TGF-β signaling
hsa04012:ErbB signaling pathway	83	0.540	1.470E-6	1.279	PTK2, AKT1, RAF1, GSK3B, MAP2K1, HRAS, PTK2	proliferation migration, differentiation, angiogenesis
hsa05212:Pancreatic cancer	70	0.456	1.618E-6	1.303	AKT1, JAK1, SMAD2, RALB, RAF1, IKBKG,	cell cycle, anti-apoptosis
hsa04010:MAPK signaling pathway	231	1.504	1.764E-6	1.159	FAS, JMJD7-PLA2G4B, MAP3K7, AKT1, TNFRSF1A, PLA2G6, GADD45A, NF1,	proliferation, differentiation, inflammation
hsa04360:Axon guidance	118	0.768	2.690E-6	1.225	PTK2, SEMA4B, MET, NTN4, RGS3, PLXNA3, CXCL12, EPHA5, LIMK2,	cell growth
hsa04722:Neurotrophin signaling pathway	113	0.735	7.413E-6	1.221	AKT1, RPS6KA3, RAF1, RAP1A, GSK3B, MAP2K1, HRAS, YWHAQ,	differentiation, cell survival
hsa05214:Glioma	61	0.397	1.589E-5	1.298	CDK6, AKT1, ATK2, GRB2, RAF1, MDM2	proliferation, P53 signaling

DISCUSSION

Recently, several reports show that microRNA expression profiles in human or plant cells change in response to particles (Bollati et al., 2010; Bourdon et al., 2012; Frazier et al., 2014; Sun et al., 2015). Titanium dioxide NPs regulate microRNAs associated with plant growth and developmental genes (Frazier et al., 2014), and diesel exhaust particles induce an alteration in microRNA expression associated with inflammation in human airway cells (Jardim et al., 2009).

In order to assess the potential biological mechanisms of citrate- and chitosan-AuNPs exposure, the putative targets of 17 microRNAs whose expression was significantly altered after citrate- and chitosan-AuNPs exposure were identified. Based on putative targets, candidate signaling pathways were predicted. The results suggest that up-regulated microRNAs by citrate-AuNPs were related to endocytosis and DNA modification in biological process categories, and they were related to migration and metastasis including adherens junction, leukocyte transendothelial migration, and VEGF signaling pathway based on the KEGG pathway. In addition, up-regulated microRNA by chitosan-AuNPs were related to transcription in biological process, and related to cell cycle, apoptosis, and differentiation including Wnt signaling pathway, TGF-beta signaling pathway, Jak-STAT signaling pathway based on the KEGG pathway. Moreover, down-regulated microRNAs by chitosan-AuNPs were related to transcription and cell metabolism in biological processes, and related to

proliferation, apoptosis, and differentiation including focal adhesion, ErbB signaling pathway, MAPK signaling pathway, and Neurotrophin signaling pathway based on the KEGG pathway.

Increasing bioinformatics reports indicate that miR-198 is involved in cancer progression such as cell proliferation, apoptosis, migration, and metastasis. The enriched pathway of target genes of has-mir-198 was involved in tumor growth and metastasis (Tan et al., 2011; Wang et al., 2014; Yang et al., 2014). As the metastasis suppressor, miR-198 inhibits the motility of hepatocarcinoma cells (Tan et al., 2011) and the proliferation of A549 cells (Yang et al., 2014). As with the previous studies, up-regulated miR-198 expression by treatment with citrate-AuNPs was found to be associated with cell migration and metastasis such as VEGF signaling. Since microRNAs negatively regulate gene expression, it can be assumed that the up-regulation of miR-198 by treatment with citrate-AuNPs suppresses the expression levels of migration and metastasis genes.

Other reports suggest that predicted targets of microRNAs enriched with Wnt, TGF-β, and Jak-STAT signaling pathways were related to self-renewal and differentiation (Bakhshandeh et al., 2012b; Yu et al., 2012). In addition, several microRNAs enriched in Wnt and TGF-β signaling regulate genes were associated with determining cell fate during mesenchymal stem cell differentiation (Chen et al., 2014; Mei et al., 2013). Moreover, the modulation of osteo-specific microRNAs induced transient osteogenesis by regulating genes related to Wnt and TGF-beta signaling pathways (Bakhshandeh et al., 2012a).

Likewise other studies, the results show that the predicted target genes of up-regulated microRNAs by treatment with chitosan-AuNPs were classified as relating to cell cycle, apoptosis, and differentiation including Wnt, TGF-β, and Jak-STAT signaling pathway. Thus, up-regulated microRNAs treated with chitosan-AuNPs suppress gene expression related to cell differentiation.

Recently, 20 nm citrate-AuNPs induce an alteration in microRNAs expression related to mRNA processing and MAPK signaling pathway (Huang et al., 2015b). In addition, several reports identified the role of altered microRNA expression (Lin et al., 2010b; Liu et al., 2012). The miR-149 induces apoptosis by inhibiting Akt1 and E2F1 in the human neuroblastoma (Lin et al., 2010b). Also, the miR-93 and miR-149 expression regulates cancer stem cell regulatory genes resulting in the inhibition of cell differentiation (Liu et al., 2012; Wang et al., 2012). The miR-502 inhibits cell growth and autophagy in human colon cancer *in vitro* and *in vivo* (Zhai et al., 2013), and the miR-501 expression promotes cell proliferation of renal cell carcinoma (Mangolini et al., 2014). Moreover, the mir-34c which had interaction sites in Nanog2 enhances mouse spermatogonial stem cells differentiation (Yu et al., 2014). Following these reports, down-regulated microRNAs by chitosan-AuNPs mainly regulate target genes associated with proliferation, apoptosis, and cell differentiation

According to results, the prediction of target genes sharing signaling pathways suggests that microRNAs treated with citrate-AuNPs may regulate gene expression in metastasis. In addition, microRNAs altered by chitosan-AuNPs may regulate gene expression in cell proliferation, apoptosis, and cell differentiation.

CHAPTER IV

Chitosan-gold nanoparticles promote osteogenic differentiation of human adipose-derived mesenchymal stem cells through Wnt/β-catenin signaling pathway

ABSTRACT

Gold nanoparticles (AuNPs) are attractive materials for use in biomedicine due to their physical properties. Increasing evidence suggests that several nanoparticles induce the differentiation of human mesenchymal stem cells into osteoblasts and adipocytes. In this study, we hypothesized that chitosan-AuNPs promote the osteogenic differentiation of human adipose-derived mesenchymal stem cells (hADSCs). For the evaluation of osteogenic differentiation, alizarin red s staining, an proliferation assay, and a real-time RT-PCR analysis were performed. In order to examine specific signaling pathways, immunofluorescence and a Western blotting assay were performed.

The results demonstrate that chitosan-AuNPs increase the deposition of calcium content and the expression of marker genes relating to osteogenic differentiation in hADSCs at the concentrations that does not decrease cell viability. Also, the results of Western blotting and immunofluorescence assays indicate that chitosan-AuNPs promote osteogenesis through the Wnt/β-catenin signaling pathway. Therefore, chitosan-AuNPs can be used as a reagent for promoting bone formation.

INTRODUCTION

Transplant engineering of stem cells is a potential therapeutic method for the regeneration of damaged tissue, such as with osteoporosis, which is becoming an important issue and health problem (Compston et al., 2014; Maxson et al., 2012; McDonald et al., 1999; Oyen et al., 2011; Ren et al., 2012; Sanfelix-Genoves et al., 2011). Human mesenchymal stem cells (hMSCs) derived from various tissues, including bone marrow, adipose tissue, and umbilical cord blood, possess multi-lineage differentiating potentials (Pittenger et al., 1999). Interests in the therapeutic potential of stem cells isolated from adipose tissue, called adipose-derived stem cells (ADSCs), has grown due to a less expensive acquisition and greater available quantities than bone marrow (Gimble and Guilak, 2003; Kern et al., 2006; Toupadakis et al., 2010; Wagner et al., 2005). However, MSCs derived from various sources have limited proliferation activity and differentiation potentials (Chen et al., 2012; Vemuri et al., 2011). Therefore, it appears that developing new technologies to stimulate the differentiation of MSCs is required.

Recently, gold nanoparticles (AuNPs) have been suggested as useful medical vehicles for regenerative tools due to their non-toxic effects, as compared to other types of nanoparticles (NPs) (Peer et al., 2007; Zhang et al., 2008a). Various forms of AuNPs are known to be involved in the differentiation of hMSCs into various types of cells. For example, gold-coated iron oxide (Gold/Fe_3O_4) and graphene stimulate the neural differentiation of rat olfactory

bulb neural stem cells, and graphene oxide-encapsulated AuNPs are attractive detection materials for neural stem cell differentiation (Kim et al., 2013; Wang et al., 2013a). In addition, it has been proposed that AuNPs regulate the myocardiac differentiation of MSC (Orza et al., 2011; Ravichandran et al., 2014). Many reports suggest that AuNPs promote the differentiation of hMSCs into osteoblasts (Phillips et al., 2010; Zhang et al., 2014). Citrate-reduced AuNPs stimulate the osteogenic differentiation of bone marrow-derived MSCs through the mitogen-activated protein kinase (MAPK) signaling pathway, and the osteogenic differentiation of fibroblasts was enhanced by an AuNPs-hydrogel complex through the bone morphogenic protein (BMP) signaling pathway (Heo et al., 2014; Yi et al., 2010). Influence of various nanomaterials on stem cell differentiation was studied (Ilie et al., 2012). However, research regarding the effects of chitosan-AuNPs on the differentiation of hMSCs has not been reported.

In the present study, the effect of chitosan-AuNPs on the differentiation of human adipose-derived mesenchymal stem cells (hADSCs) as a switch to determine cell fate into osteoblasts and the relating signaling pathway in cell differentiation was investigated.

MATERIALS AND METHODS

Characterization of chitosan-conjugated AuNPs

In this study, the same chitosan-AuNPs which were examined in chapter II were used. In summary, positively charged AuNPs were prepared using the chitosan reduction method. The average diameter of chitosan-AuNPs was ~17 nm, and the zeta potentials were ~42 mV. The hydrodynamic diameters of chitosan-AuNPs were ~40 nm rom the dynamic light scattering measurements.

Culture of hADSCs

The hADSCs were purchased from ATCC (PCS-500-011) and cultured in low-glucose Dulbecco's modified Eagle's medium (Gibco, NY, USA) with 10% fetal bovine serum and 1% antibiotics (Sigma-Aldrich, St. Louis, USA) incubating at 37°C in 5% CO_2. The culture medium was replaced every 3 days during the experiments

TEM

The uptake of chitosan-AuNPs was examined using a transmission electron microscopy (TEM). The hADSCs were plated into 6-well culture plates at 3 × 10^3 cells/cm^2. After cell confluent, chitosan-AuNPs were added to the growth medium and incubated at 37°C in 5% CO_2 for 24 h. Analysis using a TEM was operated in the Integrative Research Support Center in School of Medicine, the

Catholic University of Korea.

Cell viability assay

The cell viability of hADSCs was assessed using a cell counting kit (CCK)-8 (Dojindo, Japan). Cells were seeded in 96-well culture plates at 3×10^3 cells/cm^2. After cell confluent, chitosan-AuNPs were added to the culture medium. Wells containing the culture medium and NPs without cells were used as blanks. After 72 h of incubation, 10 μL of the CCK-8 solution was added to the medium and incubated for 4 h at 37°C. The absorbance of the optical density (OD) at 450 nm was measured using a microplate reader (Tecan, Switzerland). The cell viability (%) was calculated according to the formula: $(OD_{sample}-OD_{blank})/(OD_{control}-OD_{blank}) \times 100$.

Proliferation of hADSCs

The proliferation of the hADSCs was determined using an alamarBlue® assay. Briefly, hADSCs were seeded in each well of 96-well plates at a density of 3×10^3 cells/cm^2 and incubated for 72 h. After cell confluent, an osteogenic-inducing medium (OM) containing 100 nM dexamethasone (Calbiochem, Germany), 50 μM L-ascorbic acid 2-phosphate sequimagnesium salt hydrate (Sigma-Aldrich, St. Louis, USA), and 10 mM beta-glycerophosphate disodium salt hydrate (Sigma-Aldrich, St. Louis, USA) was added to each well with different concentrations of chitosan-AuNPs and incubated for 10, 14, and 21 days. Wells containing OM and NPs without cells were used as blanks. At each

time point, 20 μL alamarBlue® solution (Invitrogen, NY, USA) was added to the medium and incubated for 4 h at 37°C. The absorbance at 570 nm and 620 nm was measured using a microplate reader (Tecan, Switzerland).

Alizarin red s for mineralization

The osteogenic differentiation rates of hADSCs in the presence of chitosan-AuNPs were determined by an alizarin red s (ARS) staining assay. The hADSCs were seeded in a six-well culture plates at a cell density of 3×10^3 cells/cm^2 and cultured for 10, 14, and 21 days in OM and chitosan-AuNPs. Briefly, the cells were fixed with 80% ethanol for 1 h at room temperature. After being washed with distilled water, they were stained with 60 mM ARS (pH 4.2) for 15 min at room temperature. A quantitation of ARS staining was performed by elution with 10% (w/v) cetylpyridinium chloride (Sigma-Aldrich, St. Louis, USA) for 20 min at room temperature, and the absorbance was measured at 570 nm. The mineralization ratio was normalized to the proliferation ratio.

Oil red o for lipid accumulation

The adipogenic differentiation rates of hADSCs in the presence of chitosan-AuNPs were determined by oil red o (ORO) staining assay. After osteogenic induction, cells were washed with distilled water, and stained with 0.6% (w/v) ORO solution (60% isopropanol) for 15 min at room temperature. For quantitation, cells were washed with distilled water to remove unbound dye, and 2 mL isopropyl alcohol was added to well of the culture plates. After 20 min,

the absorbance was measured by a microplate reader at 510 nm. The lipid accumulation ratio was normalized with proliferation ratio.

Real-time RT-PCR analysis

Total RNA was isolated from the differentiated cells, which were treated with chitosan-AuNPs for 10, 14, and 21 days using a Hybrid-R prep kit (GeneAll, Korea) according to the manufacturer's protocol. Reverse transcription was performed using M-MLV reverse transcriptase (Invitrogen, NY, USA). The relative mRNA expression of the osteogenic differentiation marker genes was normalized to the GAPDH gene and expressed as a fold change relative to the growth medium (GM) group. The PCR conditions were an initial step at 95°C for 30 sec and 40 denaturation cycles of 95°C for 5 sec and annealing at 60°C for 45 sec. Steps at 95°C for 15 sec, 60°C for 1 min, and 95°C for 15 sec was added to minimize nonspecific products. The results were analyzed by comparing the $2^{-[delta][delta]Ct}$ values of the mRNA of cells treated with chitosan-AuNPs to those of the cells in OM. Table 1 represents the list of primers used for real-time RT-PCR.

Table 1. Primers for real-time RT-PCR analysis

Gene (Acc. No.)	Sequences	Product size (bp)
Alkaline Phosphatase (NM_000478.4)	F 5'-CCTCCTCGGAAGACACTCTG-3' R 5'-GCAGTGAAGGGCTTCTTGTC-3'	139
Bone sialoprotein (NM_004967.3)	F 5'-AAAGTGAGAACGGGGAACCT-3' R 5'-GATGCAAAGCCAGAATGGAT-3'	161
Osteocalcin (NM_001199662.1)	F 5'-GACTGTGACGAGTTGGCTGA-3' R 5'-CTGGAGAGGAGCAGAACTGG-3'	119
GAPDH (NM_002046.4)	F 5'-CTCTGCTCCTCCTGTTCGAC-3' R 5'-ACGACCAAATCCGTTGACTC-3'	112

Western blotting analysis

A western blotting assay was applied to study the protein expressions of hADSCs related to the β-catenin signaling pathway. Proteins were extracted and subjected to 10% sodium dodecyl sulfate-polyacrylamide gel electrophoresis for the detection of active-form β-catenin, then transferred to polyvinylidene fluoride membranes. The membranes were blocked with 5% skim milk in tris-buffered saline with Tween 20 for 1 h at room temperature. Membranes were reacted with primary antibodies overnight at 4°C. Primary antibodies were as follows: anti-non-phosphorylated β-catenin (1:500, Millipore, MA, USA) and β-actin (1:1000, Santa Cruze, CA, USA), and the β-actin protein was used as the control.

Immunofluorescence for translocation of non-phosphorylated β-catenin into the nucleus

The hADSCs were plated to confocal dishes (Nunc™ Lab-Tek chamber slides, Thermo Scientific, MA, USA) at a density of 3×10^3 cells/cm^2 and cultured for 7, 10, 14, and 21 days in an OM treated with chitosan-AuNPs. The cells were fixed with 4% paraformaldehyde for 15 min. Fixed cells were incubated with an active-form β-catenin (Millipore, MA, USA) antibody for 48 h at 4°C, then incubated with a secondary antibody, which was conjugated with Alexa Flour® 555 for 1 h at room temperature. Cells were stained with 2-(4-amidinophenyl)-6-indolecarbamidine dihydrochloride (DAPI) for nucleus staining. Confocal images were acquired with a LSM 710 confocal laser

scanning microscope (Carl Zeiss, Germany) operated in the National Center for Inter- University Research Facilities (Seoul National University, Korea).

Statistical analysis

Data was generally presented as the mean ± standard error (SE), and the statistical differences between the experimental groups were analyzed by Student's *t*-test using statistical software Origin 8.0. $P < 0.05$ was considered statistically significant.

RESULTS

Uptake of chitosan-AuNPs in hADSCs

In order to identify uptake of chitosan-AuNPs in hADSCs, internalized chitosan-AuNPs at a concentration of 1 ppm were measured using a TEM. The concentration of chitosan-AuNPs added for TEM was 1 ppm. Most of the internalized chitosan-AuNPs were detected in cytosol as shown in Figure 1. However, in this TEM images, chitosan-AuNPs internalized into hADSCs were not inside endosomal vesicles.

Effect of chitosan-AuNPs on hADSC viability and proliferation

To determine the the effect of chitosan-AuNPs on cell viability and proliferation of hADSCs, cell viability assay and proliferation assay were performed. In cell viability assays, hADSCs were exposured for 72 h in a GM that did not contain osteogenic-inducing substances (Figure 2A). As shown in Figure 2A, chitosan-AuNPs had no effect on the cell viability of hADSCs at a concentration of up to 10 ppm. Also, to determine the proliferation of the hADSCs in osteogenic-inducing conditions, a proliferation assay was examined at 10, 14, and 21 days in an OM containing chitosan-AuNPs (Fig. 2B). This result indicates that the value of OD was significantly increased in all experimental groups in a time-dependent manner. However, there is no statistical significance in the difference

between the OM only group and the OM containing chitosan-AuNPs group.

Chitosan-AuNPs promote the osteogenic differentiation of hADSCs

In order to confirm the effect of chitosan-AuNPs on the osteogenic differentiation of hADSCs in osteogenic-inducing conditions, osteogenic differentiation was determined by measuring the mineralized calcium deposition. The result shows that the mineralized calcium deposition increased more in the hADSCs containing OM with chitosan-AuNPs group than in the OM only group in a time-dependent manner (Figure 3A). Statistical differences between the experimental groups were also analyzed by One-way ANOVA. Differences between experimental groups in 21 days were statistically significant ($p < 0.05$). In 21 day, the mineralized calcium deposition increased in the containing AuNPs groups up to 1.4-fold at a concentration of 0.5 ppm and 1.35-fold at 1 ppm, as compared to the OM only group (Figure 3B). Therefore, chitosan-AuNPs stimulated the differentiation of hADSCs by osteogenesis.

Expression of osteogenic differentiation specific genes in hADSCs

To measure the expressions of specific genes involved with the osteogenic differentiation of hADSCs in OM containing chitosan-AuNPs, real-time RT-PCR analysis was carried out. Statistical analysis was carried out by student's t-

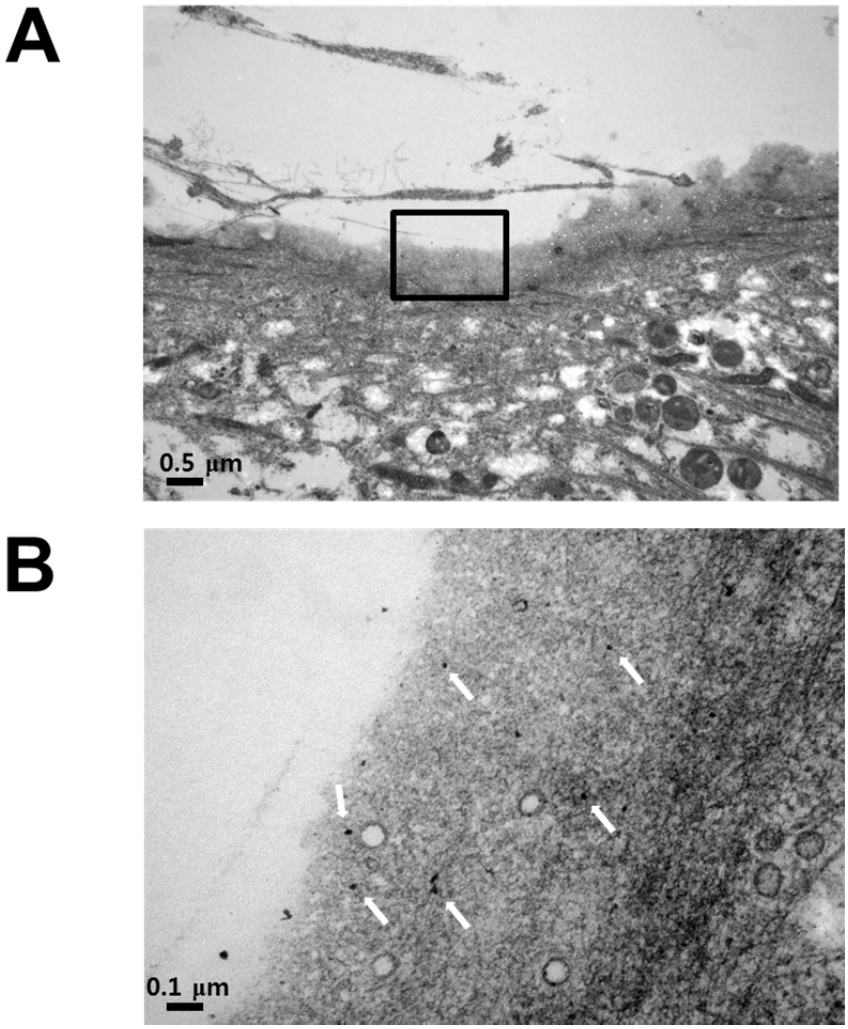

FIGURE 1. TEM images of hADSC exposed to chitosan-AuNPs. hADSCs were exposed to chitosan-AuNPs for 24 h and them fixed for TEM. (A) chitosan-AuNPs were internalized in cell membrane as magnified in the (B) image. The scale bars in the (A) and (B) are 0.5 μm and 0.1 μm.

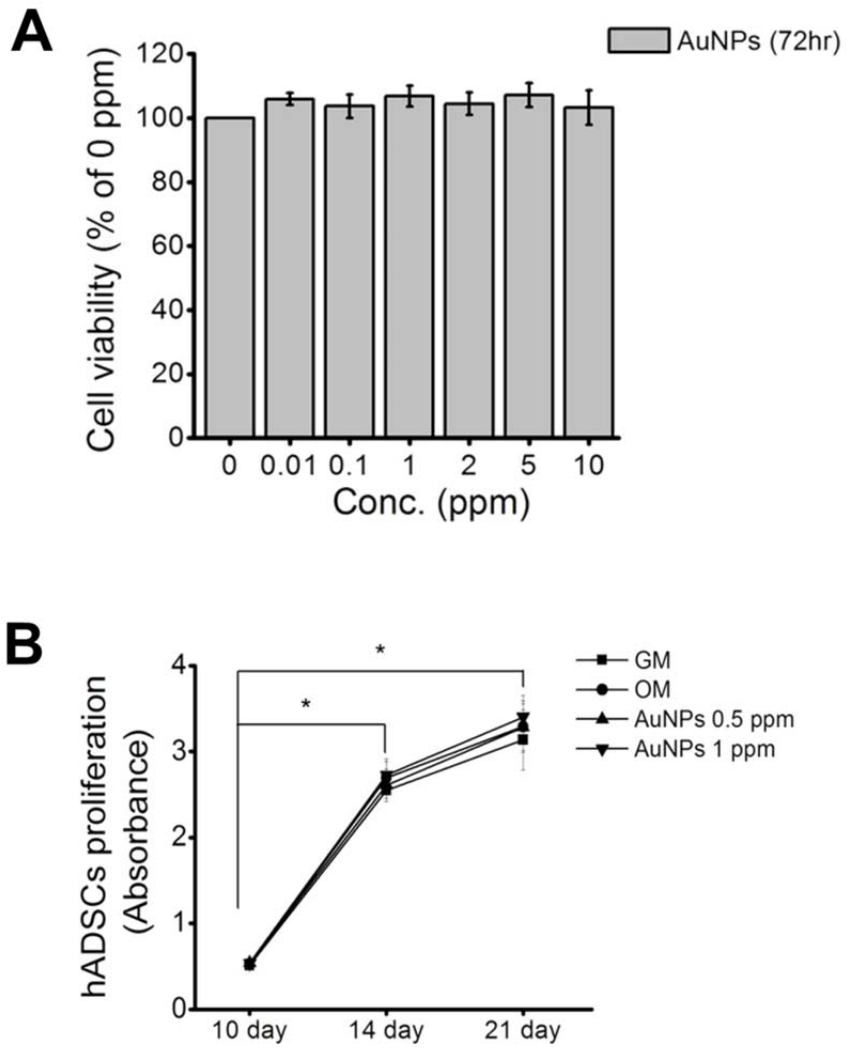

Figure 2. Effects of chitosan-AuNPs. (A) cell viability of hADSCs for 72 h in a growth medium (GM) (n = 6) and (B) cell proliferation of hADSCs for 10, 14, and 21 day after the induction of osteogenic differentiation (n = 5). Results are mean ± SE of the triplicate experiments.

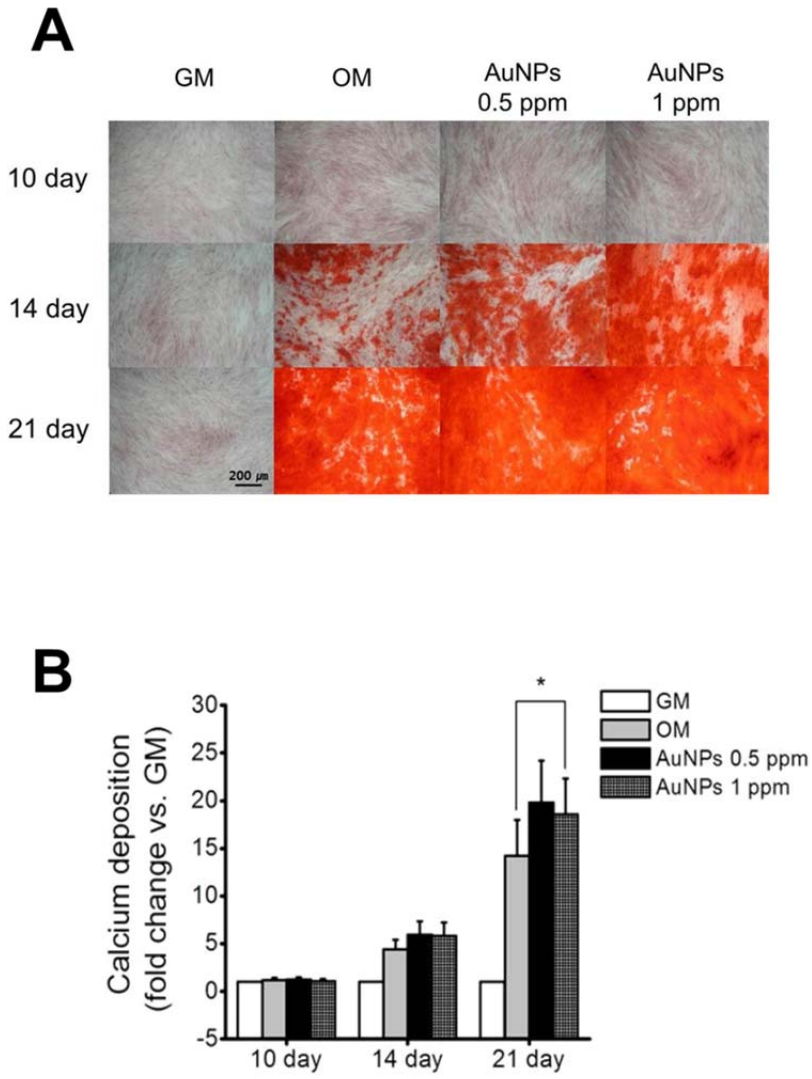

Figure 3. Effect of chitosan-AuNPs on the mineralization of hADSCs. (A) stained calcium deposition by alizarin red s (B) quantitation of mineralization through the elution of alizarin red s from stained mineral deposits (n = 6). Results are mean ± SE of the triplicate experiments, (*) $p < 0.05$.

test. The result shows that the alkaline phosphatase (ALP) mRNA expression level increased more in the cells containing chitosan-AuNPs group as compared to the OM only group at 10 day (Figure 4A). The ALP mRNA expression level in the OM only group showed a maximal value at 14 day, and it decreased at 21 day. In the OM containing chitosan-AuNPs group, the ALP mRNA expression levels increased at 10 day when compared to the OM only group, and the levels were sustained at 14 day and 21 day. Statistical differences of ALP expression between the experimental groups were also analyzed by One-way ANOVA. Differences between experimental groups in 14 days were statistically significant ($p < 0.05$). The BSP mRNA expression levels in the OM containing chitosan-AuNPs group at 0.5 ppm and 1 ppm were higher than in the OM only group at 14 day and 21 day (Figure 4B). In the OM only group, the bone sialoprotein (BSP) mRNA level decreased in a time-dependent manner. However, the BSP mRNA level in the OM containing chitosan-AuNPs group increased up to 14 day and then decreased at 21 day, as compared to the OM only group. The osteocalcin (OSC) mRNA expression levels in the OM containing chitosan-AuNPs group were significantly higher than in the OM only group at 10 day and 14 days (Figure 4C). Statistical differences of OSC expression between the experimental groups were also analyzed by One-way ANOVA. Differences between experimental groups in 10 days and 14 days were statistically significant ($p < 0.05$).

Figure 4. mRNA expression of osteogenic marker genes in hADSCs treated with chitosan-AuNPs for 10, 14, and 21 day. (A) alkaline phosphatase (ALP); (B) bone sialoprotein (BSP); (C) osteocalcin (OSC) (n = 9). Results are mean ± SE of the triplicate experiments.

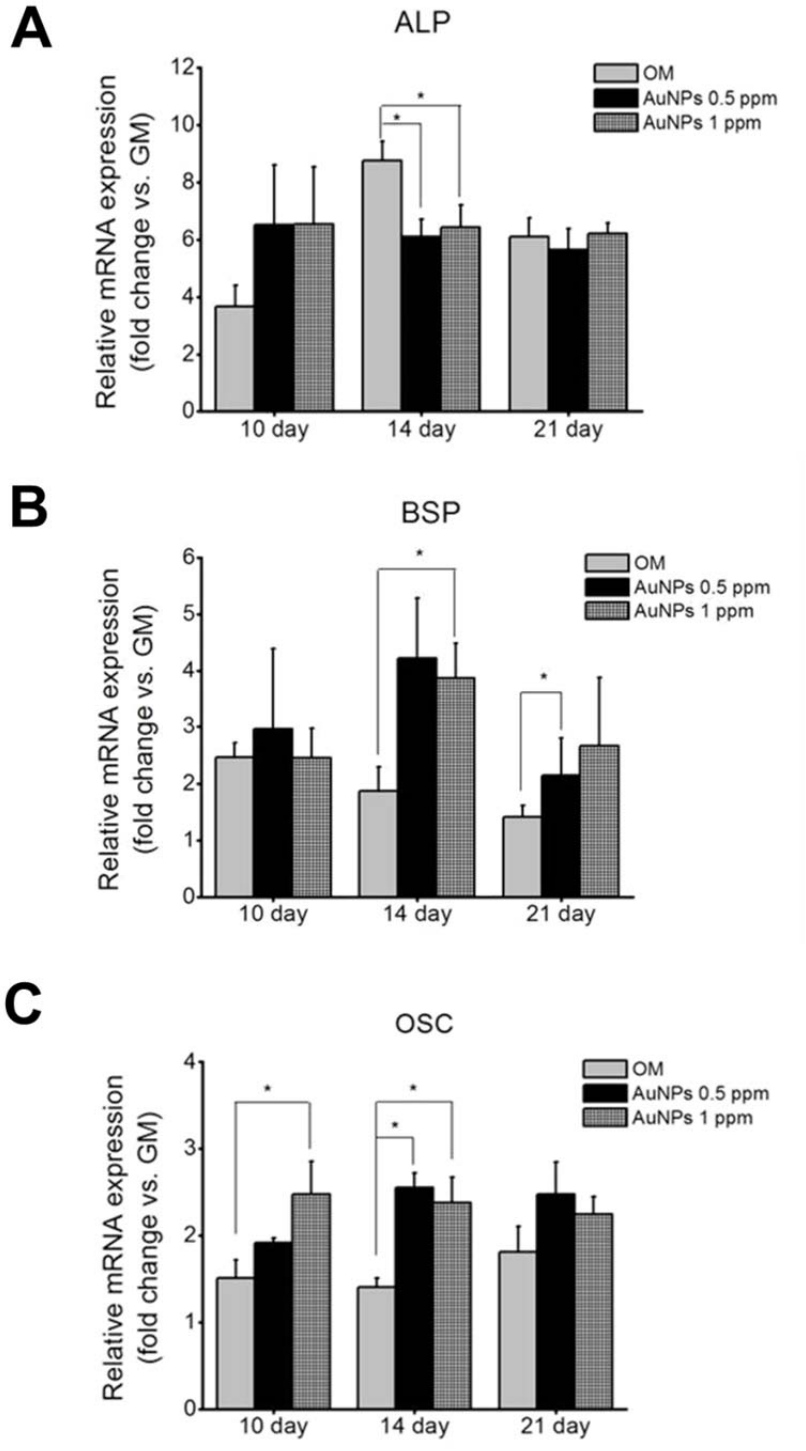
A
ALP
Relative mRNA expression
(fold change vs. GM)
OM
AuNPs 0.5 ppm
AuNPs 1 ppm
10 day
14 day
21 day
B
BSP
C
OSC

Chitosan-AuNPs do not affect the adipogenic differentiation in osteogenic- inducing hADSCs

The effect of chitosan-AuNPs on the adipogenic differentiation of hADSCs in osteogenic-inducing conditions was determined by measuring lipid droplets stained by ORO dye. In our study, the accumulation of lipid droplets was slightly increased in the OM only group and the OM containing chitosan-AuNPs group (Figure 5). However, the degree of accumulation was weak when compared to the mineralization, and it was similar between the OM only group and the OM containing chitosan-AuNPs group. Therefore, the adipogenic differentiation of hADSCs was not induced by chitosan-AuNPs in OM conditions.

Chitosan-AuNPs enhance the osteogenic differentiation of hADSCs through the Wnt/β-catenin signaling pathway

To confirm the signaling pathway related to osteogenic differentiation in hADSCs, we examined non-phosphorylated β-catenin in protein levels. Non-phosphorylated β-catenin protein levels increased in the OM containing chitosan-AuNPs group at 7 day, as compared to the OM only group (Figure 6A). The translocation of non-phosphorylated β-catenin into the nuclei of the OM group was determined by using an immunofluorescent antibody (Figure 6B). The translocation of non- phosphorylated β-catenin into nuclei of the OM containing chitosan-AuNPs group was greater than in the OM only group at 7

day and 10 day. After 10 day, the degree of translocated non-phosphorylated β-catenin proteins was similar between the OM only group and the OM containing chitosan-AuNPs group.

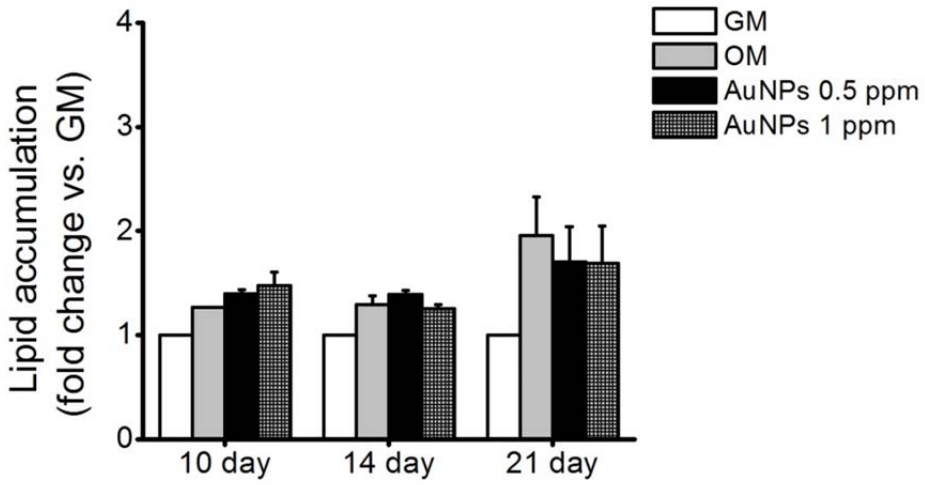

Figure 5. Effect of chitosan-AuNPs on adipogenic differentiation. Lipid accumulation of hADSCs treated with chitosan-AuNPs after 10, 14, and 21 day of culturing (n = 5). Results are mean ± SE of the triplicate experiments.

Figure 6. Activation of the osteogenic signaling pathway by chitosan-AuNPs. (A) western blot analysis of the non-phosphorylated β-catenin protein expression after treatment with chitosan-AuNPs for 7 day. (B) translocation of non-phosphorylated β-catenin into the nuclei of hADSCs treated with chitosan-AuNPs for 7, 10, 14, and 21 day.

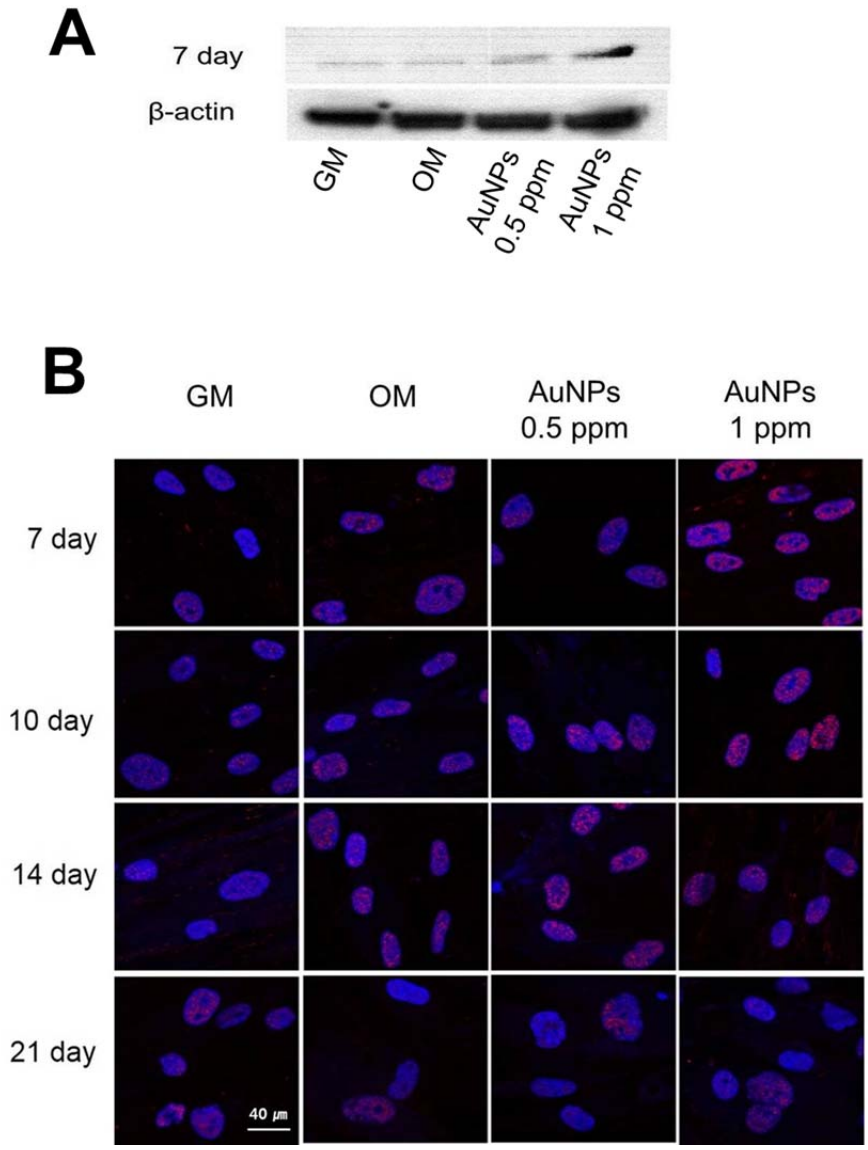
A
7 day
β-actin
GM
OM
AuNPs 0.5 ppm
AuNPs 1 ppm
B
GM
OM
AuNPs 0.5 ppm
AuNPs 1 ppm
7 day
10 day
14 day
21 day
40 μm

DISCUSSION

In the present study, we identified the promoting effect of chitosan-AuNPs on osteogenic differentiation of hADSCs through accumulation of activated phosphorylated beta-catenin into nucleus.

Recent studies suggest that the anionic AuNPs are endocytosed into cells, while half the amounts of cationic AuNPs escape the endocytotic pathway (Cho et al., 2009). Cationic AuNPs may directly diffuse into cytosol by generating disruption on the cell membrane (Lin et al., 2010a). The results indicate that chitosan-AuNPs entered into hADSCs through direct diffusion or escaping the endocytotic pathway. The degree of uptake and subcellular localization in cell systems shows different cytotoxicity (Xia et al., 2006). In particular, gold nanostars located in the nucleus are more toxic compared to the gold nanostars located in the cytosol (Dam et al., 2012). Therefore, it is possible that chitosan-AuNPs located in membrane is lack of cytotoxicity in hADSCs.

Over the past few years, the interactions of AuNPs with cell have been researched to confirm their uptake, distribution, and cytotoxicity. Recent evidence indicates that AuNPs decrease cell viability and differentiation of bone marrow MSCs through triggered necrosis by excessive ROS generation (Fan et al., 2011). In particular, excessive reactive oxygen species (ROS) cause damage to MSCs, whereas low levels of ROS enhance osteogenesis of MSCs (Atashi et al., 2015). According to results, chitosan-AuNPs enhance osteogenic differentiation of hADSCs. Pristine AuNPs without any appropriate

modifications are generally unstable because of high surface energy. Thus, a stabilizer should be added to apply AuNPs into cells (Alanazi et al., 2010). In the present study, chitosan was used in the reduction of AuNPs as a stabilizer. Several researches suggest that chitosan enhance mineralization of bone marrow-derived hMSCs by upregulating genes associated with mineralization and calcium-binding proteins (Mathews et al., 2011; Muzzarelli, 2011). In particular, multiwall carbon nanotube scaffolds modified with chitosan enhance proliferation and mineralization of MG-63 cells more than chitosan scaffolds (Venkatesan et al., 2012). Corresponding with previous studies, chitosan-AuNPs stimulate osteogenic differentiation of hADSCs on conditions not reduced cell viability.

In the osteogenic differentiation of hMSCs, bone formation is a complex biological process involving several tightly regulated gene expression patterns of bone-related proteins, and specific marker genes, such as OSC, osteopontin, and BSP, were expressed according to the progress of differentiation (Stein and Lian, 1993). ALP is a key regulator of the early-stage differentiation of bone marrow stromal cells, and gradually decreased as proceeding through differentiation into osteoblasts (Malaval et al., 1994). Lian and Stein (1995) suggest that the peak levels of the ALP mRNA represent the matrix maturation period, and the cellular levels of the ALP mRNA in the heavily mineralized stage decreased (Lian and Stein, 1995). The BSP gene is up-regulated by promoting bone formation (Ganss et al., 1999), and the OSC gene is a key marker for the late maturation of osteoblasts and the expression of OSC is concomitantly up-regulated by more advanced osteoblasts (Choi et al., 2011;

Stein and Lian, 1993). According to the integrated real-time RT-PCR results, the expressions of the osteogenic marker genes are more activated by the chitosan-AuNPs group.

Several studies demonstrate that the Wnt/β-catenin signaling pathway is initially involved in osteoblast differentiation (D'Alimonte et al., 2013; Guidotti et al., 2013; Heo et al., 2010). Wnt/β-catenin signaling inhibits adipogenic differentiation and alters the cell fate from adipocyte to osteoblast in hADSCs (Li et al., 2008). Some studies suggest that various type of nanoparticles act in hMSCs by different action mechanism. Adipogenic and osteogenic differentiation of hMSCs added with silver nanoparticles is inhibited by the Ag^{+} ion, which suppresses the expression of marker genes, and SH-SY5Y cells treated with silver nanoparticles differentiate into neuronal cells through ROS activating the ERK-AKT pathway (Dayem et al., 2014; Sengstock et al., 2014). Also, AuNPs enhance the osteogenic differentiation of mesenchymal stem cells through the activation of the MAPK and bone morphogenic protein signaling pathways (Heo et al., 2014; Yi et al., 2010). However, the mechanism of the action of the chitosan-AuNPs in hADSCs has not been clear. Several researches suggested that mechanical stimulation by AuNPs enhance osteogenesis and inhibit adipogenesis through activation of Wnt/β-catenin signaling (Case et al., 2008; Niziolek et al., 2012; Robinson et al., 2006; Sen et al., 2008). According to results, stimulation by uptake of chitosan-AuNPs in hADSCs promote the differentiation of hADSCs into osteoblasts through non-phosphorylated β-catenin accumulation, as it enhances the switching of the hADSC cell fate from adipocyte to osteoblast.

GENERAL CONCLUSION

Due to their unique characteristics, gold nanoparticles (AuNPs) are new potential tools for medical therapeutic treatments including drug delivery and promoting the regenerations of damaged tissues. AuNPs are known to be less toxic than other types of nanoparticles (NPs) and easily functionalized with various polymers.

In particular, citrate- and chitosan-AuNPs used in this study are less toxic than silver nanoparticles on human lung adenocarcinoma cells. In previous study, cell viability was decreased by silver nanoparticles at concentrations from 0 μg/mL to 2.8 μg/mL as concentration-dependent manner, and IC_{50} value was calculated at 0.8 μg/mL (n=3) which value is 30-fold less than IC_{50} of AuNPs (data not shown). However, because even a small amount of AuNPs toxicity can have an adverse effect on cells, estimating cytotoxicity prior to application in any medical fields is important.

Taking the above results as a whole, Figure 1 demonstrates in detail the effects of surface-modified AuNPs on cells. Surface-modified AuNPs with citrate and chitosan have cytotoxic effects on human lung cancer cells as concentration-dependent manners. Positively charged chitosan-AuNPs were more easily absorbed than negatively charged citrate-AuNPs by cancer cells due to electric interaction with the charged surface of the AuNPs and a negatively charged plasma membrane. As a result, the plasma membrane was more ruptured by positively charged chitosan-AuNPs. In absorbing AuNPs, extrinsic

and intrinsic apoptosis mechanisms were activated by citrate-AuNPs. On the other hand, the apoptosis mechanism and necrosis were activated by chitosan-AuNPs. Therefore, positively charged chitosan-AuNPs were more toxic than negatively charged citrate-AuNPs in human lung cancer cells. In addition, the effect of citrate- and chitosan-AuNPs on cell functions was different. The expression of the microRNAs was altered by the citrate- and chitosan-AuNPs. The microRNAs altered by the citrate-AuNPs were involved in cell migration and metastasis at the concentration that decreased cell viability by 20%. The microRNAs up-regulated by chitosan-AuNPs were related to cell cycle, apoptosis, and cell differentiation at the concentration that decreased cell viability by 20%. In addition, the microRNAs down-regulated by chitosan-AuNPs were related to proliferation, apoptosis, and differentiation. Based on microRNA expression profiling results, cell functions such as cell development and differentiation were altered by the exposure of chitosan-AuNPs. Thus, the uptake of chitosan-AuNPs in human adipose-derived mesenchymal stem cells induced osteogenic differentiation through activation of a cell differentiation related signaling pathway by chitosan-AuNPs at the concentration that does not decrease cell viability.

The AuNPs synthesized with adding stabilizer such as citrate and chitosan can present cytotoxicity on human cells depending on concentrations even though AuNPs stabilizing with citrate or chitosan are known to be less toxic than other NPs. Furthermore, the exposure of citrate- and chitosan-AuNPs alters cell functions at microRNA expression level. Thus, this study propose that surface-modified AuNPs stabilized with chitosan can be used to promote

osteogenic differentiation of human mesenchymal stem cells at a concentration that does not induce cell death after evaluating cytotoxic concentrations in damaged tissue regeneration.

Figure 1. Summary of uptake and effect of citrate- and chitosan-AuNPs on human cells. Red arrows indicate activated apoptosis mechanism by citrate-AuNPs. Yellow arrows indicate apoptosis mechanism and necrosis by chitosan-AuNPs. Blue line arrows indicate alteration of microRNA expression related to cell functions by citrate- and chitosan-AuNPs.

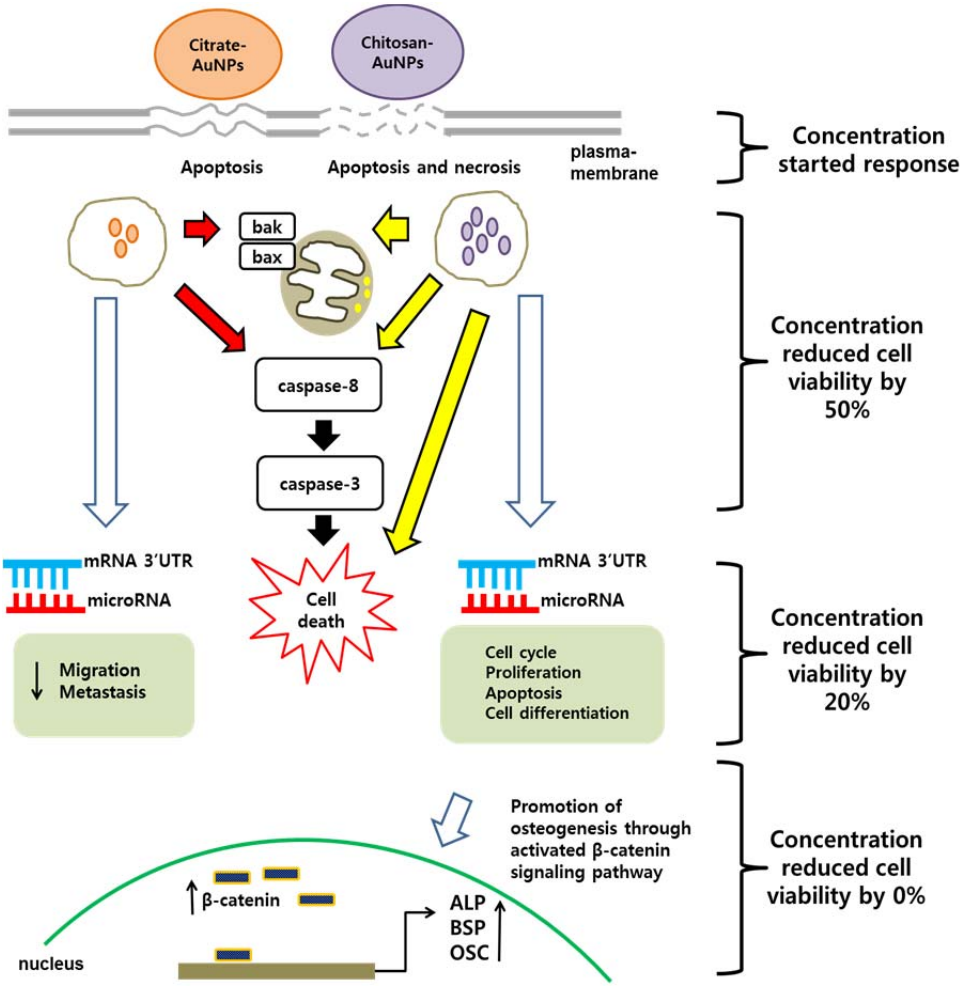
Citrate-AuNPs
Chitosan-AuNPs
plasma-membrane
Apoptosis
Apoptosis and necrosis
Concentration started response
bak
bax
caspase-8
caspase-3
Concentration reduced cell viability by 50%
mRNA 3'UTR
microRNA
Cell death
Migration
Metastasis
mRNA 3'UTR
microRNA
Cell cycle
Proliferation
Apoptosis
Cell differentiation
Concentration reduced cell viability by 20%
Promotion of osteogenesis through activated β-catenin signaling pathway
β-catenin
ALP
BSP
OSC
nucleus
Concentration reduced cell viability by 0%

REFERENCES

Agawane, G.L., Shin, S.W., Moholkar, A.V., Gurav, K.V., Yun, J.H., Lee, J.Y., Kim, J.H., 2012. Non-toxic complexing agent tri-sodium citrate's effect on chemical bath deposited ZnS thin films and its growth mechanism. J Alloy Compd. 535**,** 53-61.

Ahamed, M., Akhtar, M.J., Siddiqui, M.A., Ahmad, J., Musarrat, J., Al-Khedhairy, A.A., AlSalhi, M.S., Alrokayan, S.A., 2011. Oxidative stress mediated apoptosis induced by nickel ferrite nanoparticles in cultured A549 cells. Toxicology. 283**,** 101-108.

Akhtar, M.J., Ahamed, M., Kumar, S., Siddiqui, H., Patil, G., Ashquin, M., Ahmad, I., 2010. Nanotoxicity of pure silica mediated through oxidant generation rather than glutathione depletion in human lung epithelial cells. Toxicology. 276**,** 95-102.

Alanazi, F.K., Radwan, A.A., Alsarra, I.A., 2010. Biopharmaceutical applications of nanogold. Saudi Pharm J. 18**,** 179-193.

Albanese, A., Chan, W.C., 2011. Effect of gold nanoparticle aggregation on cell uptake and toxicity. ACS Nano. 5**,** 5478-5489.

Alivisatos, A.P., 1996. Semiconductor clusters, nanocrystals, and quantum dots. Science. 271**,** 933-937.

Alkilany, A.M., Murphy, C.J., 2010. Toxicity and cellular uptake of gold nanoparticles: what we have learned so far? J Nanopart Res. 12**,** 2313-2333.

Alvarez-Garcia, I., Miska, E.A., 2005. MicroRNA functions in animal development and human disease. Development. 132**,** 4653-4662.

Alwi, R., Telenkov, S., Mandelis, A., Leshuk, T., Gu, F., Oladepo, S., Michaelian, K., 2012. Silica-coated super paramagnetic iron oxide nanoparticles (SPION) as biocompatible contrast agent in biomedical photoacoustics. Biomed Opt Express. 3**,** 2500-2509.

Arnida, Malugin, A., Ghandehari, H., 2010. Cellular uptake and toxicity of gold nanoparticles in prostate cancer cells: a comparative study of rods and

spheres. J Appl Toxicol. 30**,** 212-217.

Arora, S., Jain, J., Rajwade, J.M., Paknikar, K.M., 2008. Cellular responses induced by silver nanoparticles: In vitro studies. Toxicol Lett. 179**,** 93-100.

Arvizo, R.R., Miranda, O.R., Thompson, M.A., Pabelick C.M., Bhattacharya, R., Robertson, J.D., Rotello, V.M., Prakash, Y.S., Mukherjee, P., 2010. Effect of nanoparticle surface charge at the plasma membrane and beyond. Nano Lett. 10**,** 2543-2548.

Atashi, F., Modarressi, A., Pepper, M.S., 2015. The role of reactive oxygen species in mesenchymal stem cell adipogenic and osteogenic differentiation: a review. Stem Cells Dev. 24**,** 1150-1163.

Auffan, M., Rose, J., Bottero, J.Y., Lowry, G.V., Jolivet, J.P., Wiesner, M.R., 2009. Towards a definition of inorganic nanoparticles from an environmental, health and safety perspective. Nat Nanotechnol. 4**,** 634-641.

Baek, D., Villen, J., Shin, C., Camargo, F.D., Gygi, S.P., Bartel, D.P., 2008. The impact of microRNAs on protein output. Nature. 455**,** 64-71.

Bakhshandeh, B., Soleimani, M., Hafizi, M., Paylakhi, S.H., Ghaemi, N., 2012a. MicroRNA signature associated with osteogenic lineage commitment. Mol Biol Rep. 39**,** 7569-7581.

Bakhshandeh, B., Soleimani, M., Paylakhi, S.H., Ghaemi, N., 2012b. A microRNA signature associated with chondrogenic lineage commitment. J Genet. 91**,** 171-182.

Bakthavathsalam, P., Rajendran, V.K., Mohammed, J.A.B., 2012. A direct detection of Escherichia coli genomic DNA using gold nanoprobes. J Nanobiotech. 10, 1-10.

Banker, D.E., Groudin, M., Norwood, T., Appelbaum, F.R., 1997. Measurement of spontaneous and therapeutic agent-induced apoptosis with BCL-2 protein expression in acute myeloid leukemia. Blood. 89**,** 243-255.

Bartel, D.P., 2004. MicroRNAs: genomics, biogenesis, mechanism, and function. Cell. 116**,** 281-297.

Bastus, N.G., Comenge, J., Puntes, V., 2011. Kinetically controlled seeded growth synthesis of citrate-stabilized gold nanoparticles of up to 200 nm: size focusing versus ostwald ripening. Langmuir. 27**,** 11098-11105.

Beer, C., Foldbjerg, R., Hayashi, Y., Sutherland, D.S., Autrup, H., 2012. Toxicity of silver nanoparticles-nanoparticle or silver ion? Toxicol Lett. 208**,** 286-292.

Betel, D., Wilson, M., Gabow, A., Marks, D.S, Sander, C., 2008. The microRNA.org resource: targets and expression. Nucleic Acids Res. 36**,** D149-153.

Blasiak, B., van Veggel, F.C.J.M., Tomanek, B., 2013. Applications of nanoparticles for MRI cancer diagnosis and therapy. J Nanomater. 2013, ID148578.

Boatright, K.M., Salvesen, G.S., 2003. Mechanisms of caspase activation. Curr Opin Cell Biol. 15**,** 725-731.

Boisselier, E., Astruc, D., 2009. Gold nanoparticles in nanomedicine: preparations, imaging, diagnostics, therapies and toxicity. Chem Soc Rev. 38**,** 1759-1782.

Bollati, V., Marinelli, B., Apostoli, P., Bonzini, M., Nordio, F., Hoxha, M., Pegoraro, V., Motta, V., Tarantini, L., Cantone, L., Schwartz, J., Bertazzi, P.A., Baccarelli, A., 2010. Exposure to metal-rich particulate matter modifies the expression of candidate microRNAs in peripheral blood leukocytes. Environ Health Perspect. 118**,** 763-768.

Bose, T., Latawiec, D., Mondal, P.P., Mandal, S., 2014. Overview of nano-drugs characteristics for clinical application: the journey from the entry to the exit point. J Nanopart Res. 16. 1-25.

Bourdon, J.A., Saber, A.T., Halappanavar, S., Jackson, P.A., Wu, D., Houggard, K.S., Jacobsen, N.R., Williams, A., Vogel, U., Wallin, H., Yauk, C.L., 2012. Carbon black nanoparticle intratracheal installation results in large and sustained changes in the expression of miR-135b in mouse lung. Environ Mol Mutagen. 53**,** 462-468.

Bouwmeester, H., Dekkers, S., Noordam, M.Y., Hagens, W.I., Bulder, A.S., de

Heer, C., ten Voorde, S.E., Wijbhoven, S.W., Marvin, H.J., Sips, A.J., 2009. Review of health safety aspects of nanotechnologies in food production. Regul Toxicol Pharm. 53**,** 52-62.

Brandenberger, C., Muhlfeld, C., Ali, Z., Lenz, A.G., Schmid, O., Parak, W.J., Gehr, P., Rothen-Rutishauser, B., 2010. Quantitative evaluation of cellular uptake and trafficking of plain and polyethylene glycol-coated gold nanoparticles. Small. 6**,** 1669-1678.

Burda, C., Chen, X., Narayanan, R., El-Sayed, M.A., 2005. Chemistry and properties of nanocrystals of different shapes. Chem Rev. 105**,** 1025-1102.

Burklew, C.E., Ashlock, J., Winfrey, W.B., Zhang, B., 2012. Effects of aluminum oxide nanoparticles on the growth, development, and microRNA expression of tobacco (Nicotiana tabacum). PLoS One. 7**,** e34783.

Calin, G.A., Liu, C.G., Sevignani, C., Ferracin, M., Felli, N., Dumitru, C.D., Shimizu, M., Cimmino, A., Zupo, S., Dono, M., Dell'Aquila, M.L., Alder, H., Rassenti, L., Kipps, T.J., Bullrich, F., Negrini, M., Croce, C.M., 2004. MicroRNA profiling reveals distinct signatures in B cell chronic lymphocytic leukemias. Proc Natl Acad Sci U S A. 101**,** 11755-11760.

Case, N., Ma, M., Sen, B., Xie, Z., Gross, T.S., Rubin, J., 2008. Beta-catenin levels influence rapid mechanical responses in osteoblasts. J Biol Chem. 283**,** 29196-29205.

Castro-Sesquen, Y.E., Gilman, R.H., Galdos-Cardenas, G., Ferrufino, L., Sanchez, G., Valencia Ayala, E., Liotta, L., Bern, C., Luchini, A., Working group on chagas disease in, Bolivia and Peru, 2014. Use of a novel chagas urine nanoparticle test (chunap) for diagnosis of congenital chagas disease. PLoS Negl Trop Dis. 8**,** e3211.

Chao, T.I., Xiang, S., Chen, C.S., Chin, W.C., Nelson, A.J., Wang, C., Lu, J., 2009. Carbon nanotubes promote neuron differentiation from human embryonic stem cells. Biochem Biophys Res Commun. 384**,** 426-430.

Chao, T.I., Xiang, S., Lipstate, J.F., Wang, C., Lu, J., 2010. Poly(methacrylic acid)-grafted carbon nanotube scaffolds enhance differentiation of hESCs into neuronal cells. Adv Mater. 22**,** 3542-3547.

Chen, H.T., Lee, M.J, Chen, C.H., Chuang, S.C., Chang, L.F., Ho, M.L., Hung, S.H., Fu, Y.C., Wang, Y.H., Wang, H.I., Wang, G.J., Kang, L., Chang, J.K., 2012. Proliferation and differentiation potential of human adipose-derived mesenchymal stem cells isolated from elderly patients with osteoporotic fractures. J Cell Mol Med. 16**,** 582-593.

Chen, L., Hou, J., Ye, L., Chen, Y., Cui, J., Tian, W., Li, C., Liu, L., 2014. MicroRNA-143 regulates adipogenesis by modulating the MAP2K5-ERK5 signaling. Sci Rep. 4**,** 3819.

Chithrani, B.D., Ghazani, A.A., Chan, W.C., 2006. Determining the size and shape dependence of gold nanoparticle uptake into mammalian cells. Nano Lett. 6**,** 662-668.

Cho, E.C., Xie, J., Wurm, P.A., Xia, Y., 2009. Understanding the role of surface charges in cellular adsorption versus internalization by selectively removing gold nanoparticles on the cell surface with a I2/KI etchant. Nano Lett. 9**,** 1080-1084.

Choi, M.H., Noh, W.C., Park, J.W., Lee, J.M., Suh, J.Y., 2011. Gene expression pattern during osteogenic differentiation of human periodontal ligament cells in vitro. J Periodontal Implant Sci. 41**,** 167-175.

Choi, S.Y., Jeong, S., Jang, S.H., Park, J., Park, J.H., Ock, K.S., Lee, S.Y., Joo, S.W., 2012. In vitro toxicity of serum protein-adsorbed citrate-reduced gold nanoparticles in human lung adenocarcinoma cells. Toxicol In Vitro. 26**,** 229-237.

Clift, M.J.D., Rothen-Rutishauser, B., Brown, D.M., Duffin, R., Donaldson, K., Proudfoot, L, Guy, K., Stone, V., 2008. The impact of different nanoparticle surface chemistry and size on uptake and toxicity in a murine macrophage cell line. Toxicol Appl Pharmacol. 232**,** 418-427.

Compston, J.E., Flahive, J., Hooven, F.H., Anderson, F.A.Jr., Adachi, J.D., Boonen, S., Chapurlat, R.D., Cooper, C., Diez-Perez, A., Greenspan,

S.L., LaCroix, A.Z., Lindsay, R., Netelenbos, J.C., Pfeischifter, J., Roux, C., Saag, K.G., Silverman, S., Siris, E.S., Watts, N.B., Gehlbach, S.H., Glow Investigators, 2014. Obesity, health-care utilization, and health-related quality of life after fracture in postmenopausal women: global longitudinal study of osteoporosis in women (GLOW). Calcif Tissue Int. 94**,** 223-231.

Connor, E.E., Mwamuka, J., Gole, A., Murphy, C.J., Wyatt, M.D., 2005. Gold nanoparticles are taken up by human cells but do not cause acute cytotoxicity. Small. 1**,** 325-327.

Coulter, J.A., Jain, S., Butterworth, K.T., Taggart, L.E., Dickson, G.R., McMahon, S.J., Hyland, W.B., Muir, M.F., Trainor, C., Hounsell, A.R., O'Sullivan, J.M., Schettino, G., Currell, F.J., Hirst, D.G., Prise, K.M., 2012. Cell type-dependent uptake, localization, and cytotoxicity of 1.9 nm gold nanoparticles. Int J Nanomed. 7**,** 2673-2685.

Cregan, S.P., MacLaurin, J.G., Craig, C.G., Robertson, G.S., Nicholson, D.W., Park, D.S., Slack, R.S., 1999. Bax-dependent caspase-3 activation is a key determinant in p53-induced apoptosis in neurons. J Neurosci. 19**,** 7860-7869.

Creighton, C.J., Nagaraja, A.K., Hanash, S.M., Matzuk, M.M., Gunaratne, P.H., 2008. A bioinformatics tool for linking gene expression profiling results with public databases of microRNA target predictions. RNA. 14**,** 2290-2296.

D'Alimonte, I., Lannutti, A., Pipino, C., Di Tomo, P., Pierdomenico, L., Cianci, E., Antonucci, I., Marchisio, M., Romano, M., Stuppia, L., Caciagli, F., Pandolfi, A., Ciccarelli, R., 2013. Wnt signaling behaves as a "master regulator" in the osteogenic and adipogenic commitment of human amniotic fluid mesenchymal stem cells. Stem Cell Rev. 9**,** 642-654.

Dam, D.H., Lee, J.H., Sisco, P.N., Co, D.T., Zhang, M., Wasielewski, M.R., Odom, T.W., 2012. Direct observation of nanoparticle-cancer cell nucleus interactions. ACS Nano. 6**,** 3318-3326.

Daniel, M.C., Astruc, D., 2004. Gold nanoparticles: assembly, supramolecular

chemistry, quantum-size-related properties, and applications toward biology, catalysis, and nanotechnology. Chem Rev. 104**,** 293-346.

Darlington, T.K., Neigh, A.M., Spencer, M.T., Nguyen, O.T., Oldenburg, S.J., 2009. Nanoparticle characteristics affecting environmental fate and transport through soil. Environ Toxicol Chem. 28**,** 1191-1199.

Dayem, A.A., Kim, B., Gurunathan, S., Choi, H.Y., Yang, G., Saha, S.K., Han, D., Han, J., Kim, K., Kim, J.H., Cho, S.G., 2014. Biologically synthesized silver nanoparticles induce neuronal differentiation of SH-SY5Y cells via modulation of reactive oxygen species, phosphatases, and kinase signaling pathways. Biotechnol J. 9**,** 934-943.

De Jong, W.H., Borm, P.J.A., 2008. Drug delivery and nanoparticles: applications and hazards. Int J Nanomed. 3**,** 133-149.

Delong, R.K., Reynolds, C.M., Malcolm, Y., Schaeffer, A., Severs, T., Wanekaya, A., 2010. Functionalized gold nanoparticles for the binding, stabilization, and delivery of therapeutic DNA, RNA, and other biological macromolecules. Nanotechnol Sci Appl. 3**,** 53-63.

Dembereldorj, U., Choi, S.Y., Ganbold, E.O., Song, N.W., Kim, D., Choo, J., Lee, S.Y., Kim, S., Joo, S.W., 2014. Gold nanorod-assembled PEGylated graphene-oxide nanocomposites for photothermal cancer therapy. Photochem Photobiol. 90**,** 659-666.

Duceppe, N., Tabrizian, M., 2010. Advances in using chitosan-based nanoparticles for in vitro and in vivo drug and gene delivery. Expert Opin Drug Deliv. 7**,** 1191-1207.

Duchesne, L., Gentili, D., Comes-Franchini, M., Fernig, D.G., 2008. Robust ligand shells for biological applications of gold nanoparticles. Langmuir. 24**,** 13572-13580.

Dweep, H., Sticht, C., Pandey, P., Gretz, N., 2011. miRWalk--database: prediction of possible miRNA binding sites by "walking" the genes of three genomes. J Biomed Inform. 44**,** 839-847.

El-Sayed, M.A., 2004. Small is different: shape-, size-, and composition-dependent properties of some colloidal semiconductor nanocrystals.

Acc Chem Res. 37, 326-333.

Eustis, S., el-Sayed, M.A., 2006. Why gold nanoparticles are more precious than pretty gold: noble metal surface plasmon resonance and its enhancement of the radiative and nonradiative properties of nanocrystals of different shapes. Chem Soc Rev. 35, 209-217.

Fan, J.H., Li, W.T., Hung, W.I., Chen, C.P., Yeh, J.M., 2011. Cytotoxicity and differentiation effects of gold nanoparticles to human bone marrow mesenchymal stem cells. Biomed Engineer: Appli, Basis and Comm. 23, 141-152.

Fang, C., Bhattarai, N., Sun, C., Zhang, M., 2009. Functionalized nanoparticles with long-term stability in biological media. Small. 5, 1637-1641.

Faunce, T.A., White, J., Matthaei, K.I., 2008. Integrated research into the nanoparticle-protein corona: a new focus for safe, sustainable and equitable development of nanomedicines. Nanomedicine (Lond). 3, 859-866.

Ferrari, M., 2005. Cancer nanotechnology: opportunities and challenges. Nat Rev Cancer. 5, 161-171.

Frazier, T.P., Burklew, C.E., Zhang, B., 2014. Titanium dioxide nanoparticles affect the growth and microRNA expression of tobacco (Nicotiana tabacum). Funct Integr Genomics. 14, 75-83.

Frohlich, E., 2012. The role of surface charge in cellular uptake and cytotoxicity of medical nanoparticles. Int J Nanomed. 7, 5577-5591.

Ganss, B., Kim, R.H., Sodek, J., 1999. Bone sialoprotein. Crit Rev Oral Biol Med. 10, 79-98.

Geiser, M., Rothen-Rutishauser, B., Kapp, N., Schurch, S., Kreyling, W., Schulz, H., Semmler, M., Im Hof, V., Heyder, J., Gehr, P., 2005. Ultrafine particles cross cellular membranes by nonphagocytic mechanisms in lungs and in cultured cells. Environ Health Persp. 113, 1555-1560.

Ghosh, P., Han, G., De, M., Kim, C.K., Rotello, V.M., 2008a. Gold nanoparticles in delivery applications. Adv Drug Deliv Rev. 60, 1307-1315.

Ghosh, P.S., Kim, C.K., Han, G., Forbes, N.S., Rotello, V.M., 2008b. Efficient gene delivery vectors by tuning the surface charge density of amino acid-functionalized gold nanoparticles. ACS Nano. 2**,** 2213-2218.

Gimble, J., Guilak, F., 2003. Adipose-derived adult stem cells: isolation, characterization, and differentiation potential. Cytotherapy. 5**,** 362-369.

Godovski, D.Y., 1995. Electron behavior and magnetic-properties of polymer nanocomposites. Thermal Electrical Conduct Polym Mater. 119**,** 79-122.

Goodman, C.M., McCusker, C.D., Yilmaz, T., Rotello, V.M., 2004. Toxicity of gold nanoparticles functionalized with cationic and anionic side chains. Bioconjug Chem. 15**,** 897-900.

Govorov, A.O., Richardson, H.H., 2007. Generating heat with metal nanoparticles. Nano Today. 2**,** 30-38.

Gratton, S.E., Ropp, P.A., Pohlhaus, P.D., Luft, J.C., Madden, V.J., Napier, M.E., DeSimone, J.M., 2008. The effect of particle design on cellular internalization pathways. Proc Natl Acad Sci USA. 105**,** 11613-11618.

Guidotti, S., Facchini, A., Platano, D., Olivotto, E., Minguzzi, M., Trisolino, G., Filardo, G., Cetrullo, S., Tantini, B., Martucci, E., Facchini, A., Flamigni, F., Borzi, R.M., 2013. Enhanced osteoblastogenesis of adipose-derived stem cells on spermine delivery via beta-catenin activation. Stem Cells Dev. 22**,** 1588-1601.

Gupta, A.K., Gupta, M., 2005. Synthesis and surface engineering of iron oxide nanoparticles for biomedical applications. Biomaterials. 26**,** 3995-4021.

Halappanavar, S., Jackson, P., Williams, A., Jensen, K.A., Hougaard, K.S., Vogel, U., Yauk, C.L., Wallin, H., 2011. Pulmonary response to surface-coated nanotitanium dioxide particles includes induction of acute phase response genes, inflammatory cascades, and changes in microRNAs: a toxicogenomic study. Environ Mol Mutagen. 52**,** 425-439.

Halleux, C., Sottile, V., Gasser, J.A., Seuwen, K., 2001. Multi-lineage potential of human mesenchymal stem cells following clonal expansion. J Musculoskelet Neuronal Interact. 2**,** 71-76.

Harisinghani, M.G., Barentsz, J., Hahn, P.F., Deserno, W.M., Tabatabaei, S., van

de Kaa, C.H., de la Rosette, J., Weissleder, R., 2003. Noninvasive detection of clinically occult lymph-node metastases in prostate cancer. N Engl J Med. 348**,** 2491-2499.

Haynes, C.L., 2010. The emerging field of nanotoxicology. Anal Bioanal Chem. 398**,** 587-588.

Heo, D.N., Ko, W.K., Bae, M.S., Lee, J.B., Lee, D.W., Byun, W., Lee, C.H., Kim, E.C., Jung, B.Y., Kwan, I.K., 2014. Enhanced bone regeneration with a gold nanoparticle–hydrogel complex. J Mater Chem B. 11**,** 1584-1594.

Heo, J.S., Lee, S.Y., Lee, J.C., 2010. Wnt/beta-catenin signaling enhances osteoblastogenic differentiation from human periodontal ligament fibroblasts. Mol Cells. 30**,** 449-454.

Heymer, A., Haddad, D., Weber, M., Gbureck, U., Jakob, P.M., Eulert, J., Noth, U., 2008. Iron oxide labelling of human mesenchymal stem cells in collagen hydrogels for articular cartilage repair. Biomaterials. 29**,** 1473-1483.

Hirn, S., Semmler-Behnke, M., Schleh, C., Wenk, A., Lipka, J., Schaffler, M., Takenaka, S., Moller, W., Schmid, G., Simon, U., Kreyling, W.G., 2011. Particle size-dependent and surface charge-dependent biodistribution of gold nanoparticles after intravenous administration. Eur J Pharm Biopharm. 77**,** 407-416.

Hu, W., Peng, C., Lv, M., Li, X., Zhang, Y., Chen, N., Fan, C., Huang, Q., 2011. Protein corona-mediated mitigation of cytotoxicity of graphene oxide. ACS Nano. 5**,** 3693-3700.

Huang da, W., Sherman, B.T., Lempicki, R.A., 2009. Systematic and integrative analysis of large gene lists using DAVID bioinformatics resources. Nat Protoc. 4**,** 44-57.

Huang, H.Z., Yang, X.R., 2004. Synthesis of chitosan-stabilized gold nanoparticles in the absence/presence of tripolyphosphate. Biomacromol. 5**,** 2340-2346.

Huang, J., Shu, Q., Wang, L., Wu, H., Wang, A.Y., Mao, H., 2015a. Layer-by-

layer assembled milk protein coated magnetic nanoparticle enabled oral drug delivery with high stability in stomach and enzyme-responsive release in small intestine. Biomaterials. 39**,** 105-113.

Huang, X., Li, M., Green, D.C., Williams, D.S., Patil, A.J., Mann, S., 2013. Interfacial assembly of protein-polymer nano-conjugates into stimulus-responsive biomimetic protocells. Nat Commun. 4**,** 2239. 1-9.

Huang, Y., Lu, X., Qu, Y.H., Yang, Y.M., Wu, S., 2015b. MicroRNA sequencing and molecular mechanisms analysis of the effects of gold nanoparticles on human dermal fibroblasts. Biomaterials. 37**,** 13-24.

Hussain, S.M., Hess, K.L., Gearhart, J.M., Geiss, K.T., Schlager, J.J., 2005. In vitro toxicity of nanoparticles in BRL 3A rat liver cells. Toxicol In Vitro. 19**,** 975-983.

Ilie, I., Ilie, R., Mocan, T., Bartos, D., Mocan, L., 2012. Influence of nanomaterials on stem cell differentiation: designing an appropriate nanobiointerface. Int J Nanomed. 7**,** 2211-2225.

Issa, B., Obaidat, I.M., Albiss, B.A., Hail, Y., 2013. Magnetic nanoparticles: surface effects and properties related to biomedicine applications. Int J Mol Sci. 14**,** 21266-21305.

Jain, P.K., Huang, X., El-Sayed, I.H., El-Sayed, M.A., 2008. Noble metals on the nanoscale: optical and photothermal properties and some applications in imaging, sensing, biology, and medicine. Acc Chem Res. 41**,** 1578-1586.

Jardim, M.J., Fry, R.C., Jaspers, I., Dailey, L., Diaz-Sanchez, D., 2009. Disruption of microRNA expression in human airway cells by diesel exhaust particles is linked to tumorigenesis-associated pathways. Environ Health Perspect. 117**,** 1745-1751.

Jena, P., Mohanty, S., Mallick, R., Jacob, B., Sonawane, A., 2012. Toxicity and antibacterial assessment of chitosan-coated silver nanoparticles on human pathogens and macrophage cells. Int J Nanomed. 7**,** 1805-1818.

Jeong, S., Choi, S.Y., Park, J.H., Seo, J.H., Park, J., Cho, K.C., Joo, S.W., Lee, S.Y., 2011. Low-toxicity chitosan gold nanoparticles for small hairpin

RNA delivery in human lung adenocarcinoma cells. J Mater Chem. 21, 13853-13859.

Kamaly, N., Xiao, Z., Valencia, P.M., Radovic-Moreno, A.F., Farokhzad, O.C., 2012. Targeted polymeric therapeutic nanoparticles: design, development and clinical translation. Chem Soc Rev. 41, 2971-3010.

Kang, B., Mackey, M.A., El-Sayed, M.A., 2010. Nuclear targeting of gold nanoparticles in cancer cells induces DNA damage, causing cytokinesis arrest and apoptosis. J Am Chem Soc. 132, 1517-1519.

Karlsson, H.L., Gustafsson, J., Cronholm, P., Moller, L., 2009. Size-dependent toxicity of metal oxide particles-a comparison between nano- and micrometer size. Toxicol Lett. 188, 112-118.

Kawata, K., Osawa, M., Okabe, S., 2009. In vitro toxicity of silver nanoparticles at noncytotoxic doses to HepG2 human hepatoma cells. Environ Sci Technol. 43, 6046-6051.

Kean, T., Thanou, M., 2010. Biodegradation, biodistribution and toxicity of chitosan. AdvanDrug Deliv Rev. 62, 3-11.

Kern, S., Eichler, H., Stoeve, J., Kluter, H., Bieback, K., 2006. Comparative analysis of mesenchymal stem cells from bone marrow, umbilical cord blood, or adipose tissue. Stem Cells. 24, 1294-1301.

Khan, A.K., Rashid, R., Murtaza, G., Zahra, A., 2014. Gold nanoparticles: synthesis and applications in drug delivery. Trop J Pharm Res. 13, 1169-1177.

Khan, J.A., Pillai, B., Das, T.K., Singh, Y., Maiti, S., 2007. Molecular effects of uptake of gold nanoparticles in HeLa cells. Chembiochem. 8, 1237-1240.

Khlebtsov, N., Dykman, L., 2011. Biodistribution and toxicity of engineered gold nanoparticles: a review of in vitro and in vivo studies. Chem Soc Rev. 40, 1647-1671.

Kim, B.Y., Rutka, J.T., Chan, W.C., 2010. Nanomedicine. N Engl J Med. 363, 2434-2443.

Kim, S., Choi, J.E., Choi, J., Chung, K.H., Park, K., Yi, J., Ryu, D.Y., 2009.

Oxidative stress-dependent toxicity of silver nanoparticles in human hepatoma cells. Toxicol In Vitro. 23**,** 1076-1084.

Kim, T.H., Lee, K.B., Choi, J.W., 2013. 3D graphene oxide-encapsulated gold nanoparticles to detect neural stem cell differentiation. Biomaterials. 34**,** 8660-8670.

Kim, V.N., 2005. MicroRNA biogenesis: coordinated cropping and dicing. Nat Rev Mol Cell Biol. 6**,** 376-385.

Kodiha, M., Wang, Y.M., Hutter, E., Maysinger, D., Stochaj, U., 2015. Off to the organelles-killing cancer cells with targeted gold nanoparticles. Theranostics. 5**,** 357-370.

Krek, A., Grun, D., Poy, M.N., Wolf, R., Rosenberg, L., Epstein, E.J., MacMenamin, P., da Piedade, I., Gunsalus, K.C., Stoffel, M., Rajewski, N., 2005. Combinatorial microRNA target predictions. Nat Genet. 37**,** 495-500.

Kumar, S., Gandhi, K.S., Kumar, R., 2007. Modeling of formation of gold nanoparticles by citrate method. IndustEng Chem Res. 46**,** 3128-3136.

Lagos-Quintana, M., Rauhut, R., Lendeckel, W., Tuschl, T., 2001. Identification of novel genes coding for small expressed RNAs. Science. 294**,** 853-858.

Lan, Z., Yang, W.X., 2012. Nanoparticles and spermatogenesis: how do nanoparticles affect spermatogenesis and penetrate the blood-testis barrier. Nanomedicine (Lond). 7**,** 579-596.

Lee, H., Kang, T., Yoon, K.A., Lee, S.Y., Joo, S.W., Lee, K., 2010. Colorimetric detection of mutations in epidermal growth factor receptor using gold nanoparticle aggregation. Biosens Bioelectron. 25**,** 1669-1674.

Lee, P.C., Meisel, D., 1982. Adsorption and surface-enhanced raman of dyes on silver and gold. J phys chem. 86**,** 3391-3395.

Lee, S., Choi, S.U.S., Li, S., Eastman, J.A., 1999. Measuring thermal conductivity of fluids containing oxide nanoparticles. J Heat Transfer-Transac Asme. 121**,** 280-289.

Lee, W.C., Lim, C.H., Shi, H., Tang, L.A., Wang, Y., Lim, C.T., Loh, K.P., 2011.

Origin of enhanced stem cell growth and differentiation on graphene and graphene oxide. ACS Nano. 5**,** 7334-7341.

Levy, R., Thanh, N.T., Doty, R.C., Hussain, I., Nichols, R.J., Schiffrin, D.J., Brust, M., Fernig, D.G., 2004. Rational and combinatorial design of peptide capping ligands for gold nanoparticles. J Am Chem Soc. 126**,** 10076-10084.

Levy, R., 2006. Peptide-capped gold nanoparticles: towards artificial proteins. Chembiochem. 7**,** 1141-1145.

Levy, R., Shaheen, U., Cesbron, Y., See, V., 2010. Gold nanoparticles delivery in mammalian live cells: a critical review. Nano Rev. 1, 1-18.

Li, H.X., Luo, X., Liu, R.X., Yang, Y.J., Yang, G.S., 2008. Roles of Wnt/beta-catenin signaling in adipogenic differentiation potential of adipose-derived mesenchymal stem cells. Mol Cell Endocrinol. 291**,** 116-124.

Lian, J.B., Stein, G.S., 1995. Development of the osteoblast phenotype: molecular mechanisms mediating osteoblast growth and differentiation. Iowa Orthop J. 15**,** 118-140.

Limbach, L.K., Wick, P., Manser, P., Grass, R.N., Bruinink, A., Stark, W.J., 2007. Exposure of engineered nanoparticles to human lung epithelial cells: Influence of chemical composition and catalytic activity on oxidative stress. Environ Sci Technol. 41**,** 4158-4163.

Lin, J., Zhang, H., Chen, Z., Zheng, Y., 2010a. Penetration of lipid membranes by gold nanoparticles: insights into cellular uptake, cytotoxicity, and their relationship. ACS Nano. 4**,** 5421-5429.

Lin, R.J., Lin, Y.C., Yu, A.L., 2010b. miR-149* induces apoptosis by inhibiting Akt1 and E2F1 in human cancer cells. Mol Carcinog. 49**,** 719-727.

Liu, S., Xu, L., Zhang, T., Ren, G., Yang, Z., 2010. Oxidative stress and apoptosis induced by nanosized titanium dioxide in PC12 cells. Toxicology. 267**,** 172-177.

Liu, S., Patel, S.H., Ginestier, C., Ibarra, I., Martin-Trevino, R., Bai, S., McDermott, S.P., Shang, L., Ke, J., Ou, S.J., Heath, A., Zhang, K.J., Korkaya, H., Clouthier, S.G., Charafe-Jauffret, E., Birnbau, D., Hannon,

G.J., Wicha, M.S., 2012. MicroRNA93 regulates proliferation and differentiation of normal and malignant breast stem cells. PLoS Genet. 8**,** e1002751.

Lu, J.M., Wang, X., Marin-Muller, C., Wang, H., Lin, P.H., Yao, Q., Chen, C., 2009. Current advances in research and clinical applications of PLGA-based nanotechnology. Expert Rev Mol Diagn. 9**,** 325-41.

Lynch, I., Salvati, A., Dawson, K.A., 2009. Protein-nanoparticle interactions: What does the cell see? Nat Nanotechnol. 4**,** 546-547.

Mahapatro, A., Singh, D.K., 2011. Biodegradable nanoparticles are excellent vehicle for site directed in-vivo delivery of drugs and vaccines. J Nanobiotech. 9**,** 55, 1-11.

Malaval, L., Modrowski, D., Gupta, A.K., Aubin, J.E., 1994. Cellular expression of bone-related proteins during in vitro osteogenesis in rat bone marrow stromal cell cultures. J Cell Physiol. 158**,** 555-572.

Mangolini, A., Bonon, A., Volinia, S., Lanza, G., Gambari, R., Pinton, P., Russo, G.R., Del Senno, L., Dell'Atti, L., Aguiari, G., 2014. Differential expression of microRNA501-5p affects the aggressiveness of clear cell renal carcinoma. FEBS Open Bio. 4**,** 952-965.

Marie, E., Landfester, K., Antonietti, M., 2002. Synthesis of chitosan-stabilized polymer dispersions, capsules, and chitosan grafting products via miniemulsion. Biomacromolecules. 3**,** 475-481.

Mathews, S., Gupta, P.K., Bhonde, R., Totey, S., 2011. Chitosan enhances mineralization during osteoblast differentiation of human bone marrow-derived mesenchymal stem cells, by upregulating the associated genes. Cell Prolif. 44**,** 537-549.

Maxson, S., Lopez, E.A., Yoo, D., Danikovitch-Miagkova, A., Leroux, M.A., 2012. Concise review: role of mesenchymal stem cells in wound repair. Stem Cells Transl Med. 1**,** 142-149.

Maynard, A.D., Aitken, R.J., Butz, T., Colvin, V., Donaldson, K., Oberdorster, G., Philbert, M.A., Ryan, J., Seaton, A., Stone, V., Tinkle, S.S., Tran, L., Walker, N.J., Warheit, D.B., 2006. Safe handling of nanotechnology.

Nature. 444**,** 267-269.

McConnell, W.P., Novak, J.P., Brousseau, L.C., Fuierer, R.R., Tenet, R.C., Feldheim, D.L, 2000. Electronic and optical properties of chemically modified metal nanoparticles and molecularly bridged nanoparticle arrays. J Phys Chem B. 104**,** 8925-8930.

McDonald, J.W., Liu, X.Z., Qu, Y., Liu, S., Mickey, S.K., Turetsky, D., Gottlieb, D.I., Choi, D.W., 1999. Transplanted embryonic stem cells survive, differentiate and promote recovery in injured rat spinal cord. Nat Med. 5**,** 1410-1412.

Mei, Y., Bian, C., Li, J., Du, Z., Zhou, H., Yang, Z., Zhao, R.C., 2013. miR-21 modulates the ERK-MAPK signaling pathway by regulating SPRY2 expression during human mesenchymal stem cell differentiation. J Cell Biochem. 114**,** 1374-1384.

Mieszawska, A.J., Mulder, W.J., Fayad, Z.A., Cormode, D.P., 2013. Multifunctional gold nanoparticles for diagnosis and therapy of disease. Mol Pharm. 10**,** 831-847.

Minones-Moyano, E., Porta, S., Escaramis, G., Rabionet, R., Iraola, S., Kagerbauer, B., Espinosa-Parrilla, Y., Ferrer, I., Estivill, X., Marti, E., 2011. MicroRNA profiling of Parkinson's disease brains identifies early downregulation of miR-34b/c which modulate mitochondrial function. Hum Mol Genet. 20**,** 3067-3078.

Murphy, C.J., Sau, T.K., Gole, A.M., Orendorff, C.J., Gao, J., Gou, L., Hunyadi, S.E., Li, T., 2005. Anisotropic metal nanoparticles: Synthesis, assembly, and optical applications. J Phys Chem B. 109**,** 13857-13870.

Muzzarelli, R.A.A., 2011. Chitosan composites with inorganics, morphogenetic proteins and stem cells, for bone regeneration. Carbohyd Polym. 83**,** 1433-1445.

Nam, J.M., Thaxton, C.S., Mirkin, C.A., 2003. Nanoparticle-based bio-bar codes for the ultrasensitive detection of proteins. Science. 301**,** 1884-1886.

Nayak, T.R., Jian, L., Phua, L.C., Ho, C.K., Ren, Y., Pastorin, G., 2010. Thin

films of functionalized multiwalled carbon nanotubes as suitable scaffold materials for stem cells proliferation and bone formation. ACS Nano. 4**,** 7717-7725.

Nel, A., Xia, T., Malder, L., Li, N., 2006. Toxic potential of materials at the nanolevel. Science. 311**,** 622-627.

Nie, S.M., Xiang, Y., Kim, G.J., Simons, J.W., 2007. Nanotechnology applications in cancer. Annu Rev Biomed Eng. 9**,** 257-288.

Niziolek, P.J., Warman, M.L., Robling, A.G., 2012. Mechanotransduction in bone tissue: The A214V and G171V mutations in Lrp5 enhance load-induced osteogenesis in a surface-selective manner. Bone. 51**,** 459-465.

Oberdorster, G., Sharp, Z., Atudorei, V., Elder, A., Gelein, R., Kreyling, W., Cox, C., 2004. Translocation of inhaled ultrafine particles to the brain. Inhal Toxicol. 16**,** 437-445.

Orrenius, S., Zhivotovsky, B., Nicotera, P., 2003. Regulation of cell death: the calcium-apoptosis link. Nat Rev Mol Cell Biol. 4**,** 552-565.

Orza, A., Soritau, O., Olenic, L., Diudea, M., Florea, A., Rus Ciuca, D., Biris, A.S., 2011. Electrically conductive gold-coated collagen nanofibers for placental-derived mesenchymal stem cells enhanced differentiation and proliferation. ACS Nano. 5**,** 4490-4503.

Oyen, J., Brudvik, C., Gjesdal, C.G., Tell, G.S., Lie, S.A., Hove, L.M., 2011. Osteoporosis as a risk factor for distal radial fractures: a case-control study. J Bone Joint Surg Am. 93**,** 348-356.

Paciotti, G.F., Kingston, D.G.I., Tamarkin, L., 2006. Colloidal gold nanoparticles: A novel nanoparticle platform for developing multifunctional tumor-targeted drug delivery vectors. Drug DevelopRes. 67**,** 47-54.

Palombo, M., Deshmukh, M., Myers, D., Gao, J., Szekely, Z., Sinko, P.J., 2014. Pharmaceutical and toxicological properties of engineered nanomaterials for drug delivery. Annu Rev Pharmacol Toxicol. 54**,** 581-598.

Pan, Y., Neuss, S., Leifert, A., Fischler, M., Wen, F., Simon, U., Schmid, G.,

Brandau, W., Jahnen-Dechent, W., 2007. Size-dependent cytotoxicity of gold nanoparticles. Small. 3**,** 1941-1949.

Pan, Y., Leifert, A., Ruau, D., Neuss, S., Bornemann, J., Schmid, G., Brandau, W., Simon-U., Jahnen-Dechent, W., 2009. Gold nanoparticles of diameter 1.4 nm trigger necrosis by oxidative stress and mitochondrial damage. Small. 5**,** 2067-2076.

Panda, K.K., Achary, V.M., Krishnaveni, R., Padhi, B.K., Sarangi, S.N., Sahu, S.N., Panda, B.B., 2011. In vitro biosynthesis and genotoxicity bioassay of silver nanoparticles using plants. Toxicol In Vitro. 25**,** 1097-1105.

Pantic, I., Markovic, L., 2011. Antibody-labeled gold nanoconjugates in experimental physiology and cancer research. Rev Adv Mater Sci. 29**,** 126-129.

Park, J., Bauer, S., Schlegel, K.A., Neukam, F.W., von der Mark, K., Schmuki, P., 2009. TiO2 nanotube surfaces: 15 nm--an optimal length scale of surface topography for cell adhesion and differentiation. Small. 5**,** 666-671.

Patra, H.K., Banerjee, S., Chaudhuri, U., Lahiri, P., Dasgupta, A.K., 2007. Cell selective response to gold nanoparticles. Nanomedicine. 3**,** 111-119.

Peer, D., Karp, J.M., Hong, S., Farokhzad, O.C., Margalit, R., Langer, R., 2007. Nanocarriers as an emerging platform for cancer therapy. Nat Nanotechnol. 2**,** 751-760.

Pernodet, N., Fang, X., Sun, Y., Bakhtina, A., Ramakrishnan, A., Sokolov, J., Ulman, A., Rafailovich, M., 2006. Adverse effects of citrate/gold nanoparticles on human dermal fibroblasts. Small. 2**,** 766-773.

Perumal, O.P., Inapagolla, R., Kannan, S., Kannan, R.M., 2008. The effect of surface functionality on cellular trafficking of dendrimers. Biomaterials. 29**,** 3469-3476.

Phillips, J.E., Petrie, T.A., Creighton, F.P., Garcia, A.J., 2010. Human mesenchymal stem cell differentiation on self-assembled monolayers presenting different surface chemistries. Acta Biomater. 6**,** 12-20.

Pittenger, M.F., Mackay, A.M., Beck, S.C., Jaiswal, R.K., Douglas, R., Mosca,

J.D., Moorman, M.A., Simonetti, D.W., Craig, S., Marshak, D.R., 1999. Multilineage potential of adult human mesenchymal stem cells. Science. 284**,** 143-147.

Pokharkar, V., Dhar, S., Bhumkar, D., Mali, V., Bodhankar, S., Prasad, B.L., 2009. Acute and subacute toxicity studies of chitosan reduced gold nanoparticles: a novel carrier for therapeutic agents. J Biomed Nanotech. 5**,** 233-239.

Ravichandran, R., Sridhar, R., Venugopal, J.R., Sundarrajan, S., Mukherjee, S., Ramakrishna, S., 2014. Gold nanoparticle loaded hybrid nanofibers for cardiogenic differentiation of stem cells for infarcted myocardium regeneration. Macromol Biosci. 14**,** 515-525.

Ren, G., Chen, X., Dong, F., Li, W., Ren, X., Zhang, Y., Shi, Y., 2012. Concise review: mesenchymal stem cells and translational medicine: emerging issues. Stem Cells Transl Med. 1**,** 51-58.

Richardson, H.H., Carlson, M.T., Tandler, P.J., Hernandez, P., Govorov, A.O., 2009. Experimental and theoretical studies of light-to-heat conversion and collective heating effects in metal nanoparticle solutions. Nano Lett. 9**,** 1139-1146.

Richardson, S.C.W., Kolbe, H.J.V., Duncan, R., 1999. Potential of low molecular mass chitosan as a DNA delivery system: biocompatibility, body distribution and ability to complex and protect DNA. Int J Pharm. 178**,** 231-243.

Ricles, L.M., Nam, S.Y., Sokolov, K., Emelianov, S.Y., Suggs, L.J., 2011. Function of mesenchymal stem cells following loading of gold nanotracers. Int J Nanomed. 6**,** 407-416.

Robinson, J.A., Chatterjee-Kishore, M., Yaworsky, P.J., Cullen, D.M., Zhao, W., Li, C., Kharode, Y., Sauter, L., Babij, P., Brown, E.L., Hill, A.A., Akhte, M.P., Johnson, M.L., Recker, R.R., Komm, B.S., Bex, F.J., 2006. Wnt/beta-catenin signaling is a normal physiological response to mechanical loading in bone. J Biol Chem. 281**,** 31720-31728.

Rothen-Rutishauser, B.M., Schurch, S., Haenni, B., Kapp, N., Gehr, P., 2006.

Interaction of fine particles and nanoparticles with red blood cells visualized with advanced microscopic techniques. Environ Sci Technol. 40**,** 4353-4359.

Sahu, D., Kannan, G.M., Vijayaraghavan, R., Anand, T., Khanum, F., 2013. Nanosized zinc oxide induces toxicity in human lung cells. ISRN Toxicol. 2013**,** ID316075.

Sanfelix-Genoves, J., Hurtado, I., Sanfelix-Gimeno, G., Reig-Molla, B., Peiro, S., 2011. Impact of osteoporosis and vertebral fractures on quality-of-life. a population-based study in Valencia, Spain (The FRAVO Study). Health Qual Life Outcomes. 9**,** 1-10.

Sardar, R., Funston, A.M., Mulvaney, P., Murray, R.W., 2009. Gold nanoparticles: past, present, and future. Langmuir. 25**,** 13840-13851.

Schaeublin, N.M., Braydich-Stolle, L.K., Schrand, A.M., Miller, J.M., Hutchison, J., Schlager, J.J., Hussain, S.M., 2011. Surface charge of gold nanoparticles mediates mechanism of toxicity. Nanoscale. 3**,** 410-420.

Selbach, M., Schwanhausser, B., Thierfelder, N., Fang, Z., Khanin, R., Rajewsky, N., 2008. Widespread changes in protein synthesis induced by microRNAs. Nature. 455**,** 58-63.

Sen, B., Xie, Z., Case, N., Ma, M., Rubin, C., Rubin, J., 2008. Mechanical strain inhibits adipogenesis in mesenchymal stem cells by stimulating a durable beta-catenin signal. Endocrinology. 149**,** 6065-6075.

Sengstock, C., Diendorf, J., Epple, M., Schildhauer, T.A., Koller, M., 2014. Effect of silver nanoparticles on human mesenchymal stem cell differentiation. Beilstein J Nanotechnol. 5**,** 2058-2069.

Sharma, V., Park, K., Srinivasarao, M., 2009. Colloidal dispersion of gold nanorods: Historical background, optical properties, seed-mediated synthesis, shape separation and self-assembly. Mater Sci Eng R-Report. 65**,** 1-38.

Shen, J., Vakifahmetoglu, H., Stridh, H., Zhivotovsky, B., Wiman, K.G., 2008. PRIMA-1MET induces mitochondrial apoptosis through activation of

caspase-2. Oncogene. 27**,** 6571-6580.

Shevach, M., Fleischer, S., Shapira, A., Dvir, T., 2014. Gold nanoparticle-decellularized matrix hybrids for cardiac tissue engineering. Nano Lett. 14**,** 5792-5796.

Shi, H., Magaye, R., Castranova, V., Zhao, J., 2013. Titanium dioxide nanoparticles: a review of current toxicological data. Part Fibre Toxicol. 10**,** 1-33.

Simpson, C.A., Huffman, B.J., Gerdon, A.E., Cliffel, D.E., 2010. Unexpected toxicity of monolayer protected gold clusters eliminated by PEG-thiol place exchange reactions. Chem Res Toxicol. 23**,** 1608-1616.

Sohaebuddin, S.K., Thevenot, P.T., Baker, D., Eaton, J.W., Tang, L., 2010. Nanomaterial cytotoxicity is composition, size, and cell type dependent. Part Fibre Toxicol. 7**,** 1-17.

Spadaccio, C., Rainer, A., Trombetta, M., Vadala, G., Chello, M., Covino, E., Denaro, V., Toyoda, Y., Genovese, J. A., 2009. Poly-L-lactic acid/hydroxyapatite electrospun nanocomposites induce chondrogenic differentiation of human MSC. Ann Biomed Eng. 37**,** 1376-1389.

Sperling, R.A., Parak, W.J., 2008. Biological applications of gold nanoparticles. Chem Soc Rev. 37**,** 1896-1908.

Sperling, R.A., Parak, W.J., 2010. Surface modification, functionalization and bioconjugation of colloidal inorganic nanoparticles. Philos Trans A Math Phys Eng Sci. 368**,** 1333-1383.

Stein, G.S., Lian, J.B., 1993. Molecular mechanisms mediating proliferation/differentiation interrelationships during progressive development of the osteoblast phenotype. Endocr Rev. 14**,** 424-442.

Su, F.X., Wang, L.M., Sun, Y.Y., Liu, C.H., Duan, X. R., Li, Z.P., 2015. Highly sensitive detection of CpG methylation in genomic DNA by AuNP-based colorimetric assay with ligase chain reaction. ChemCommun. 51**,** 3371-3374.

Sun, B., Liu, R., Ye, N., Xiao, Z.D., 2015. Comprehensive evaluation of microRNA Expression profiling reveals the neural signaling specific

cytotoxicity of superparamagnetic iron oxide nanoparticles (SPIONs) through N-Methyl-D-Aspartate Receptor. Plos One. 10, e121617.

Tan, S., Li, R., Ding, K., Lobie, P.E., Zhu, T., 2011. miR-198 inhibits migration and invasion of hepatocellular carcinoma cells by targeting the HGF/c-MET pathway. FEBS Lett. 585**,** 2229-2234.

Teodoro, J.S., Simoes, A.M., Duarte, F.V., Rolo, A.P., Murdoch, R.C., Hussain, S.M., Palmeira, C.M., 2011. Assessment of the toxicity of silver nanoparticles in vitro: a mitochondrial perspective. Toxicol In Vitro. 25**,** 664-670.

Tervonen, T., Linkov, I., Figueira, J.R., Steevens, J., Chappell, M., Merad, M., 2009. Risk-based classification system of nanomaterials. J Nanopart Res. 11**,** 757-766.

Tiwari, P.M., Vig, K., Dennis, V.A., Singh, S.R., 2011. Functionalized gold nanoparticles and their biomedical applications. Nanomaterials. 1**,** 31-63.

Tong, L., Wei, Q.S., Wei, A., Cheng, J.X., 2009. Gold nanorods as contrast agents for biological imaging: optical properties, surface conjugation and photothermal effects. Photochem Photobiol. 85**,** 21-32.

Tosi, G., Bortot, B., Ruozi, B., Dolcetta, D., Vandelli, M.A., Forni, F., Severini, G.M., 2013. Potential use of polymeric nanoparticles for drug delivery across the blood-brain barrier. Curr Med Chem. 20**,** 2212-2225.

Toupadakis, C.A., Wong, A., Genetos, D.C., Cheung, W.K., Borjesson, D.L., Ferraro, G.L., Galuppo, L.D., Leach, J.K., Owens, S.D., Yellowley, C.E., 2010. Comparison of the osteogenic potential of equine mesenchymal stem cells from bone marrow, adipose tissue, umbilical cord blood, and umbilical cord tissue. Am J Vet Res. 71**,** 1237-1245.

Tsukahara, T., Haniu, H., 2011. Nanoparticle-mediated intracellular lipid accumulation during C2C12 cell differentiation. Biochem Biophys Res Commun. 406**,** 558-563.

Turkevich, J., Stevension, P.C., Hillier, J., 1951. A study of the nucleation and growth processes in the sysnthesis of the colloidal gold. Discuss Farad

Soci. 55-75.

Uboldi, C., Bonacchi, D., Lorenzi, G., Hermanns, M.I., Pohl, C., Baldi, G., Unger, R.E., Kirkpatrick, C.J., 2009. Gold nanoparticles induce cytotoxicity in the alveolar type-II cell lines A549 and NCIH441. Part Fibre Toxicol. 6**,** 1-12.

Uehara, N., 2010. Polymer-functionalized gold nanoparticles as versatile sensing materials. Anal Sci. 26**,** 1219-1228.

Unfried, K., Albrecht, C., Klotz, L.O., Mikecz, A.V., Beck, S.G., Schins, R.P.F., 2007. Cellular responses to nanoparticles: Target structures and mechanisms. Nanotoxicology. 1**,** 52-71.

Vamanu, C.I., Cimpan, M.R., Hol, P.J., Sornes, S., Lie, S.A., Gjerdet, N.R., 2008. Induction of cell death by TiO2 nanoparticles: studies on a human monoblastoid cell line. Toxicol In Vitro. 22**,** 1689-1696.

Vemuri, M.C., Chase, L.G., Rao, M.S., 2011. Mesenchymal stem cell assays and applications. Methods Mol Biol. 698**,** 3-698.

Venkatesan, J., Ryu, B., Sudha, P.N., Kim, S.K., 2012. Preparation and characterization of chitosan-carbon nanotube scaffolds for bone tissue engineering. Int J Biol Macromol. 50**,** 393-402.

Vetrone, S.A., Huarng, M.C., Alocilja, E.C., 2012. Detection of non-PCR amplified S. enteritidis genomic DNA from food matrices using a gold-nanoparticle DNA biosensor: a proof-of-concept study. Sensors (Basel). 12**,** 10487-10499.

Vijayakumar, S., Ganesan, S., 2012. In Vitro Cytotoxicity Assay on Gold Nanoparticles with Different Stabilizing Agents. J Nanomater. 2012**,** ID734398.

Volinia, S., Calin, G.A., Liu, C.G., Ambs, S., Cimmino, A., Petrocca, F., Visone, R., Iorio, M., Roldo, C., Ferracin, M., Prueitt, R.L., Yanaihara, N., Lanza, G., Scarpa, A., Vecchione, A., Negrini, M., Harris, C.C., Croce, C.M., 2006. A microRNA expression signature of human solid tumors defines cancer gene targets. Proc Natl Acad Sci U S A. 103**,** 2257-2261.

Wagner, W., Wein, F., Seckinger, A., Frankhauser, M., Wirkner, U., Krause, U.,

Blake, J., Schwager, C., Eckstein, V., Ansorge, W., Ho, A.D., 2005. Comparative characteristics of mesenchymal stem cells from human bone marrow, adipose tissue, and umbilical cord blood. Exp Hematol. 33**,** 1402-1416.

Wang, F., Gao, F., Lan, M., Yuan, H., Huang, Y., Liu, J., 2009. Oxidative stress contributes to silica nanoparticle-induced cytotoxicity in human embryonic kidney cells. Toxicol In Vitro. 23**,** 808-815.

Wang, M., Li, Z., Qiao, H., Chen, L., Fan, Y., 2013a. Effect of Gold/Fe3O4 Nanoparticles on Biocompatibility and Neural Differentiation of Rat Olfactory Bulb Neural Stem Cells. J Nanomater. 2013**,** 1-7.

Wang, M., Wang, J., Kong, X., Chen, H., Wang, Y., Qin, M., Lin, Y., Chen, H., Xu, J., Hong, J., Chen, Y.X., Zou, W., Fang, J.Y., 2014. MiR-198 represses tumor growth and metastasis in colorectal cancer by targeting fucosyl transferase 8. Sci Rep. 4**,** 6145, 1-10.

Wang, R.B., Billone, P.S., Mullett, W.M., 2013b. Nanomedicine in Action: An Overview of Cancer Nanomedicine on the Market and in Clinical Trials. J Nanomater. 2013**,** ID629681.

Wang, Y., Zheng, X., Zhang, Z., Zhou, J., Zhao, G., Yang, J., Xia, L., Wang, R., Cai, X., Hu, H., Zhu, C., Nie, Y., Wu, K., Zhang, D., Fan, D., 2012. MicroRNA-149 inhibits proliferation and cell cycle progression through the targeting of ZBTB2 in human gastric cancer. PLoS One. 7**,** e41693.

Wei, D., Qian, W., 2008. Facile synthesis of Ag and Au nanoparticles utilizing chitosan as a mediator agent. Colloids Surf B Biointerfaces. 62**,** 136-142.

Xia, T., Kovochich, M., Brant, J., Hotze, M., Sempf, J., Oberley, T., Sioutas, C., Yeh, J.I., Wiesner, M.R., Nel, A.E., 2006. Comparison of the abilities of ambient and manufactured nanoparticles to induce cellular toxicity according to an oxidative stress paradigm. Nano Lett. 6**,** 1794-1807.

Xu, B.S., Tanaka, S., 1999. Behavior and bonding mechanisms of aluminum nanoparticles by electron beam irradiation. NanostructMater. 12**,** 915-918.

Xu, S., Witmer, P.D., Lumayag, S., Kovacs, B., Valle, D., 2007. MicroRNA (miRNA) transcriptome of mouse retina and identification of a sensory organ-specific miRNA cluster. J Biol Chem. 282**,** 25053-66.

Yah, C.S., 2013. The toxicity of Gold Nanoparticles in relation to their physiochemical properties. Biomedical Research-India. 24**,** 400-413.

Yang, B., Guo, H., Zhang, Y., Dong, S., Ying, D., 2011. The microRNA expression profiles of mouse mesenchymal stem cell during chondrogenic differentiation. BMB Rep. 44**,** 28-33.

Yang, J., Zhao, H., Xin, Y., Fan, L., 2014. MicroRNA-198 inhibits proliferation and induces apoptosis of lung cancer cells via targeting FGFR1. J Cell Biochem. 115**,** 987-995.

Ye, Y., Wang, C., Du, P., Falzon, M., Seitz, P.K., Cooper, C.W., 2001. Overexpression of parathyroid hormone-related protein enhances apoptosis in the rat intestinal cell line, IEC-6. Endocrinology. 142**,** 1906-1914.

Yen, H.J., Hsu, S.H., Tsai, C.L., 2009. Cytotoxicity and immunological response of gold and silver nanoparticles of different sizes. Small. 5**,** 1553-1561.

Yguerabide, J., Yguerabide, E.E., 1998. Light-scattering submicroscopic particles as highly fluorescent analogs and their use as tracer labels in clinical and biological applications. Anal Biochem. 262**,** 157-76.

Yi, C., Liu, D., Fong, C.C., Zhang, J., Yang, M., 2010. Gold nanoparticles promote osteogenic differentiation of mesenchymal stem cells through p38 MAPK pathway. ACS Nano. 4**,** 6439-6448.

Yildirimer, L., Thanh, N.T., Loizidou, M., Seifalian, A.M., 2011. Toxicology and clinical potential of nanoparticles. Nano Today. 6**,** 585-607.

Yu, M., Mu, H., Niu, Z., Chu, Z., Zhu, H., Hua, J., 2014. miR-34c enhances mouse spermatogonial stem cells differentiation by targeting Nanos2. J Cell Biochem. 115**,** 232-242.

Yu, X., Li, H., Ren, X., 2012. Interaction between regulatory T cells and cancer stem cells. Int J Cancer. 131**,** 1491-1498.

Zapol, P., Curtiss, L.A., 2007. Organic molecule adsorption on TiO2 nanoparticles: A review of computational studies of surface interactions. J Comput Theor Nanos. 4**,** 222-230.

Zhai, H., Song, B., Xu, X., Zhu, W., Ju, J., 2013. Inhibition of autophagy and tumor growth in colon cancer by miR-502. Oncogene. 32**,** 1570-1579.

Zhang, B., Pan, X., 2009. RDX induces aberrant expression of microRNAs in mouse brain and liver. Environ Health Perspect. 117**,** 231-240.

Zhang, D., Liu, D., Zhang, J., Fong, C., Yang, M., 2014. Gold nanoparticles stimulate differentiation and mineralization of primary osteoblasts through the ERK/MAPK signaling pathway. Mater Sci Eng C Mater Biol Appl. 42**,** 70-77.

Zhang, J., Saltzman, M., 2013. Engineering biodegradable nanoparticles for drug and gene delivery. Chem Eng Prog. 109**,** 25-30.

Zhang, L., Gu, F.X., Chan, J.M., Wang, A.Z., Langer, R.S., Farokhzad, O.C., 2008a. Nanoparticles in medicine: therapeutic applications and developments. Clin Pharmacol Ther. 83**,** 761-769.

Zhang, L.W., Monteiro-Riviere, N.A., 2009. Mechanisms of quantum dot nanoparticle cellular uptake. Toxicol Sci. 110**,** 138-155.

Zhang, X., 2015. Gold nanoparticles: recent advances in the biomedical applications. Cell Biochem Biophys. 72, 771-775.

Zhang, Y., Yang, M., Portney, N.G., Cui, D., Budak, G., Ozbay, E., Ozkan, M., Ozkan, C.S., 2008b. Zeta potential: a surface electrical characteristic to probe the interaction of nanoparticles with normal and cancer human breast epithelial cells. Biomed Microdevices. 10**,** 321-328.

ABSTRACT IN KOREAN

국문초록

표면 변형된 금 나노 입자의 세포 생존도 및 골분화에 대한 작용

최선영

서울대학교 대학원

수의과대학 수의생명과학 전공

(수의약리학)

(지도교수: 이소영)

독특한 물리적, 화학적 성질을 갖는 나노 입자를 약물전달, 암세포 표적, 조직재생과 같은 바이오 의학 분야에서 활용하고자 하는 연구가 활발히 진행되고 있다. 다른 나노 입자에 비해 독성이 없다고 알려진 금 나노 입자의 경우, 용매에 분산되어 있는 콜로이드 형태의 입자로 널리 사용된다. 그러므로, 이때 발생하는 전기화학적 불안정성을 예방하고자 안정제를 첨가하여 합성하게 된다. 안정제로 변형시킨 금 나노 입자는 생체안정성이 높고 특정 단백질이나 항체 등과 쉽게 결합

할 수 있어 약물 전달체, 진단 검출도구로 응용되고 있다. 더욱이, 조직 재생 의학에서 성체줄기세포의 분화를 촉진하는 치료 도구로 연구되고 있다. 그러나, 최근 금 나노 입자의 크기, 형태, 표면 전하, 또는 세포의 종류에 따라 세포에 대한 독성을 나타낸다는 연구 결과가 발표되고 있다. 또한, 금 나노 입자의 생리적, 생물학적 효과가 세포 타입 의존적으로 다르다는 연구가 발표되었다. 본 연구에서는 구연산염(sodium citrate)과 키토산(chitosan)으로 표면을 변형시킨 금 나노 입자의 폐암 세포에 대한 독성을 측정하고, 금 나노 입자의 노출에 따른 microRNA 발현 변화를 통해 세포 기능의 변화를 예측하였다. 또한 키토산-금 나노 입자의 성체줄기세포에 대한 골 분화 촉진 효과를 연구하였다.

본 연구의 결과는 구연산염과 키토산으로 변형시켜 다른 전하를 나타내는 금 나노 입자가 세포사멸 또는 괴사를 통해 농도 의존적으로 폐암세포에 대한 독성을 나타내는 것을 확인하였다. 또한, 구연산염과 키토산으로 변형시킨 금 나노 입자에 노출되었을 때 폐암 세포에서 전사 후 조절 인자인 microRNA의 발현이 변화하였다. 구연산염-금 나노 입자에 의해 발현이 증가한 microRNA는 세포 이주, 전이와 관련이 있다. 키토산-금 나노 입자에 의해 발현이 증가된 microRNA는 세포 증식, 세포 사멸, 분화와 관련이 있다. 또한, 키토산-금 나노 입자에 의해 발현이 감소된 microRNA는 세포 증식, 세포 사멸, 세포 발

달 신호 전달과 관련이 있다. 세포 분화와 관련된 연구에서, 키토산-금 나노 입자가 세포 생존도가 감소하지 않는 농도에서, Wnt/β-catenin 신호전달체계의 활성화를 통하여 지방조직유래 성체 줄기세포의 골 분화를 촉진시키는 것을 관찰하였다. 그러므로, 본 연구 결과는 구연산염과 키토산으로 표면을 변형시킨 금 나노 입자를 조직 재생을 촉진 시키기 위한 치료 도구로써 활용할 수 있으며, 금 나노 입자를 바이오 의학적으로 응용하기 전, 세포에 대한 독성 평가가 반드시 선행되어야 한다는 것을 보여준다.

본 연구는 다음과 같은 측면에 중점을 두었다. (1) 구연산염-금 나노 입자와 키토산-금 나노입자의 세포 독성 효과 (Chapter I and II), (2) 구연산염-, 키노산-금 나노입자에 의한 microRNA 발현 변화 (Chapter III), (3) 키토산-금 나노 입자에 의한 지방조직유래 성체줄기세포에 대한 골분화 촉진 (Chapter IV).

주요어: 구연산염-금 나노 입자, 키토산-금 나노 입자, 세포독성,
마이크로 알앤에이, 성체줄기세포, 무기화작용, Wnt/β-catenin

학번: 2009-21640